ISAS - INTERNATIONAL SCHOOL FOR ADVANCED STUDIES

THEORETICAL MODELS OF ACTIVE GALACTIC NUCLEI

A thesis submitted for the degree of

Doctor Philosophiae

Candidate:

Piergiovanni Madau

Supervisor:

Professor M.A. Abramowicz

Trieste - September 1987

CONTENTS

ACKNOWLEDGMENTS

My greatest debt of gratitude is owed to M.A. Abramowicz for his advice, supervision and patience.

I have benefitted from stimulating conversations on AGNs and related topics with O. Blaes, G. de Zotti, J. Krolik, M. Malkan, L. Maraschi, S. Phinney, D. Raine, R. Svensson, A. Treves and G. Zamorani.

I am also grateful to L. Maraschi and A.Treves for their hospitality at the University of Milano, to S. Phinney and D. Eardley who allowed me to enjoy a stimulating extended program on AGNs at the Institute for Theoretical Physics (Santa Barbara), and to the director of the 1986 Erice School on "AGNs, Neutron Stars and Jets" for financial support.

I also wish to express my gratitude to prof. D.W. Sciama, a constant source of encouragement and ideas, not always readily exploited.

My friend and collegue G. Ghisellini deserves special thanks for a long and fruitful collaboration, and for his patience in leading me into the world of relativistic plasmas.

Finally I thank my parents, to whom this thesis is dedicated.

FOREWORD

To the reader of this thesis, I can only recall, as Akhmatova wrote: "*..if only you knew from what kind of garbage high poetry shamelessly arises..*" and ask him to wait, trustfully, for the high poetry.

INTRODUCTION

Active Galactic Nuclei have been classified on the basis of the observed luminosity, presence or absence of broad emission lines, presence or absence of low-excitation emission lines, level of radio power, radio extended morphology, degree of polarization, degree of variability, relative prominence of IR/UV/X-ray continuum emission, flat or steep radio spectra, relative prominence of continuum vs lines, and space density. This frighteningly long list of known observed properties, however, hides what in the last decade have become the building blocks of a unified phenomenology.

The first step in this direction has been, of course, the habit of using the term AGN (Active Galactic Nucleus) to cover everything (for a recent review on AGNs see Lawrence 1987). In the general basic framework within which the observed phenomenology is interpreted, the "prime mover" at the center is responsible for phenomena ranging in lengthscale from the central continuum source ($\sim 10^{13}$-10^{17}cm) which is the underlying powerhouse, to the broad emission line region ($\sim 10^{17}$-10^{18}cm), the compact flat-spectrum radio source ($\sim 10^{18}$-10^{20}cm), the narrow emission line region ($\sim 10^{19}$-10^{21}cm), and the jets of plasma ($\sim 10^{18}$-10^{22}cm) which supply energy and material to the extended radio lobes ($\sim 10^{22}$-10^{25}cm).

Active nuclei are responsible for emission all the way from the lowest radio frequencies to the highest gamma-ray energies. For most AGNs the bolometric luminosity is unknown and, in many cases, the bulk of the emitted power may emerge in the unseen UV/X region.

The most recent discovery of the nuclear activity is that it is commonly manifested in the production of jets of plasma that emerge from the nucleus. We know that the central engine does accelerate and collimate material on lengthscales $\ll 1$ pc, but it is not clear what is being accelerated; whether it is a relativistic electron-proton or a lighter electron-positron plasma (see Phinney 1983, Begelman, Blandford & Rees 1984).

It is now 23 years (soon after the discovery of quasars) since it has been realized that the power supply is gravitational in origin. The most popular class of explanations for the AGN powerhouse involves the accretion of gas onto a supermassive black hole. The evidence that a great deal of mass is squeezed within a very small volume, a more efficient mechanism to convert rest mass energy into radiation, and the idea that the likely evolutionary endpoint of any massive central condensation in the nucleus of a galaxy is a runaway collapse, suggest that massive black holes are the prime movers of the nuclear activity (see the review by Rees 1984). Needless to say, the most persuasive argument for this idea are essentially theoretical, and we have no proof that black holes do harbor in galactic nuclei (or indeed anywhere else).

The immediate consequence of a relativistic central potential well is that a characteristic jet speed is of order the escape velocity $\sim c(r_G/r)$. The strongest evidence for relativistic bulk velocities is in the apparent superluminal motion of radio luminous blobs which is observed in some compact sources.

A simplified conceptual framework, which tentatively organizes the different forms of nuclear activity, involves different regimes of gas accretion onto the black hole and the presence of a relativistic outflow from the nucleus. The likely

candidate parameters of the theoretical space are:

1) *the viewing angle* ϑ. Due to Doppler beaming along the direction of motion of the radiation emitted from material in a relativistic jet, the orientation angle of the jet-axis with respect to the line of sight may affect the source appearance and statistics;

2) *the mass of the black hole* M, which governs the linear scale r_G, the dynamical timescale r_G/c and the Eddington luminosity L_E;

3) the amount of matter surrounding it or, less trivially, the *dimensionless accretion rate* $\dot{m}=\dot{M}c^2/L_E$. Different modes of accretion with angular momentum would produce different kinds of emission spectra and convey gravitational energy into different output channels, such as nuclear luminosity or bulk kinetic energy of the jets.

Several theoretical pictures have been proposed in the past few years (with differing degrees of success) to unify different classes of AGNs. Unified schemes involving relativistic beaming have been proposed for radio-quiet and radio-loud quasars (Scheuer & Readhead 1979), steep-spectrum and flat-spectrum radio quasars (Orr & Browne 1982), BL Lac objects and radio-galaxies (Blandford & Rees 1978), quasars and OVVs (Blandford & Konigl 1979).

From the observational point of view, it has also become clear that: first, there is an evolutionary link between Seyfert 1 galaxies and QSOs (Weedman 1985) and second, inclination and dust obscuration are probably at the base of the observed differences between Type 1 and Type 2 Seyfert galaxies (Lawrence & Elvis 1982, Antonucci & Miller 1985).

The physics of accretion flows onto black holes may be the 'Rosetta Stone' for such a complex phenomenology. Unified schemes which invoke different accretion regimes have been proposed by Rees et al (1982), Phinney (1983), Blandford (1984), Begelman (1985). The basic physics of accretion was developed in the early 70's. For a long time the only theoretical description of an accretion disk was based on the 'standard model' of Shakura & Sunyaev (1973) which basically assumed small vertical thickness of the disk and accretion rates much lower than the Eddington value.

It was realized in the late 70's that super-Eddington accretion rates do not necessarily imply any dramatic consequence for the equilibrium structure of the disk (Paczynski & Wiita 1980, Abramowicz, Calvani & Nobili 1980). The shapes of theoretical disk models in such accretion regimes are toroidal, somewhat resembling a sphere with two deep and narrow funnels along the rotation axis.

Despite its initial promises as an origin of radiation pressure driven and collimated outflows, the theory of thick accretion disks is still in its infancy. This is because the structure of accretion flows with $\dot{m} \gg 1$ is considerably more complicated than the structure of $\dot{m} \ll 1$ flows described by the standard thin accretion disk model. In addition to the complications genuine to regimes with $\dot{m} \gg 1$, these flows share all the difficulties found in the subcritical $\dot{m} \ll 1$ regime as well as those connected with the lack of understanding viscosity and other dissipative processes.

On the other hand, observational estimates of the masses of the central black hole in AGNs, from which the values of $\dot{m}$ can be inferred, are very uncertain. Most of them are based on measurements of the broad emission-line widths and on the

assumption that they reflect the Keplerian motion of gas clouds in the central potential well; sub-Eddington luminosities are derived in this way. However, larger values of $\dot{m}$ cannot be excluded, especially if the ratio L(UV/X)/L(opt) is very large. Smaller central masses and $\dot{m} \gg 1$ are obviously allowed in the case of outward radiatively accelerated clouds.

The black hole masses are estimated in chapter I of this thesis following a different approach, i.e. through the study of the statistical properties of the collectivity of AGNs: space density and evolutionary (the redshift dependence) behaviour. We also derive from the observations constraints on the radiation mechanisms and on the physical conditions in the emission region, which then may favour one or another of the proposed central engines.

In chapter II we present the basic theory of non-thermal radiation processes and relativistic beaming. The emphasis is now placed on the importance of the viewing angle for the observed global energetics of individual objects and for the statistics of AGNs.

The physics of accretion flows onto massive black holes is described in chapter III. The control parameter is now the accretion rate. The general approach is to consider as fundamental the problem of energy generation and try to derive the main features of the emission spectra associated with different accretion regimes.

The thermal spectrum of a radiation-supported torus is computed in chapter IV. Again, the main feature is found to be the dependence of the observed spectrum on the viewing angle. The occultation of the innermost disk region due to self-shadowing and

the enhancement of the radiation field which results from the multiple scatterings of photons off the funnel walls, are self-consistently taken into account.

A modest 'unified scheme' is suggested on the basis of this spectral behaviour. Basically, radiation tori would represent the powerhouse of optically bright QSOs. High and low-inclination systems would be responsible, respectively, for the optical/UV and UV/soft X-ray thermal excesses which are observed in their spectra. The shielding of the outer regions from the primary ionizing radiation source may explain the strong, low-excitation Fe II emission lines which are typically observed in these objects.

CHAPTER I: AN INTRODUCTION TO THE ACTIVE GALACTIC NUCLEI

I.1) Nomenclature and the hosts

The classification of various kinds of Active Galactic Nuclei has been traditionally based on their spectrum and morphology. This crowd of objects has generated a confusing nomenclature: QSOs, QSRs, BL Lacs, Type 1, 1.5 and 2 Seyfert galaxies, HPQs, OVVs, RGs, BLRGs, NLRGs, BALQSOs, blazar, N-galaxies, LINERs, and so on. Some confusion has resulted from the vagueness of the boundaries between different categories; for example 3C 120 has been called a Seyfert galaxy, a radio galaxy, an N galaxy and a quasars. I will not try in this chapter to give a detailed treatment of the taxonomy of AGNs and of their observed energetics and spectra (see, e.g. the proceedings of the recent conferences held in Manchester (Dyson 1985), Santa Cruz (Miller 1985), Trieste (Giuricin et al. 1986) and Bangalore (Swarup & Kapahi 1986).

Some of the relevant properties of AGNs will be discussed in the next chapters. For the sake of the discussion I will rather adopt the following qualitative terminology.

A *QSO* is a stellar appearing object at large redshift which show strong continuum emission all the way from the far IR to X-rays, and broad (FWHM>3000 km/s) permitted and narrow forbidden emission lines. It is optically more luminous than a first-ranked cluster elliptical galaxy $M_V < -21.5 + 5\log h$, where $h=H_o/100$ $Kms^{-1}Mpc^{-1}$. Roughly 10% of QSOs are radio loud QSRs, in the sense

that $L_R > 10^{-3} L_{opt}$.

A *Seyfert galaxy* is essentially a QSO scaled down to be less luminous than its surrounding spiral galaxy. They are relatively weak radio sources. Type 2 Seyferts are distinguished from Type 1 Seyferts by the absence of broad wings to the permitted emission lines (it is a recent discovery by Antonucci & Miller 1985, that the archetypical Seyfert 2 galaxy, NGC 1068, is a Seyfert 1 hidden inside a torus of absorbing stuff).

A *radio galaxy* (RG) is an active galaxy with radio emission comparable or greater than its optical emission and characterized by radio-emitting structures which extend up to thousands of kiloparsecs from the central galaxy. The *classical doubles* were the first type recognized, with the two large radio-lobes collinear with the central galaxy.

High Polarization Quasars (HPQs) share many of the distinctive features of *BL Lacertae* objects, namely flat radio spectra, rapid radio, optical, X-ray variability, high and strongly variable optical polarization. The BL Lac objects tend to be less luminous than the HPQs and have weak or no detectable emission lines. The two classes are usually grouped together under the common denomination of *blazar* (Angel & Stockman 1980).

It has been realized that the distinction between active galaxies and normal ones is not clear cut, as well; in fact, there is considerable evidence that the majority of spiral galaxies show some kind of activity not directly related to stellar sources in their nuclei. In particular, about 80% of nuclei in early-type (Sa,Sb) spirals have low-ionisation nuclear emission region (*LINERs*, see Keel 1985).

These objects are obviously very common, with a space density

almost two orders of magnitude above that of classical Seyfert nuclei. Fitting LINERs' spectra requires more hard-photons than stars can provide (Ferland & Netzer 1983); the invoked mechanisms for producing low-ionisation spectra are photoionisation by a very dilute power-law continuum source and/or shock heating. LINERs represent relatively low luminosity objects ($L(H_\alpha) < 10^{40}$erg/s).

The nature of the host galaxies of QSOs is an important clue in understanding the formation of QSOs, their fuelling mechanism and the relation between QSOs and active galaxies. It has been known for many years that the majority of Seyfert galaxies are spirals, that radio galaxies are universally giant ellipticals and that BL Lacs appear located in ellipticals rather spiral galaxies (Miller 1981).

Imaging studies have shown that:

- virtually all QSOs and active galaxies with redshift $z \leq 0.5$ have extended nebulosities (Gehren et al. 1984);

- the mean absolute blue magnitude of galaxies underlyng radio-loud quasars: $M_B \simeq -21.11 + 5\log h$ is comparable to the mean value of $M_B \simeq -21.5 + 5\log h$ found for the brightest cluster galaxies (Smith et al. 1986,hereafter S86). The QSO point sources optically dominate their hosts : $L_{NUCL} / L_{GAL} \simeq 7$;

- the radio-loud quasar host galaxies are typically a magnitude more luminous than the radio-quiet quasar host galaxies, which are in turn typically a magnitude more luminous than Seyfert galaxies;

- host galaxies of QSOs are generally drawn from the

high-luminosity exponential tail of the Schechter galaxy luminosity function (see figure 1). If the optical luminosity of the QSO host is not boosted by processes associated with the nuclear activity (such as QSO-induced bursts of star formation), the preferential association of quasars with luminous host galaxies places important constraints on QSO evolution model ;

- a trend is observed for elliptical (disk) galaxy models to be preferred for the radio-loud (radio-quiet) QSOs ;

- the morphologically peculiar host galaxies frequently observed are suggestive of tidal interactions with nearby companions (Stockton & McKenty 1987). QSOs seem to be usually situated in cluster of galaxies (Yee & Green 1984).

Spectroscopic studies (Boroson & Oke 1984, Boroson,Persson & Oke 1985) show two clearly distinct groups:

I) *extended steep-spectrum* radio sources with strong O [III] emission lines in the nebulosity and in the nuclear narrow line region and weak or absent nuclear Fe II emission lines;

II) *compact flat-spectrum* radio sources and radio-quiet objects with weak or absent nebular and nuclear emission lines and prominent Fe II nuclear emission lines.

This dichotomy is thus apparent in a variety of properties at so many size scales, from the Broad Line Region (~ 10^{17}- 10^{18} cm) through the underlying host galaxy (1-10 kpc) up to the extended radio emission (100 Kpc). Some very basic difference must exist between these two groups of QSOs, suggesting the controlling

factor being located in the central regions of QSOs. The most likely explanation (Boroson, Persson & Oke 1985) involves geometrical effects in group II preventing the ionizing radiation from reaching the nebular gas. Absorption of the primary ionizing photons by a dense and optically thick torus would result in weaker O [III] line emission, allowing more of the iron to remain Fe II, thus relatively increasing the strength of the optical Fe II emission. This kind of argument will be discussed extensively in chapter IV.

The basic, still unsettled question at issue in dealing with low-luminosity active nuclei and with the properties of the collectivity of QSOs is whether nearly all luminous galaxies pass through an active phase at some time in their life or has only a small fraction of them ever exhibited quasar activity in the past. The search for clues to this question will lead us into the intricate world of quasar *demography*.

I.2) Quasar demography

Within the usual framework of a Friedmann universe it has long been known that the space density of quasars increases steeply with distance out of a redshift $z \simeq 3$ at least, in the sense that either the intrinsic power or the number of sources was greater in the past (see, e.g. Veron 1983 for a review).

The evidence for evolution of optically selected quasars is based on the distribution of their optical magnitudes. If the number-magnitude relation for quasars is written in the form :

$$\log N\ (<B) = a + b \cdot B$$

where N is the number of QSOs per square degree brighter than magnitude B, the determination of b provides an estimate of the rate of cosmological evolution of quasars. Early estimates of b were ~0.75. If quasars had a uniform space distribution in a Friedman universe, then b=0.35 (Schmidt 1978). The value expected for uniformly distributed objects in Euclidean space is b=0.6.

The evolution is a consequence of the variation of the quasar luminosity function (LF) with time. Two basic alternative scenarios for this evolution have been historically proposed:

i) *pure density evolution* (PDE, Schmidt 1972), in which all quasars of all luminosities scale up in numbers as we observe to higher z. In this picture the past LF was the same in shape as the local LF but shifted uniformly to higher densities;

ii) *pure luminosity evolution* (PLE, Mathez 1976), in which the number of quasars per unit comoving volume does not change, but their luminosity sistematically increases with z. In this picture the shape of the LF is again preserved and the evolution involves a uniform shift to brighter luminosities in the past of long-lived individual objects or of a statistical ensemble of short-lived events.

A luminosity-dependent density evolution model (LDDE) has been suggested by Schmidt & Green (1983) for optical quasars, in which the amount of density evolution is dependent on luminosity, the most luminous sources evolving most rapidly (in analogy with the evolution pattern of radio-sources,see e.g. Peacock & Gull

1981). This differential evolution model involves a change in the shape of the LF, the latter being flatter at higher z.

The evolution of the LF is described by a volume density ϕ (L,z). In the case of PDE, one has:

$$\phi(L,z) = \phi(L) \cdot f_D(z)$$

while for a PLE model it is

$$\phi(L,z) = 1/f_L(z) \cdot \phi(L/f_L(z)) \quad .$$

In both cases it is assumed that the evolution functions $f_L(z)$ and $f_D(z)$ are independent on L. Now,if the luminosity function $\phi(L)$ is a power-law : $\phi(L) = AL^{-m}$, density evolution with arbitrary $f_D(z)$ is locally equivalent to luminosity evolution with $f_L^{m-1} = f_D$. Unfortunately, in the case of optically selected QSOs, the LF derived from the ultraviolet excess bright quasar survey (limited to $z \leq 2$ and $B<20$) is well described by a single power-law over 2 or 3 decades in luminosity, with a slope that is almost identical at all redshifts (see,e.g. Marshall 1986).

Different models of evolution give thus rise to indistinguishable results. At magnitudes fainter than 20, however, the differences between the models diverge; in particular, PDE predicts a continuing steep rise whereas PLE show a flattening of the counts. A turnover in the number-magnitude counts has been actually suggested by Koo & Kron (1982) to explain the low surface densities of multicolor-selected QSOs at faint $B<22.5$; this supported the conclusion of Zamorani et al.(1981) that the X-ray background is exceeded unless the counts flatten before $B \simeq 22$.

Based on a new catalogue of faint ($B<21$) QSOs, Boyle et al.(1987) have recently shown that the steep slope $d\log N/dB \simeq 0.86$ exhibited by the number-magnitude relation flattens significantly

beyond B≃ 19.5 to dlogN/dB≃ 0.32. The low surface density at faint magnitudes is in agreement with recent multicolor spectroscopic surveys by Koo & Kron (1987) and Marano,Zamorani & Zitelli (1987). The flattening of the quasar counts is direct evidence that the steep power-law LF of distant quasars must turn over and that PDE model must be abandoned, the observed surface density at B≃ 20.7 being a factor 10 down on that predicted (Boyle et al. 1987).

Now, for a power-law spectrum $S_\nu \propto \nu^{-\alpha}$, the monochromatic luminosity is :

$$L_\nu = 4\pi S_\nu D_L^2 (1+z)^{\alpha-1}$$

where $D_L = 1.85\cdot 10^{28}\cdot(1+z-(1+z)^{0.5})\ h^{-1}$cm (for $\Omega_o=1$) is the luminosity distance. Hereafter, when not explicitly indicated, numerical values will be quoted assuming h=1, $\Omega_o=1$. In dealing with optical samples we need a conversion between optical magnitudes and flux densities. For a $\nu^{-0.5}$ spectrum, we have (Schmidt & Green 1983):

$$M_B = -2.5\cdot\log L_\nu(4400\ \text{Å}) + 51.84 \quad .$$

The luminosity function is related to the number of quasars per square degree at redshift z with apparent magnitude B by the equation:

$$N(B,z)dBdz = \phi(M_B,z)dM_B dV/dz \qquad (1.1)$$

where dV is the comoving volume element in a unit area of the sky: $dV = c/H_o D_L^2 (1+z)^{-3.5} dz$.

As expected from the N(B) counts,the LF does exhibit a break at faint absolute magnitudes. The z dependence of this break is consistent with a uniform shift towards higher luminosities in the past. The evolution of QSOs at $z \leq 2.2$ can thus be simply

parametrized with a pure luminosity evolution of the form (Boyle et al. 1987, Marshall 1987):

$$L(z) = L(z=0)\cdot(1+z)^{k} \qquad (1.2)$$

with $k=3.5$ for $\Omega_o=1$. In other words QSOs statistically conserve their number since $z \approx 2.2$, but they fade off by a factor ~ 50 on average, with a timescale of 5 Gyr.

The best fit (differential) QSO LF, evolved back to z=0, is given by a two power-law form:

$$\phi(L,z=0)=\phi^*/L^*\cdot\left[(L/L^*)^{3.6} + (L/L^*)^{1.2}\right]^{-1} \qquad (1.3)$$

where $\phi^*=1.2\cdot10^{-5}\ h^3 Mpc^{-3}$, and $L^*=0.072$ (in units of 10^{30} erg/s/Hz at 4400 Å) corresponds to $M_B^*=-20.3+5\log h$ and represents the position of the break (Marshall 1987). This LF matches both in shape and space density the Seyfert 1 & 1.5 LF (Cheng et al. 1985, Weedman 1986, Boyle et al. 1987, Marshall 1987), strongly supporting an evolutionary link between Seyfert galaxies and QSOs. The form given in eq.(1.3) is truncated somewhat arbitrarily below $M_B=-17.5$, which corresponds to the faintest Seyfert nuclei.

The galaxy luminosity function is given by:

$$\Psi(L)=\Psi^*/L_G^*\cdot(L/L_G)^{-1.3}\exp(-L/L^*) \qquad (1.4)$$

where $\Psi^*=1.4\cdot10^{-2}\ h^3\ Mpc^{-3}$ and L_G^* corresponds to $M_B^*=-19.4$ (Schechter 1976, Davis & Huchra 1982). Then at least 0.1-1% of all bright galaxies contains a *dead quasar* (see figure 2).

If all galaxies undergo a quasar phase, QSOs must have a very short lifetime, less than ~ 1% of the look-back time to z=2: $t(z)\simeq6.5\cdot10^{9}(1-(1+z)^{-3/2})\ h^{-1}$ yr. In this case the parametrization

$L(z) \propto (1+z)^{3.5}$ would represent the evolution in average luminosity for ~100 successive generations of short-lived ~ 10^7 yr objects, the present day population of which would be represented by Seyfert galaxies. However, a special arrangement would be required between the rate of QSOs births and deaths to keep ϕ^* roughly constant with cosmic epoch, as observed. Indeed the simplest physical interpretation of PLE is one in which there is a single generation of objects, with individual long-lived ~ 10^9yr QSOs formed prior to z=2.2. They would gradually dim in luminosity, the endpoint of their evolution being the Seyfert galaxies.

I.3) Weighing black holes

In the single-generation scenario, a lower limit to the total energy radiated away by individual sources can be found integrating in look-back time up to z=2.2. In the framework of massive black hole models for the QSO central engine, the total accreted mass accumulated in the black hole during this time is:

$$M(z=0)/M_\odot \simeq 1.2 \cdot 10^{10} \cdot \epsilon_{0.1}^{-1} K_{BC} \cdot 10^{-0.4(M_B+24)} \quad h^{-3} \qquad (1.5)$$

where K_{BC} is the bolometric correction to $(\nu L_\nu)_B$, and ϵ is the efficiency of mass to radiation conversion.

In the case,e.g. of 3C 273 ($K_{BC} \simeq 10$, $M_B = -25.5$), this yields the enormous mass of $4.5 \cdot 10^{11}$ h^{-3} $M_\odot$. Although 3C 273 is a unique object, probably a statistical outlier, very massive black holes $M \approx 10^9$-10^{10} $M_\odot$ in the nuclei of low z QSOs and Seyfert galaxies are generally predicted in the long-lived quasar

evolution model. Half of the total accreted mass is actually accumulated in the first $\sim 6 \cdot 10^8$ yr of their lifetime (if they were born at $z \simeq 2$).

A characteristic luminosity associated with a gravitating mass is the Eddington luminosity, at which radiation pressure on free electrons balances gravity:

$$L_E = 4\pi cGM/k_T = 1.3 \cdot 10^{38}\ M/M_\odot \qquad (1.6)$$

where k_T is the Thomson opacity. Equations (1.5) and (1.6) imply that the local QSOs radiates at very sub-Eddington luminosities:

$$L(z=0)/L_E(z=0) \simeq 10^{-3} \epsilon_{0.1}\ h\ . \qquad (1.7)$$

This ratio increases with redshift, the mass accumulated in the black hole obviously decreasing with z as it approaches the "turn-on" time (arbitrarily set in at $z_{on}=2.2$, see figure 3). More in general, it is easy to derive:

$$L(z)/L_E(z) \simeq 8.96 \cdot 10^{-3} (1+z)^{3.5} \cdot \epsilon_{0.1}/((1+z_{on})^2 - (1+z)^2)\ .$$

$$M(z)/M(z=0) \simeq \left[(1+z_{on})^2 - (1+z)^2\right]/\left[(1+z_{on})^2 - 1\right] \qquad (1.8)$$

On the other hand, in the single generation evolution model, luminosities are expected to be well below the Eddington limit because the source lifetime:

$$\tau = M/\dot{M} \simeq 4.4 \cdot 10^7\ \epsilon_{0.1} (L/L_E)\ \ \mathrm{yr} \qquad (1.9)$$

is very short if $L \geq L_E$; here $\dot{M}$ is the black hole accretion rate.

Hence a black hole eating at the Eddington limit would grow exponentially with time on an e-folding timescale of $4.4 \cdot 10^7$ yr. The time necessary to a *primeval* seed $10 M_\odot$ black hole (a' la Cygnus X-1)to grow at the Eddington rate up to $10^8 M_\odot$ is

$\sim 7 \cdot 10^8$ yr.

A more general argument to constraint the masses of hypothetical black holes from the statistics of QSOs has been given by Soltan (1982) (see also Phinney 1983, Peacock 1987). The total comoving energy density radiated by all quasars is:

$$U = \iint L\, \phi(L,z)\, dL dt \qquad (1.10)$$

where integrals are over the entire range of quasar redshifts and bolometric luminosities. From equation (1.1) we derive:

$$U = 4\pi/c \int (1+z) dz \int N(S,z) S dS \quad .$$

The energy density U is independent of H_o and Ω_o. Let us compute the integral in eq.(1.10) taking the optical LF given in (1.3) and the PLE evolution law (1.2), and integrate, to be conservative, only up to z=2.2. The total radiated energy density (now) is:

$$U_{QSO}(z \leq 2.2) \simeq 700\ K_{BC}\ M_\odot c^2 \quad Mpc^{-3} \qquad (1.11)$$

with K_{BC} being the rather uncertain bolometric correction, $K_{BC} \simeq 5$. Integration up to z=3 would increase this estimate by a factor ~1.6 (the value of U_{QSO} can be compared with the microwave background energy density $U_{MWB} \simeq 7.5 \cdot 10^6 \cdot M_\odot c^2$ Mpc^{-3}, or the closure rest mass energy density $U_C \simeq 3 \cdot 10^{11} \cdot M_\odot c^2$ Mpc^{-3}, see Phinney 1983).

The mass density accumulated in black holes is then $\epsilon^{-1} U_{QSO}$. We must divide this number for a space density of relic objects to get the average black hole mass which is lurking in a galactic nucleus. Integrating the LF given in (1.3), we find:

$$\phi(M_B < -17) \simeq 5 \cdot 10^{-5}\ h^3 Mpc^{-3} \quad .$$

such that a burnt mass:

$$M_{BH} \simeq 10^8 M_\odot \; K_{BC} \; \epsilon_{0.1}^{-1} \; h^{-3} \quad M_\odot$$

should exist, on average, in the cores of Seyfert galaxies.

If, on the other hand, every galaxy brighter than $M_B^* = -19.4$ (the break in Schechter galaxy LF of eq.(1.4)) has undergone a quasar phase in its life, we have from eq. (1.4) :

$$\Psi(M_B < M_B^*) \simeq 3 \cdot 10^{-3} \; h^3 \; Mpc^{-3}$$

translating to a burnt mass per galaxy:

$$M_{BH} \simeq 2 \cdot 10^6 \; K_{BC} \; \epsilon_{0.1}^{-1} \; h^{-3} \; M_\odot \quad .$$

In this case, quasar lifetimes of order $\sim 10^8$ yr would be typical of ~ 60 successive generations of quasars. However, as shown in figure 1, QSO host galaxies are very luminous, with an average magnitude $M_B \simeq -20.5$. If the host luminosity is independent of the nuclear one (Smith et al. 1986), we can integrate again Schechter LF to give :

$$\Psi(M_B < -20.5) \simeq 1.4 \cdot 10^{-4} \; h^3 \; Mpc^{-3}$$

which yields:

$$M_{BH} \simeq 5 \cdot 10^7 \; K_{BC} \; \epsilon_{0.1}^{-1} \; h^{-3} \; M_\odot \quad .$$

It should be noted that the space density of QSOs brighter than $M_B = -17$ is about ~ 1/3 the space density of all galaxies brighter than $M_B = -20.5$, so that an evolution scenario with many generations of short-lived QSOs would be ruled out.

In deriving the typical masses of the black holes which may power quasars, an efficiency of mass to radiation conversion of

10% has been assumed. An efficiency much lower than 1% seems difficult to reconcile with the observations due to the enormous central masses required, unless the majority of galaxies do actually host a QSO.

High efficiencies favour models of disk accretion onto black holes compared to ,e.g. supermassive stars and dense star clusters ($\epsilon \simeq 10^{-4}$), or spherical accretion models ($\epsilon \simeq 10^{-3}$).

The two basic evolutionary scenarios can be summarized as follows:

i) QSOs are long-lived objects shining for $\geq 5 \cdot 10^{9}$ yr ($z \geq 2$). Such large black hole masses are involved in this case that their characteristic luminosities (at $z=0$) are very sub-Eddington : $L/L_E \simeq 10^{-3}$. Only a small fraction of the total number of galaxies $\sim 10^{-2}$ did actually undergo a quasar phase;

ii) there are ≤ 100 successive generations of short-lived objects in the timescale over which the entire population fade off. In this case the masses of the remnants are much smaller but much more common. Higher ratios L/L_E would be typical.

If, however, QSO host galaxies are drawn only from the exponential tail of the Schechter LF, the last scenario appears ruled out by the comparison of the space densities.

I.4) The cut-off and the background

Grism surveys of QSOs at high redshifts $z \geq 3$ have suggested a decline in the comoving space density of objects (Osmer 1982). It appears that $z>3$ QSOs are rare and the small number of known cases are remarkably bright.

Schmidt,Schneider & Gunn (1986) concluded that there is a severe absence of faint high-z objects compared with the extrapolation of the evolving LDDE luminosity function. This redshift cut-off might be sharply luminosity dependent, with quasars of higher intrinsic luminosity "turning-on" at higher z.

However, the relatively large number of QSOs between $3<z<3.8$ recently found by Schmidt,Schneider & Gunn (1987) rather argues for a gradual decline beyond $z \simeq 3$ of the comoving space density (Koo & Kron 1987). A decrease in comoving density beyond $z \simeq 2$ is also apparent from radio-surveys (Peacock 1987).

Besides constraining theories of QSOs birth and evolution and of galaxy formation, the existence of the redshift cut-off may have important implications for the estimates of the QSOs contribution to the diffuse UV radiation field as a function of z.

The integrated UV background is the basic ingredient for photoionisation models of the intergalactic medium (IGM) and of the "primordial" Lyman-α clouds producing absorption lines blueward of Lyα emission in QSO spectra. The local QSO volume emissivity (erg $s^{-1} cm^{-3} Hz^{-1}$) at frequency ν^*(4400 Å) is found to be, from eq. (1.3):

$$\epsilon(\nu^*, z=0) = L^* \cdot \phi^* \cdot \int \left[(L/L^*)^{3.6} + (L/L^*)^{1.2} \right]^{-1} (L/L^*) d(L/L^*) \quad . \quad (1.12)$$

The proper volume emissivity at redshift z and frequency ν is of the form:

$$\epsilon(\nu,z)=\epsilon(\nu^*,z=0)\cdot(1+z)^3\cdot f_L(z)\cdot(\nu/\nu^*)^{-\alpha} \qquad (1.13)$$

where $f_L(z)$ is the luminosity evolution law in eq.(1.2) and we have assumed a power-law continuum for the intrinsic spectrum with spectral index α. The specific intensity J_ν (erg $s^{-1}cm^{-2}Hz^{-1}sr^{-1}$) at the frequency ν_o as seen at redshift z_o is given by:

$$J_\nu(\nu_o,z_o)=1/4\pi\cdot(1+z_o)^3\cdot\int_{z_o}^{z_{on}}\epsilon(\nu,z)/(1+z)^3\cdot(dl/dz)\cdot dz \qquad (1.14)$$

with $\nu_o=(1+z_o)/(1+z)\cdot\nu$, $dl/dz=c/H_o\cdot(1+z)^{-2.5}$, and z_{on} is the quasar "turn-on" redshift. At the Lyman limit this yields:

$$J_{912}(z_o)=9.9\cdot10^{-24}(1+z)^{3+\alpha}\cdot\left[(1+z_{on})^{1.5}-(1+z)^{1.5}\right] \qquad (1.15)$$

independently on h. The result is plotted in figure 4, where I have assumed $\alpha=0.5$ and $z_{on}=4$.

A luminosity-dependent cut-off can also be imposed following Bechtold et al.(1987) and Bajtlik, Duncan & Ostriker (1987,hereafer BDO). In this case we actually evolve the low-luminosity integration limit in eq.(1.12) according to :

$$L_{min}=L_o\cdot10^{2(z-z_c)}$$

where $z_c=2.6$, $z\geq z_c$ and L_o corresponds to $M_B=-21.5+5\log h$ (see fig.4).

The important point is that the UV background at high-z has been recently estimated by fitting the distribution of absorption lines in the Lyα forests observed in QSOs spectra. The Lyman-α absorption lines shown on the blue-side of the Lyα emission line in the spectra of high z ($z\geq1.7$) QSOs are now generally regarded

as being due to a population of cosmologically distributed (lack of line clustering) intergalactic clouds (sizes 10^{21}-10^{23}cm) of "primordial" material poor in heavy elements (Sargent et al. 1980, Sargent & Boksenberg 1983).

The clouds have a temperature of ~10^4 k, they are pressure confined in a hotter adiabatically expanding IGM, and highly ionized by the diffuse background of UV photons. Typical column densities are $N_H \simeq 10^{14}$ cm^{-2}, corresponding to an optical depth at the Lyman limit: $\tau_L \simeq 6 \cdot 10^{-4}$. The distribution of observed cloud number density n in column density N_H at a given redshift z can be fitted by a power-law:

$$dn(N_H)/dN_H \simeq 10^{11} \cdot N_H^{-s} \qquad (1.16)$$

with $s \simeq 1.7$ (Carswell et al. 1984). At a given N_H, the comoving density of these clouds show clear evidence of evolution with cosmic time as:

$$dn(z)/dz = n_o \cdot (1+z)^{\gamma} \qquad (1.17)$$

with γ=2.1-2.36 (Murdoch et al. 1986, BDO) (compare this with the expected $dn/dz \propto (1+z)(1+\Omega_o z)^{-0.5}$).

However, a trend is observed within individual QSOs running counter to the overall trend of eq.(1.17), namely a turndown in the number density of Lyα absorption lines near the emission line redshift, which is referred to as the *inverse* or *proximity* effect. A likely explanation is that the effect is due to photoionisation by the QSO Lyman continuum in excess of the diffuse UV background. On the other hand, if the photoionisation model is correct, by fitting the data it is possible to *directly* infer the background of ionizing photons at large redshifts (BDO, Phinney 1987). BDO,

by studying a sample of 19 QSOs with $1.7 \leq z \leq 3.8$, have found that a roughly constant background radiation intensity given by:

$$\log J_{912} \simeq -21 \pm 0.5 \quad \text{erg s}^{-1}\text{cm}^{-2}\text{Hz}^{-1}\text{sr}^{-1}$$

does fit the data (see figure 4). This is much larger than the integrated UV emission of quasars with a luminosity-dependent cut-off at $z>2.6$, but still consistent with a PLE model with a sharp luminosity independent cut-off at $z \geq 4$. Likely possibilities are that the observed drop-off of QSOs number density at $z>2.5$ is not real, or a different source of ionizing photons, e.g. young elliptical galaxies (Bechtold et al. 1987). More data on the high-z quasar space density are clearly needed; however, from eq. (1.16) and (1.17) we can compute the optical depth in these clouds:

$$d\tau_L/dz \simeq 0.06 \cdot (1+z)^{\gamma}$$

which reaches unity at $z \leq 3$, so that searches of high-z QSOs in the blue band will clearly be inefficient.

I.5) A key to the active region : the L/R ratio

A clue to the basic physics of the violent activity in the most powerful and compact sources within AGNs is provided by the observed L/R ratio, the so-called *compactness parameter*. Short term variations in luminosity provide an upper limit for the sizes of the active region. In the absence of special geometries and relativistic effects (both probably present), the causality argument yields the minimum possible time over which such

variations are conceivable for black hole models:

$$\Delta t \geq r_G/c = 2GM/c^3 \simeq 1000 \quad M_8 \quad \text{sec}$$

where r_G is the Schwarzschild radius of a $M_8 = 10^8 M_\odot$ black hole. Periodic variations are further constrained by the shortest rotational timescales in accreting material; a common way of explaining short-lived periodic variations is to assume that the accreting disk contains a "hot spot" which is spiralling into the central black hole. Thin keplerian accretion disks around a Schwarzschild hole have their innermost stable orbit at $r_{in} = 3r_G$, thus a periodic variation could exist down to a timescale of about:

$$\Delta t = 2\sqrt{2}\pi (r_G/c) \cdot (r_{in}/r_G)^{3/2} \simeq 4.6 \cdot 10^4 \quad M_8 \quad \text{sec} \quad .$$

(A tentative detection of a 15 min periodicity in the BL Lac object OJ 287 by Carrasco ,Dultain-Hacyan and Cruz-Gonzales 1984 would be consistent with a mass $M < 2 \cdot 10^6 M_\odot$).

The maximum luminosity that can be radiated by a non-rotating object, in mechanical equilibrium under the action of gravitational force and radiation pressure, is the Eddington limit L_E. Hence, the maximum compactness parameter allowed is :

$$L_E/r_G = 2\pi c^3 m_p/\sigma_T \simeq 4 \cdot 10^{30} \quad L_{45}/R_{15} \quad \text{erg s}^{-1}\text{cm}^{-1}$$

where L_{45} and R_{15} are luminosity and size in unit of 10^{45} erg s^{-1} and 10^{15} cm, respectively (in a pure electron-positron gas, the Eddington limit is a factor m_e/m_p smaller).

A tighter constraint on L/R can be provided: if the outburst is produced by material with an optical depth to electron scattering τ_T, the photon diffusion timescale is: $\Delta t = R/c \cdot (1+\tau_T)$.

In a spherical region of radius R, the amount of energy radiated associated with the conversion of a mass M is:

$$L\Delta t=\epsilon Mc^2=(4/3)\pi R^3 n m_p c^2 \epsilon \ .$$

The photon diffusion time scales with optical depth as $(1+\tau_T)/\sqrt{\tau_T}$ and is a minimum when $\tau_T=n\sigma_T R=1$, yielding:

$$L/R=\epsilon \pi m_p c^3/3\sigma_T \simeq 7 \quad L_{45}/R_{15} \cdot \epsilon_{0.1}$$

(Fabian & Rees 1979). Since ϵ cannot exceed unity, many rapidly varying sources, such as optically violently variable (OVV) quasars and BL Lac objects, do violate this limit (see, e.g. the compilation by Bassani, Dean & Sembay 1983). For these sources, variability timescales tend to be shorter at higher energies. Most variable objects have timescales as short as weeks in the radio, and as short as hours in the optical. In the extreme case of OJ 287, a value of $L_{45}/R_{15} \simeq 100$ has been observed (Wolstencroft, Gilmore & Williams 1982) . Luminosity variations implying $L_{45}/R_{15} \simeq 10\text{-}100$ have also been detected in the X-ray band (Morini et al. 1986, Feigelson et al. 1986).

One or more of the assumptions underlying these calculations: energy from mass conversion, rather than, say magnetic flares or rotational energy, and isotropy of the emission may be violated in these sources. If the individual electrons that radiate are re-used many times, the efficiency ϵ may then be effectively $\gg 1$ (Guilbert, Fabian & Rees 1983).

The luminosity to size ratio places general constraints on the electron radiation mechanisms responsible for the continuum non-thermal emission which is a characteristic property of rapidly varying and highly polarized sources (Blandford & Rees 1978,

Cavaliere & Morrison 1980). Thermal emission mechanisms are unlikely to produce the observed polarization P~10-20% ; besides, there is no evidence for any thermal bump or cut-off in the spectra of these objects from radio to X-rays.

On its crossing a spherical region of radius R and radiation energy density U_r, the expected number of electron collisions with a photon of frequency ν is:

$$\tau_e = \sigma_T R \cdot (U_r/h\nu) \simeq 6.5 \cdot 10^5 \cdot \nu_{15}^{-1} \; L_{45}/R_{15}$$

the electrons then undergoing repeated scatterings and exchanging energy with the photons within the source (provide the Thomson regime applies, i.e. $\nu < m_e c^2/\gamma h$).

The *equipartition* magnetic field $B^2/8\pi = U_r$ is given by:

$$B \simeq 260 \; L_{45}^{1/2}/R_{15} \quad G$$

For the sake of discussion, suppose that the luminosity L is produced at optical frequencies $\nu = 10^{15} \nu_{15}$ Hz by ultrarelativistic electrons with energy γmc^2 as synchrotron radiation. In this case, electrons with Lorentz factor:

$$\gamma \simeq 1000 \; \nu_{15}^{1/2} \; R_{15}^{1/2} \cdot L_{45}^{-1/4}$$

cool on a timescale:

$$t_s \simeq 12 \; \nu_{15}^{-1/2} \; R_{15}^{3/2} \cdot L_{45}^{-3/4} \quad sec$$

The Compton drag of the ambient radiation field limits the maximum Lorentz factor attainable to: $eBc = 4/3 \cdot \sigma_T c \gamma_{max}^2 U_r$, hence

$$\gamma_{max} \simeq 10^8 \; B^{-1/2} \simeq 7 \cdot 10^6 \cdot L_{45}^{-1/4} \cdot R_{15}^{1/2}$$

(Phinney 1983). The ratio of the electron crossing time through

the source, R/c (at a velocity $v \leq c$), to the synchrotron cooling time is given by:

$$t_c/t_s \simeq 2\gamma \cdot L_{45}/R_{15}$$

thus in compact sources the cooling time will be much shorter than the crossing time, even for low Lorentz factor γ.

Replenishment of the electron energy is crucial for such strongly variable sources; that is to say, continuos reacceleration of electrons within the emission region itself must take place. Continuos injection of fresh particles without reacceleration, associated with the short radiative timescales, will pile-up cold electrons. The Thomson optical depth can be estimated as follows. If n is the number density of cool particles, the escape rate ($cm^{-3}\ s^{-1}$) is: nc/R (if, again, $v \simeq c$). The injection rate (monoenergetic injection at γ) is : $U_r c/(R\ \gamma m_e c^2)$. By balancing the injection and the escape rate, the density:

$$n = U_r/(\gamma m_e c^2)$$

and hence the Thomson optical depth can be found:

$$\tau_T \simeq 2 \cdot \gamma^{-1} \cdot L_{45}/R_{15} \quad .$$

If $\tau_T > 1$, photon diffusion enhances the radiation energy density, washes out the rapid time variations and destroys the high linear polarization characteristic of a synchrotron source (the degree of polarization being typically reduced by a factor ~1/2 for each scattering). The density N of the relativistic electrons themselves can be computed as:

$$N\dot{\gamma}m_e c^2 = U_r c/R$$

where $\dot{\gamma}$ is the cooling rate. A "Compton" optical depth: $N\sigma_T R$ can then be defined, yielding:

$$\tau_c \simeq 1/\gamma^2 \leq 1 \quad .$$

This represents the fraction of photons that can be inverse-Compton (IC) scattered by relativistic electrons; hence the IC emissivity is τ_c times the synchrotron emissivity (for more complicated models, see Zdziarski 1986, Ghisellini 1987). The ratio between the Thomson and Compton optical depths is equal to the ratio between the crossing and cooling timescales.

The plasma frequency associated with the cool electron density is:

$$\nu_p \simeq 10^7 \ \nu_{15}^{-1/4} \ L_{45}^{5/8}/R_{15}^{5/4} \quad \text{Hz} \quad .$$

At low frequencies, cold plasma suppresses the beaming effect associated with synchrotron emission (Razin effect) below $\nu_r = \gamma\nu_p$

$$\nu_r \simeq 10^{10} \ \nu_{15} \ L_{45}^{1/4}/R_{15}^{1/2} \quad \text{Hz} \quad .$$

The thermal plasma will depolarize the emitted flux if the Faraday rotation angle of the polarization plane:

$$\Delta\vartheta = e^3 n \ B \ R/(2\pi m_e^2 c^2 \nu^2) \simeq 0.02 \ \nu_{15}^{-5/2} \ L_{45}^{7/4}/R_{15}^{5/2} \quad \text{rad}$$

is greater than ~1 rad.

In the deep potential wells around black holes, the virial mean temperature per proton can reach ~100 Mev. Thermal or non-thermal gamma-ray emission is likely to occur. The active galaxies 3C 273, NGC 151, Cen A, MCG 8-11-11, NGC 1275 are known

gamma-ray sources.

As for the termination of the spectrum in the gamma-ray range, the ratio L/R again decides, determining in fact the optical depth to photon-photon interactions. If gamma-ray photons are emitted with energy $x_1>1$ (in unit of the threshold energy $m_e c^2$), they can collide with X-ray photons x_2 and electron-positron pair production can take place, provide:

$$x_1 \cdot x_2 \geq 1 \quad .$$

Because the cross-section of the process, $\simeq\sigma_T$, peaks at twice the threshold, a source can be optically thick to photon-photon pair production at x if the photon density n_γ at the photon energy 1/x is large enough. The optical depth of a source of radius R with most of the photons at x≃1 is simply:

$$\tau_{\gamma\gamma} \simeq n_\gamma(x\simeq 1)\cdot\sigma_T R = L\sigma_T/(4\pi R m_e c^3) \simeq 2\cdot L_{45}/R_{15}$$

(for a review on pair plasmas see Svensson 1986). In compact and very luminous sources, pair production may play a key role. In addition to suppressing gamma-ray emission from the source, pair creation modifies the spectrum at all lower frequencies, because the energy which would otherwise be emitted in the gamma spectrum, has to be channelled into other wavebands. If copius pair production takes place in the source, a "photosphere" of pairs would scatter the optical continuum, destroying again the high polarization and smearing out the rapid luminosity variations. The pairs in the source do not produce any Faraday rotation.

The optical depth of cool pairs can be derived by balancing the pair production and annihilation rate (Guilbert, Fabian & Rees 1983). In the saturated case (every photon above threshold is

converted into an electron-positron pair), the pair production rate at threshold can be estimated as:

$$\dot{n}_p \simeq 2 n_\gamma (x \simeq 1) c/R \quad .$$

The inverse process, pair annihilation, takes place at a rate:

$$\dot{n}_a \simeq n_+^2 \cdot \sigma_T c$$

where n_+ is the pair density. The pair Thomson optical depth is then:

$$\tau_{T+} \simeq 2 (L_{45}/R_{15})^{1/2} \quad .$$

So far we have assumed the emitting source does not undergo bulk relativistic motion. If this is not the case, the beaming of the radiation in the direction of motion and the Doppler effect will strongly affect the observed luminosity to size ratio:

$$L/R = \delta^5 \cdot (L'/R')$$

where δ is the Doppler factor and the primed quantities are measured in the rest-frame of the source. In this case we are fooled into incorrectly inferring high luminosities and short timescales by the special relativistic consequences of the source motion at a speed ~c in the observer's line of sight. But this will be the subject of the next chapter.

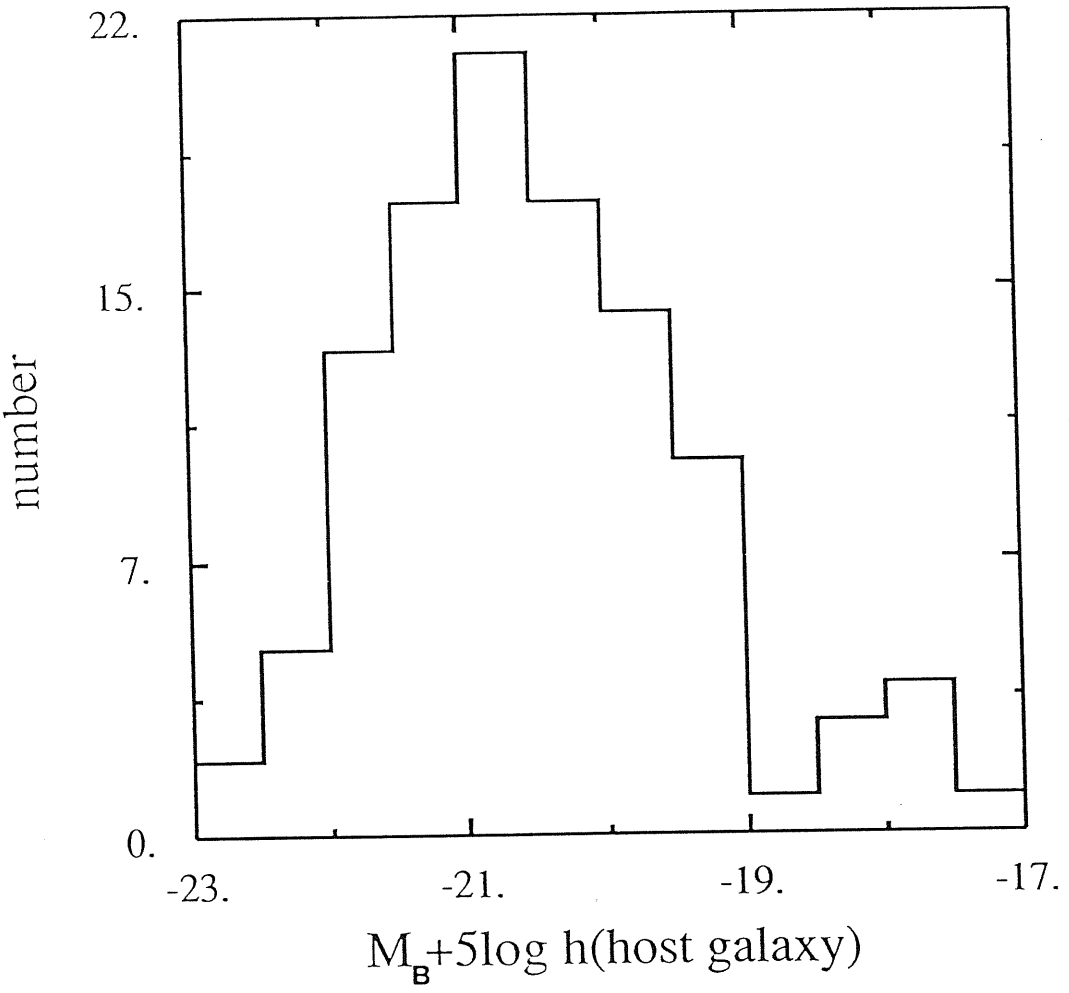

figure 1

Distribution of QSO host galaxy absolute blue magnitudes ($h=1, q_o=0$) from a compilation by Smith et al. (1986). The average magnitude is $M_B=-20.5$, to be compared with $M_B=-19.4$ for a Schechter L_G^* galaxy (see text). The host galaxies of QSOs are generally luminous systems populating the exponential tail of the galaxy luminosity function. The radio-loud host galaxies are more luminous than the radio-quiet hosts, which are more luminous, on average, than Seyfert galaxies. Radio-loud hosts are better fitted by elliptical galaxy model and radio-quiet by disk galaxy model.

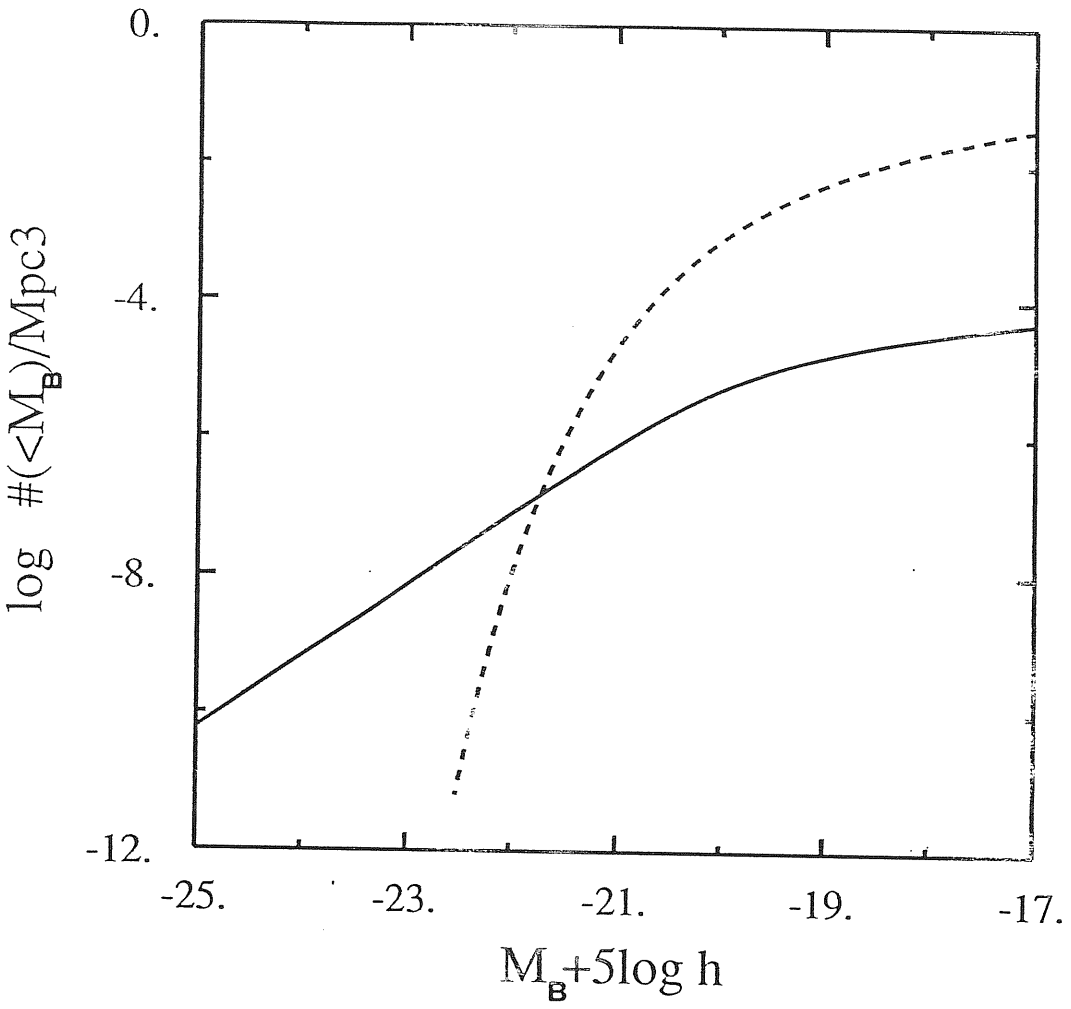

figure 2

Integral luminosity functions ($h=1, q_o=0.5$).

Dashed line: Schechter galaxy LF (from Davis & Huchra 1982). The exponential cut-off corresponds to $M_B^*=-19.4$, *where* $\Psi^*=1.4\cdot10^{-2}Mpc^{-3}$.

Solid line: QSO LF at z=0 (from Marshall 1987). $M_B=-20.3$ *represents the position of the break, where* $\phi^*=1.2\cdot10^{-5}Mpc^{-3}$. *At least 0.1% of all galaxies contains a dead quasar. The z-dependence of the break at* M_B^* *is consistent (Boyle et al. 1987) with a uniform shift towards higher luminosities in the past:* $L(z)=L(z=0)\cdot(1+z)^{3.5}$.

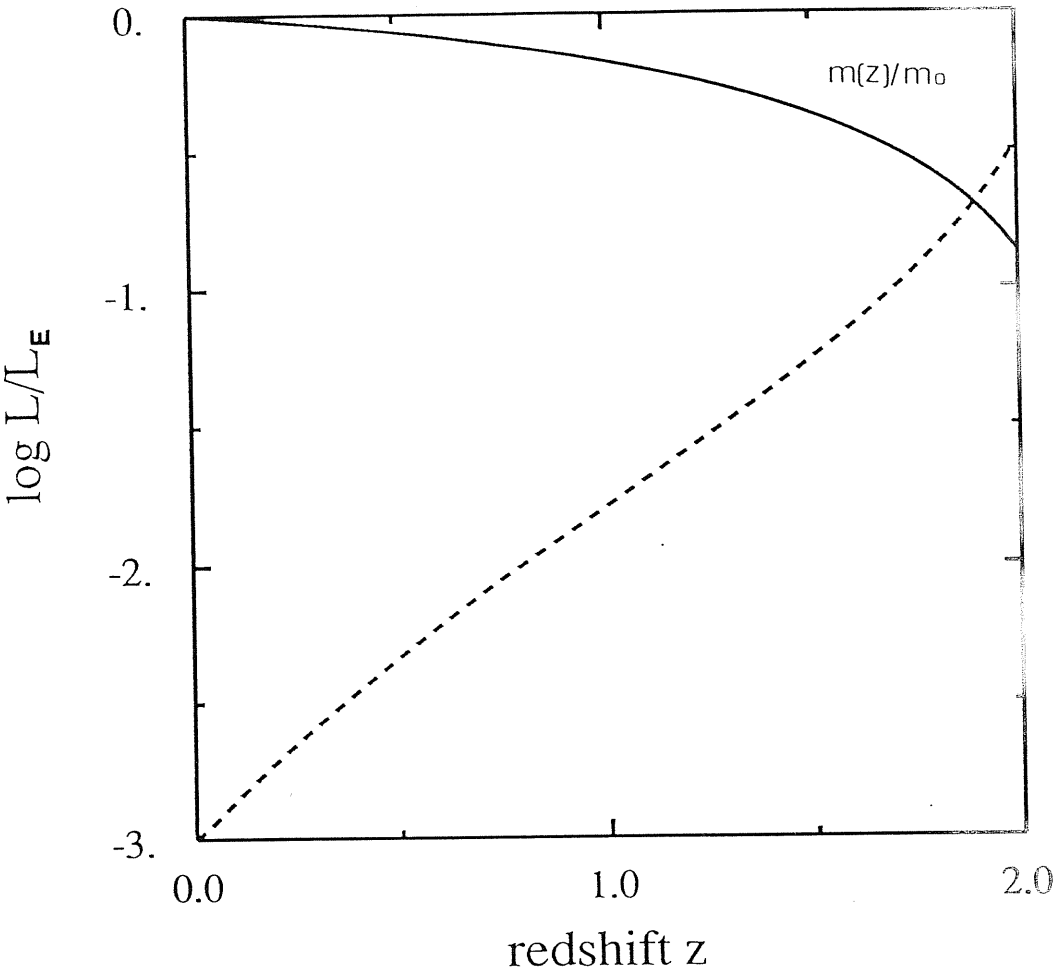

figure 3

Redshift evolution of individual quasar in a PLE model with a 'turn on' at $z_{on}=2.2$.

Solid line: The ratio $m(z)/m_o$ *of the accreted mass to the total mass at z=0,* m_o. *Half of the latter is accumulated in the first* $6 \cdot 10^8$ *yr of the source lifetime.*

Dashed line: the ratio L/L_E *as a function of z. Local QSOs radiates at very sub-Eddington luminosities. The ratio obviously increases with reshift.*

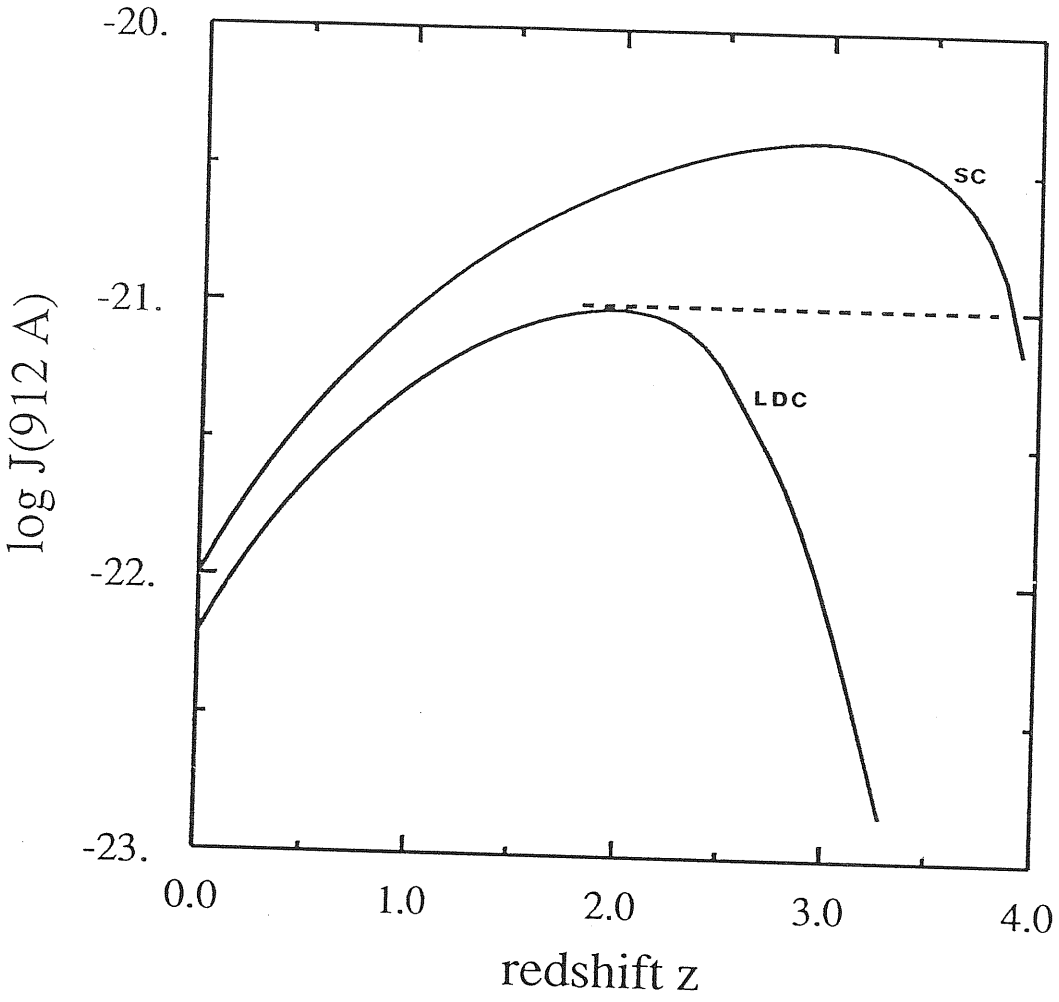

figure 4

Background radiation intensity at the Lyman limit vs redshift. Dashed line: Bajtlik, Duncan & Ostriker (1987) fit to the distribution of absorption lines in the Lyα forest of 1.7≤z≤3.8 QSOs. The value of J_ν is inferred from a local photoionization model of the so-called 'proximity effect' (see text). Solid lines: curves derived from the pure luminosity evolution model described in the text. The curve labeled SC is computed with a sharp, luminosity independent cut-off at z=4 (the 'turn-on' redshift). The curve labeled LDC is computed with a luminosity dependent cut-off at z>2.6.

CHAPTER II : THEORY OF COMPACT SOURCES

II.1) Generalities

In some cases, up to 10^{48} erg s^{-1} are emitted by AGNs without striking evidences for a characteristic photon energy, roughly an equal power being radiated for frequency decades from the far-IR to the hard X-rays. Over wide ranges of photons energies, the spectra of AGNs are well fitted by power-laws of the form $S_\nu \propto \nu^{-\alpha}$. A variety of emission mechanisms do lead to a power-law spectrum as, more in general, does the convolution of a power-law distribution of the properties of the emitting gas (ρ,T) with any emissivity $\epsilon_\nu(\rho,T)$ (see Phinney 1983).

The basic emission mechanism in observed radio sources is incoherent synchrotron radiation, produced by a population of relativistic electrons gyrating in a magnetic field. The sources of radio emission are divided into three regions (see, e.g. Kellerman & Pauliny-Toth 1981, Miley 1980):

- the diffuse, steep-spectrum ($\alpha \simeq 0.7$) radio lobes which may extend up to Mpc away from the parent galaxy or quasar;

- the narrow extended jets, beams of plasma which propagate from the nucleus to the lobes, supplying mass, momentum, energy and magnetic flux;

- the compact, flat-spectrum ($-0.3 \leq \alpha \leq 0.3$) core, characterized by

small angular sizes ~milliarcsecond (1 mas~10^{-2}pc in nearby galaxies), high surface brightness $10^{10} \leq T_b \leq 10^{13}$K, variability on timescales from months to years. Nearly all BL Lacs, QSRs and many radio-galaxies contain compact nuclei. Typical measured polarization in compact sources is only a few percent, exceeding 10% in some sources like BL Lac objects.

One of the most intriguing discoveries concerning compact cores is their frequently elongated jet-like structure (core-jet sources) and, in some cases, the striking collinearity of these elongations with the extended jets (see, for a review, Begelman Blandford & Rees 1984). An important feature of these mas jets is their asymmetry, the radio emission being one-sided. Strong jet misalignments on mas scale are often observed in core-dominated superluminal sources (e.g. 3C 273,3C 345), which may be caused by projection effects, i.e. by viewing a slightly curved jet along a line of sight which is almost parallel to the direction of motion.

The most spectacular feature observed in compact sources is, however, the so-called *superluminal motion*, namely luminous blobs or components are observed to move away from the core with a transverse apparent speed up to 10c h^{-1} (see, e.g. Cohen & Unwin 1984).

Because synchrotron emission is known to occur at radio-frequencies, the most economic way to interpret the overall power-law spectrum is thus in term of synchrotron radiation from relativistic electrons. However, due to the high compactness of these sources (inferred from variability timescales or directly observed with VLBI techniques), inverse-Compton (IC) scattering of the ambient photon field is found to be a primary cooling mechanism.

The synchrotron self-Compton (SSC) model, in which

ultra-relativistic electrons produce radio to optical synchrotron photons and scatter them to X-ray frequencies by the IC mechanism, deserves the appellation of "standard" model for the continuum spectrum (Jones,O'Dell & Stein 1974).

Although non-thermal processes do play a role in all AGNs, I will discuss here mainly sources like BL Lac objects, or OVV quasars, which are compact radio sources and exhibit overall characteristics that are clearly explained by non-thermal radiation mechanisms.

II.2) The synchrotron self-Compton model

A relativistic electron of energy $\gamma m_e c^2$ spiraling in a magnetic field B radiates a total power:

$$\dot{\gamma}_s = -(4/3)\beta^2\gamma^2\sigma_T/(m_e c)\cdot U_B \qquad (2.1)$$

where σ_T is the Thomson cross-section, U_B is the magnetic energy density and we averaged over an isotropic distribution. The mean photon energy (in units of $m_e c^2$) is:

$$x_s = (4/3)\gamma^2 x_B \qquad (2.2)$$

where $x_B = B/4.4\cdot 10^{13}$ G.

Synchrotron photons are scattered by free electrons. In the electron rest frame k' the incoming photon energy is:

$$x'_s = x_s\gamma\cdot(1-\beta\cos\vartheta) \qquad (2.3)$$

where ϑ is the angle between the photon and electron momenta in the lab frame k; x'_s then varies from $x'_s = x_s/(2\gamma)$ for $\vartheta = 0^o$ to $x'_s \simeq 2\gamma x_s$ for head-on collisions $\vartheta = \pi$. In k' the corresponding angle

ϑ' is given by:

$$tg\vartheta'=\sin\vartheta/\gamma(\cos\vartheta-\beta) \quad . \tag{2.4}$$

When $\gamma\gg1$ and $\vartheta=\pi/2$, then: $tg\vartheta'\simeq\vartheta'\simeq-1/\gamma$, thus in k' photons are concentrated in a narrow cone in the forward direction. This is called the *beaming effect*. The energy x'_c in k' after scattering is (Blumenthal & Gould 1970):

$$x'_c=x'_s/(1+x'_s\cdot(1-\cos\vartheta'_c)) \tag{2.5}$$

where ϑ'_c is the angle between the incident and scattered photon momenta. In the lab system k this energy is:

$$x_c=x'_c\gamma\cdot(1-\beta\cos\vartheta'_c) \quad . \tag{2.6}$$

The condition for Thomson scattering is: $x'_s\ll1$ (the Thomson limit condition in the case of synchrotron radiation is, by analogy: $B\ll4.4\cdot10^{13}/\gamma$ G) and so by eq.(2.5) $x'_c\simeq x'_s$. The maximum energy of the scattered photon is:

$$x_c\simeq2\gamma x'_c\simeq4\gamma^2x_s \tag{2.7}$$

this process therefore converting a low-energy photon x_s to a high energy one by the large boosting factor $4\gamma^2$.

The total IC energy loss in the Thomson limit for an isotropic photon gas is:

$$\dot{\gamma}_c=-(4/3)\beta^2\gamma^2\sigma_T/(m_ec)\cdot U_r \tag{2.8}$$

U_r being the initial radiation energy density. The mean energy of the scattered photon is :

$$x_c=(4/3)\gamma^2x_s \quad . \tag{2.9}$$

When $x'_s\geq1$, two effects act to reduce the effectiveness of the process:1) the scattering will no longer be elastic ($x'_c<x'_s$) because of electron recoil;2) the scattering probability is reduced due to the decline of the exact Compton cross-section

(Klein-Nishina formula). Energy conservation limits the maximum photon energy: $x_c \leq \gamma$ so that, from eq.(2.9) we get: $x_s < 3/(4\gamma)$. In other words not all the radiation energy density is available for scattering.

In compact sources, the ratio of the crossing time (R/c) to the electron cooling time ($\gamma/\dot{\gamma}$) at radius R is: $\gamma \cdot L_{45}/R_{15}$, much greater than unity. If electron are continuosly reaccelerated (after a complete cooling) with a source function $Q(\gamma)$ ($cm^{-3}s^{-1}$), they will reach an equilibrium distribution $N(\gamma)$ (in a cooling time) given by:

$$N(\gamma) = -\dot{\gamma}^{-1} \cdot \int_{\gamma}^{\gamma_{max}} Q(\gamma')d\gamma' \quad . \tag{2.10}$$

Any power-law injection rate: $Q(\gamma) \propto \gamma^{-s}$, with $s \leq 1$ (or a delta-function source term) yields: $N(\gamma) \simeq K\gamma^{-2}$. A steeper injection slope $s>1$ yields: $N(\gamma) \simeq K\gamma^{-(s+1)}$. In the delta-function $\delta(x-x_s)$ approximation, the production rate ($cm^{-3}s^{-1}$) of synchrotron photons can be written as (Zdziarski 1986):

$$\dot{n}_s(x_s) = c/(8a_o) \cdot N(\gamma)/\gamma \propto x_s^{-\alpha-1} \tag{2.11}$$

where a_o is the Bohr radius $a_o = 5.3 \cdot 10^{-9}$cm and α is the spectral index: $\alpha = s/2$. The electron energy is concentrated at the high energy end for $\alpha < 0.5$ and at the low energy end for $\alpha > 0.5$. Note, however, that optically thin synchrotron spectra with $\alpha < 0.5$ cannot be produced steadily at frequencies where the cooling time is much shorter than the acceleration time.

The first inverse-Compton photo-production rate is:

$$\dot{n}_c(x_c) = 0.5\sigma_T c/x_c \cdot \int n_s(x_s)\, N(\gamma)\gamma \, dx_s \tag{2.12}$$

where $n_s(x_s)$ is the synchrotron photon spectral density (in a homogeneous spherical source it is: $n_s(x_s) = (3/4) \cdot (R/c) \cdot \dot{n}_s(x_s)$,

Zdziarski 1986). Equation (2.12) yields: $\dot{n}_c(x_c) \propto x_c^{-\alpha-1}$, the synchrotron and IC flux densities being then characterized by the same spectral slope α.

Electrons of Lorentz factor γ_t self-absorb their own emitted photons x_t when the brightess temperature $T_b \equiv c^2 I_\nu/(2k\nu^2)$ is:

$$T_b \simeq \gamma_t m_e c^2/k \simeq 5 \cdot 10^9 \cdot \gamma_t \quad K \tag{2.13}$$

and:

$$\gamma_t \simeq 100 \cdot (\tau_c/B)^{1/8} \quad . \tag{2.14}$$

Here a spectral slope α=1.5 was assumed; $\tau_c = K\sigma_T R$ is a Compton optical depth $\tau_c \leq 1$, which represents the fraction of photons that are scattered by the relativistic electrons.The emissivity observed from an optically thick synchrotron source then satisfies: $\epsilon_\nu \propto \nu T_b \propto \nu^{2.5}$.

From eq. (2.1),(2.8) we derive: $\dot{\gamma}_c/\dot{\gamma}_s = U_r/U_B$. If the energy density in synchrotron photons U_r exceeds the magnetic energy density U_B, the 1^{st} IC losses - $\propto \gamma^4 U_B$ - exceed the synchrotron losses. Electrons begin to multiple scatter their own radiation -2^{nd} IC losses $\propto \gamma^6 U_B$ - and the process quickly runs away; however, no more than a few IC orders can take place in the Thomson regime, and the Klein-Nishina dimming inhibit further upscattering (Rees 1967).

When the IC is the dominant cooling mechanism, the Klein-Nishina cut-off may affect the cooling rate, which may be approximated as:

$$\dot{\gamma}_c = -(4/3)\sigma_T/(m_e c) \cdot \int^{3/4\gamma} U_r(x)dx \tag{2.15}$$

In the case of a flat radiation spectrum $U_r(x) \propto x^{-\alpha}$, with $\alpha<1$, we derive $\dot{\gamma}_c \propto \gamma^{1+\alpha}$, so the cooling is reduced and the steady electron distribution $N(\gamma)$ (and consequently the emitted photon spectrum)

is flatter than that derived for complete Thomson cooling (Rees 1967).

From eq. (2.13) and (2.14), the magnetic field B and the relativistic electron density K as function of the observable quantities x_t, $S_\nu(\nu_t)$ and of the angular size of the source ϑ_d, can be derived, although the different geometries (slab or sphere) and definition of turnover frequency employed by various authors have led to a considerable set of different numerical factors (see Urry (1984) for a discussion of this problem).

It must be stressed, however, that in no case a synchrotron self-absorption turnover with flux density $S_\nu \propto \nu^{-2.5}$ (for $\nu<\nu_t$) has been unambiguosly observed. Rather, the spectra in the radio band are *flat* ($-0.3\leq\alpha\leq0.3$), indicating a superposition of partially opaque zones whose luminosities and self-absorption frequencies *cosmic conspire* to produce a flat overall spectrum. Multifrequency VLBI observations (see, e.g. Unwin et al. 1983, 1985) strongly support this explanation.

Consider a (conical) free-jet or a spherical source in which the relativistic electron density K and the magnetic field B are power-law functions of a radial coordinate r: $K \propto r^{-n}$ and $B \propto r^{-m}$ and convolve these distributions with the self-absorbed synchrotron source function $I_\nu \propto \gamma_t \nu_t^2$, assuming an optically thin spectral index $\alpha=0.5$. The observed flux density is thus:

$$S_\nu \propto \gamma_t \nu_t^2 \cdot r^2 \propto \nu_t^{-\lambda} \qquad (2.16)$$

where $\lambda=-(17-5n-7m)/(2-2n-4m)$. For n=2, m=1, we derive $\lambda=0$. On the other hand, for a flat spectrum, $\nu_t \propto 1/r$, so that the flux at higher frequencies comes from deeper regions of the source. For n=m=2, which corresponds to conservation of magnetic flux and number of particles, we derive $\lambda=-0.7$.

In the inner emission regions, where the jet is collimated by pressure gradients, a parabolic geometry must be considered: $r=aR^{\epsilon}$, with $\epsilon<1$. Here R is a coordinate along the symmetry axis and r is in the perpendicular direction. In this case we derive $\lambda=-(11+6\epsilon-5\epsilon n-7\epsilon m)/(2-2\epsilon n-4\epsilon m)$, which is always steeper than the optically thin index α.

In fact, a parabolic geometry cannot provide a flat optically thick integrated spectrum because at low frequencies the emission is totally dominated by the outer region. Flat radio spectra can naturally be produced by conical geometries (for more complicated models see Marscher 1980, Konigl 1981, Ghisellini, Maraschi & Treves 1985).

Above $\sim 10^{12}$Hz the radio spectra of blazars invariably steepen to a characteristic $S_{\nu} \propto \nu^{-\alpha}$ ($\alpha \simeq 0.75 \div 1$) inner-core spectrum (a turnover at frequencies $\simeq 10^{13}$Hz, interpreted as a synchrotron self-absorption cut-off, has been recently observed in Seyfert galaxies by Edelson & Malkan 1986). How compact must be the core in the framework of SSC models can be estimated by deriving some fiducial numbers, in the assumption that the central engine is powered by a black hole and that all the luminosity is ultimately powered by accretion at the Eddington limit.

In spherical geometry, the radiation energy density U_E which corresponds to the Eddington luminosity L_E is:

$$U_E=(9/4)\ L_E/(4\pi R^2 c)\simeq 8.5\cdot 10^7\ M_8^{-1} r^{-2}\ \text{erg cm}^{-3} \qquad (2.17)$$

where M_8 is the mass in units of $10^8 M_{\odot}$ and r is a distance in unit of the Schwarzschild radius. A characteristic *equipartition* magnetic field strength is:

$$B\simeq 4.6\cdot 10^4\ M_8^{-1/2} r^{-1}\ \text{G} \qquad (2.18)$$

to which correspond a cyclotron frequency:

$$\nu_B \simeq 1.3 \cdot 10^{11} \quad M_8^{-1/2} r^{-1} \quad \text{Hz} \tag{2.19}$$

If relativistic electrons with a steep energy distribution: $N(\gamma)=K\gamma^{-p}$ ($p>3$, hence $\alpha>1$) radiate a luminosity L_E, neglecting the power emitted in the self-absorbed part of the synchrotron spectrum, we have:

$$L_E=(4/3)\pi R^3 m_e c^2 \cdot \int_{\gamma_t} N(\gamma)\dot{\gamma}\, d\gamma \tag{2.20}$$

which yields: $\tau_c=(p-3)\cdot\gamma_t^{p-3}$. If we assume $p=4$, then from eq. (2.14),(2.18)and (2.20) we derive:

$$\gamma_t \simeq 44 \quad M_8^{1/14} \quad r^{1/7} \tag{2.21}$$

and:

$$\nu_t=(4/3)\cdot\gamma_t^2\nu_B \simeq 3.4 \cdot 10^{14} \quad M_8^{-5/14} \quad r^{-5/7} \quad \text{Hz} \tag{2.22}$$

which is Compton scattered to a fiducial frequency:

$$\nu_c=(4/3)\gamma_t^2\nu_t \simeq 10^{18} \quad M_8^{-3/14} \quad r^{-3/7} \quad \text{Hz} \quad . \tag{2.23}$$

Now, if we impose a characteristic turnover frequency at $\nu_t=10^{12}$Hz, from eq. (2.22) we get: $r\simeq 3500\ r_G \simeq 10^{17}\ M_8$ cm (corresponding to a characteristic variability timescale $\simeq$1month), $B_E \simeq 13$ G, $\gamma_t \simeq 140$, $\nu_c \simeq 3\cdot 10^{16}$Hz.

So the very simple model considered above predicts the radio emission at the turnover frequency 10^{12}Hz to be associated with a region $\sim 10^{17}$cm in size and with a magnetic field ~10 G. In this "box", relativistic electrons with typical Lorentz factors $\simeq$150 upscatter their own synchrotron photons at UV frequencies. The brightness temperature of the box is $T_b \simeq 10^{12}$K, a limiting value which actually corresponds to the assumption $U_r = U_B$. When $T_b \gg 10^{12}$K, or equivalently $U_r \gg U_B$, the IC runaway begins and most of the

luminosity is expected at high X,gamma-ray energies (Hoyle, Burbidge and Sargent 1966).

Some bright and rapidly variable sources, mostly BL Lacs and OVV quasars, appear to exceed this limiting value by orders of magnitude, their observed X-ray fluxes, however, being orders of magnitudes *below* that predicted. In the next section we will see that the likely explanation for this is that the brightness temperature does not actually exceed 10^{12}K in the *fluid rest-frame*.

II.3) Relativistic beaming

The first suggestion that *bulk relativistic motion* might be important in compact sources was made by Rees (1966) as a possible solution for the so called Compton-catastrophe. In the modern "beam" version (Blandford & Rees 1974, 1978, Blandford & Konigl 1979), a pair of narrow relativistic jets with bulk Lorentz factor Γ squirt out of the central nucleus in opposite directions, at an angle ϑ with the line of sight. The arrival time t of photons of frequency ν is related to the proper time t' of emission with frequency ν' by the Doppler formula:

$$t/t'=\nu'/\nu=\delta \qquad (2.24)$$

where δ is the Doppler factor: $\delta=(\Gamma\cdot(1-\beta\cos\vartheta))^{-1}$. The apparent observed transverse velocity is given by:

$$\beta_a=\beta\sin\vartheta/(1-\beta\cos\vartheta) \qquad (2.25)$$

which has a maximum at $\sin\vartheta=1/\Gamma$ equals to $\Gamma\beta$ (which exceeds unity when $\beta>1/\sqrt{2}$). The source then undergoes superluminal motion.

When $\sin\vartheta=1/\Gamma$, from the aberration formula (eq.2.4) we have: $\vartheta'=\pi/2$, so in the rest frame of the source these photons are emitted perpendicular to the direction of motion. If the emitting source is a plane surface with normal along the direction of motion, it will appear *edge-on*, actually rotated, to the observer (Terrel 1959, Phinney 1985).

Because I_ν/ν^3 is proportional to the photon phase-space density, which is a Lorentz invariant, we have:

$$I_\nu(\delta\nu')=\delta^3 I'_\nu(\nu') \tag{2.26}$$

Useful relations are also (Rybicki & Lightman 1979):

$$d\Omega=\delta^{-2}d\Omega';\ dV=\delta\,dV';\ j_\nu(\delta\nu')=\delta^2 j'_\nu(\nu') \tag{2.27}$$

where j_ν is the emissivity (erg $cm^{-3}Hz^{-1}sr^{-1}$). In the observer frame the radiation is no longer isotropic but is beamed along the direction of motion within an angle of half-width $\sim 1/\Gamma$. The observed flux density from an optically thin source at large distance D is:

$$S_\nu(\nu)=\int I_\nu d\Omega=D^{-2}\int j_\nu dV=D^{-2}\delta^3\int j'_\nu(\nu')dV'=D^{-2}\delta^{2+\alpha}\int j'_\nu(\nu)dV=\delta^{2+\alpha}S'_\nu(\nu) \tag{2.28}$$

if $j_\nu\propto\nu^{-\alpha}$. This is the correct expression in the case of a steady flow, which occupies a well defined volume in the observer frame, volume which is not subject to Lorentz contraction (Lind & Blandford 1986). If the emission is coming from a moving optically thin spherical blob, the exponent $(3+\alpha)$ must instead be used. Hereafter the latter exponent will be adopted.

When the brightness temperature is estimated from the variability timescale and the Rayleigh-Jeans law, it varies like $T_b(\nu)=\delta^{3+\alpha}T'_b(\nu)$. This dependence provides a natural interpretation for the relative "absence" of inverse-Compton

scattered X-rays in sources where the observed brightness temperature exceeds 10^{12}K.

Consider, e.g. the nearest FRI radio galaxy, Centaurus A (D≃ 5Mpc). Its radio morphology is characterized by two sets of radio-lobes centered on the nuclear-component which has an angular size < 1mas. At 90 GHz Cen A shows a variability timescale of the order of months, with a radio flux ~10 Jy and spectral index $\alpha \simeq 0.5$ (Beall et al. 1978). The brightness temperature is $T_b \simeq 10^9$K. The same source, relativistically boosted with a Lorentz factor $\Gamma=5$, aimed nearly at us ($\vartheta=0^\circ$), would have a variability timescale of the order of few days, a radio flux at 90 GHz ≃3000 Jy and a correspondent brightness temperature $T_b \geq 10^{12}$K and ,placed at z≃0.1, may be called a BL Lac object!. In the beam model, the flux densities for the approaching and receding jets would be in the ratio $1:10^6$. The counterjet would therefore be unobservable ("Doppler favouritism" explanation for one-sided jets).

II.4) Beaming in blazars

Relativistic beaming is the most economic way of explaining the otherwise disparate phenomena of superluminal motion, rapid variability and one-sided jets. However, a relativistic expansion of the source was originally suggested to explain the paucity of IC scattered X-ray radiation observed in many sorces, orders of magnitudes below the flux predicted by the naive SSC theory. If the radiation from an isotropic emitting source is beamed toward the observer, the source appears more luminous than in its rest-frame. The inferred radiation density in the source is then

an overestimate of the true radiation density, and therefore the computed Compton flux too large.

In practice, the argument is turned around and the X-ray observations are used to derive a lower limit to the Doppler factor δ .The fact that the synchrotron spectrum is self-absorbed allows us to calculate the magnetic field. In a homogenous source, the observable parameters are: the synchrotron turn-over frequency ν_t, the peak radio flux density S_t, the optically thin spectral index α and the angular diameter of the source ϑ_d at ν_t, either measured from VLBI techniques or inferred from flux variability (see, e.g. Jones, O'Dell & Stein 1974, Gould 1979). With all these observable given, one can predict the first-order Compton flux given by:

$$S_c \propto S_t^{2(2+\alpha)} \cdot \nu_t^{-(5+3\alpha)} \cdot \vartheta_d^{-2(3+2\alpha)} \cdot \nu_c^{-\alpha} \quad . \qquad (2.29)$$

The sensitivity of the last equation to a change in various parameters is enormous: for α=0.5, the IC flux $\propto \vartheta_d^{-8} \cdot \nu_t^{-6.5}$!

If the source is moving relativistically, the emitted radiation is beamed in the velocity direction due to angle aberration; the observed luminosity might be considerably brighter or dimmer than the luminosity emitted in the rest-frame, depending on the direction of motion with respect to the observer. For angles smaller than

$$\vartheta_c = \sin^{-1}(2/(\Gamma+1))^{1/2} \qquad (2.30)$$

δ is greater than unity and correspondingly the source appears brighter than in its rest-frame.

From the constraint that the predicted IC X-ray radiation S_c (assuming isotropic emission) should not exceed the observed X-ray flux S_x, a lower limit on the Doppler factor of the source can be

obtained, being $S_c/S_x \propto \delta^{2(2+\alpha)}$. To estimate δ for individual sources, beside ν_t(GHz), S_t(Jy), α and ϑ_d(mas), we need to know the high energy synchrotron cut-off ν_b, the redshift z of the source and the observed X-ray flux density S_x(Jy) at the frequency ν_x(KeV). From Gould (1979), we can write:

$$\delta = f(\alpha) \cdot S_x^{-a}(\nu_x) \cdot \nu_x^{-b} \cdot S_t \cdot \nu_t^{-c} \cdot \vartheta_d^{-d} \cdot \ln^e(\nu_b/\nu_t) \cdot (1+z) \qquad (2.31)$$

where $a=1/(4+2\alpha)$, $b=\alpha/(4+2\alpha)$, $c=(5+3\alpha)/(4+2\alpha)$, $d=(3+2\alpha)/(2+\alpha)$, $e=1/(2+\alpha)$, and $f(\alpha)$ takes the values of 0.17, 0.18, 0.20, and 0.22 for α=0.25, 0.5, 0.75 and 1, respectively (Urry 1984).

Relativistic beaming of radiation is generally invoked to explain the extreme properties of blazars (Blandford & Rees 1978). Under this common denomination are grouped together two classes of objects: the BL Lacs and the High Polarization Quasars (HPQs) or OVVs. The clearest distinction between them is the presence, in HPQs, of broad emission lines. When available, redshifts of BL Lac objects indicate a smaller luminosity than HPQs.

In the beaming scenario, the core emission is strongly anisotropic while, owing to its diffuse morphology and large linear scale, off-nuclear emission is likely to be isotropic. Thus the ratio of the core to extended radio emission is also a possible indicator of viewing aspect or beaming intensity (Antonucci & Ulvestad 1985). Recently, Maraschi et al. (1986) have suggested, on the basis of the observed luminosity distributions, that unbeamed or misaligned objects may be present in the BL Lac population. They would be distinguished by the weakness of their radio emission relative to the optical or X-ray one, and should be discovered by X-ray searches.

We have attempted to directly test the beaming hypothesis in blazars (Madau, Ghisellini & Persic, 1987): we applied the

simplest homogeneous SSC model to derive the factors δ in a sample of 41 objects for which radio VLBI sizes and X-ray fluxes are available in the literature. The application of eq. (2.31) requires some care in the choice of the input parameters. Only angular source diameters measured by VLBI techniques have been used. Estimates of δ based on variability timescales, besides being distance-dependent, are misleading; in fact, due to inhomogeneity in the sources, the region responsible for flux variations may not be coincident with the radio emission region which is relevant here.

It is also important to emphasize that our sample is neither complete in any statistical sense, since no complete survey of blazar exists, nor homogeneous. Neverthless it is a large subset of all the known blazars (Moore & Stockman 1984, Ledden and O'Dell 1985). Table I lists the objects under study. When no redshift was available, we have adopted an average value of z=0.4 (Ghisellini et al. 1986, Madejski & Schwartz 1983). We have considered the observed steepening of the blazar spectra between IR and optical frequencies (Cruz-Gonzales & Huchra 1984) as an indication of the synchrotron high-energy cut-off and consequently adopted $\nu_b=10^{14}$Hz. Note that the derived value of δ is very weakly dependent on ν_b (eq. 2.31).

The flat radio spectra observed in blazar (up to ~300 GHz, Gear et al. 1985) are an indication of inhomogeneous synchrotron sources, where the observed angular size ϑ_d is a function of wavelength (see eq. 2.16). In this case the VLBI frequency corresponds to the self-absorption frequency of the observed component. Hence the Doppler factor δ must be computed at the VLBI wavelength. Inhomogenous models are much more realistic than a homogeneous sphere model, but unfortunately have many parameters

that cannot be simply or uniquely constrained. However we have checked that for reasonable values of these parameters, the derived values of δ are in good agreement with those computed in the homogeneous model we adopt here for simplicity.

The biggest uncertainty in these estimates comes from the angular size, since it is hard to determine accurately and it is raised to the largest exponent in eq. (2.31). We assumed a uniform spectral index α=0.75 for the optically thin emission. We have repeated the calculations for α=0.5 and α=1 and verified that the computed values change by no more than 30%.

It is also important to emphasize that derived values of δ lower than unity do not necessarily mean misaligned beaming of radiation, since other regions of the source can contribute to the X-ray flux by SSC or other emission mechanisms. On the other hand if the observed VLBI component is responsible for only 1% of the observed X-ray flux, the derived value of δ correspondingly increases only by a factor ~ 2.

Figure 5 show the Doppler factor distributions for BL Lac objects and HPQs. In the former case, the values of δ range from $\sim 10^{-2}$ to ~15; half of the sources have $\delta<1$. On the other hand, all HPQs are characterized by $\delta>1$, the corresponding Γ values being in the range 5-10. Such values are consistent with estimates independently derived, e.g. from models of superluminal motion (Cohen & Unwin 1984). Known superluminal sources self-consistently cluster at high δ factors.

The low δ-tail of the BL Lac distribution is mostly contributed by non radio-selected or low-redshift objects, which are of lower radio power. These sources are also characterized by a low ratio of the core to extended radio emission (the core dominance parameter) and show a tendency for a preferred optical

polarization angle (Wardle, Moore & Angel 1984). On the contrary, high δ BL Lacs are more core-dominated sources and show a wider range of polarization angle orientations.

In HPQs the highly polarized, anisotropic continuum is mixed in with isotropic emission (steady, low-polarized continuum, "blue-bump" and emission lines, see e.g. Malkan & Moore 1986). In BL Lac objects, instead, the polarized component totally dominates the observed flux. On the other hand, the δ-distributions in fig.5 indicates, on average, a larger Doppler boosting for HPQs than for BL Lacs. Although this is stricly valid only for radio emission, it is reasonable to expect, by continuity arguments, the plotted distributions to be indicative of the boosting at optical frequencies, as well. That is, one expects the polarized optical continuum to be more relativistically enhanced in HPQs than in BL Lac objects.

If this is the case, the lack of strong emission lines in BL Lacs cannot be attributed to pure geometrical effects. In this scenario, as the angle of observation decreases, the contribution of the beamed polarized component increase relative to the isotropic unpolarized one. Hence the distribution in line-to-continuum ratios in blazars would reflect their orientation with respect to the line of sight: BL Lacs would represent the extreme case, in which the Doppler boost is so large that the emission lines are washed out by the beamed continuum.

However, we find lower values of δ in objects with weak lines which probably suggests that orientation effects are not the primary cause which distinguishes weak-emission line from strong-emission line blazars and that the emission lines are intrinsically weak in BL Lac objects. Their δ-distribution may actually be bimodal, with high-δ high-luminosity BL Lacs being

intrinsically strong-emission line quasar-like objects, and with low-δ faint sources being members of a different lineless population (maybe FRI radio-galaxies, see next section).

HPQs, on the contrary, may be identified as blazars only when observed nearly face-on, the isotropic, broad-emission line and unpolarized component being intrinsically so strong than the polarized "blazar" continuum is observable only when highly boosted. As a corollary, the optical luminosity in the beam, since it does not swamp the emission lines even when directed towards us, is only a small fraction of the quasar' energy budget when Doppler enhancement is accounted for.

II.5) Unified pictures and beaming statistics

The essence of all beaming theories involves the identification of the unbeamed parent population. Since the jets from an ensemble of sources should be randomly oriented on the sky, it follows that our jet-dominated (e.g. BL Lacs) beamed objects must be a subset of some larger class of non jet-dominated objects (for a review see Peacock 1987).

Consider an ensamble of sources comprised of a pair of relativistic jets, all with the same Lorentz factor Γ, plus a stationary, isotropic component, the intrinsic jet luminosity being some fraction f of the isotropic flux I (Urry & Shafer 1984). To make life simpler, we will neglect the radiation emitted from the receding jet. The total flux observed is:

$$L(\vartheta)=(1+f\delta^{p})\cdot I \qquad (2.32)$$

where $f\delta^p \cdot I$ is the jet-component boosted by a factor δ^p. We will adopt here $p=(2+\alpha)$. A source will then appear as "beamed" when the anisotropic flux $f\delta^p \cdot I$ exceeds the isotropic one. This implies $\delta \geq (1/f)^{1/p}$ or, for a given Γ, a critical angle with the line of sight of:

$$\sin\vartheta_c \leq \left[(2\Gamma f^{1/p} - f^{2/p} - 1)/(\Gamma^2 - 1)\right]^{1/2} \qquad (2.33)$$

which reduces to (2.30) for f=1. For example, if $\Gamma=5$, a source will appear as jet-dominated within a cone of half-opening angle $\vartheta_c \simeq 35^\circ$(f=1), 20°(f=0.1), 9°(f=0.01).

The ratio of (one) jet to isotropic luminosity, $R(\vartheta)=f\delta^p$, is a minimum at $\vartheta=90^\circ$, $R_T=f/\Gamma^p$, and a maximum at $\vartheta=0^\circ$, $R_m=f(2\Gamma)^p$. The spread in the R distribution, or amplification parameter $A=R_m/R_T=2^p\Gamma^{2p}$, can be used to put constraints on the Lorentz factor Γ.

The probability that a jet will be aligned to within an angle ϑ of the line of sight is simply $(1-\cos\vartheta)$. The probability distribution in δ is easily derived as: $P(\delta)=(\beta\Gamma\delta^2)^{-1}$. Given I, the fraction of sources with observed flux $L(\vartheta)$ is:

$$P(L,I)=1/(\beta\Gamma p)\cdot f^{1/p}\cdot I^{-1}\cdot\left[L/I - 1\right]^{-(p+1)/p} \qquad (2.34)$$

for $I\cdot(1+f/\Gamma^p) \leq L \leq I\cdot(1+f(2\Gamma)^p)$. The effect of beaming is then to redistribute sources, with an intrinsic luminosity $(1+f)\cdot I$, over a wider range of apparent luminosities, corresponding -at a given Γ- to the entire range of viewing angles.

For $\Gamma \gg 1$, is $P(>L) \propto L^{-1/(2+\alpha)}$. By assuming such a radio flux-density distribution, Scheuer & Readhead (1979) suggested the radio-quiet QSOs to be the parent unbeamed population of compact radio quasars. Detailed observations of compact radio-sources have revealed, however, the presence of steep-spectrum extended radio

haloes most unlikely to be beamed; the unbeamed counterparts of compact quasars would still be strong radio-sources, much more luminous in the radio than the typical radio-quiet QSOs.

In the general case we must allow for a distribution of intrinsic luminosities $\phi(l)$. The observed space density of sources with apparent luminosity L will be:

$$\Phi(L)=\int_{l_1}^{l_2} \phi(l)\cdot P(L,l)\ dl \qquad . \qquad (2.35)$$

Consider, for simplicity, a luminosity function with a single power-law form $\phi(l)=\phi_o l^{-\beta}$, for $l_1 \leq l \leq l_2$. In the case of a broken power-law which flattens at low luminosities (see I.2), l_1 can be considered as the luminosity at the break. Let us also neglect, for the moment, the isotropic component. The limits of integration in eq. (2.35) do depend on the value of L at which it is being evaluated. For $L<l_1\cdot(2\Gamma)^p$, the apparent LF is:

$$\Phi(L)=\left[\phi_o l_1^{-c}\cdot(cp\beta\Gamma)^{-1}\right]\cdot L^{-(p+1)/p} \qquad (2.36)$$

where $c=\beta-1-1/p$. It has the same slope of the probability distribution in eq. (2.34), and the observed sources are predominantly those with $l=l_1$ spread over the full range of Doppler factors. For $L>l_1\cdot(2\Gamma)^p$, the apparent LF

$$\Phi(L)=\left[\phi_o\cdot(2\Gamma)^{pc}\cdot(cp\beta\Gamma)^{-1}\right]\cdot L^{-\beta} \qquad (2.37)$$

has the same slope of the parent LF (although the normalization is increased by a factor $\simeq\Gamma^{(2+\alpha)(\beta-1)-2}$), and the observed sources are mainly the extreme beamed ones, seen at angles $\vartheta\leq\vartheta_c$). The beamed LF will thus be a broken power-law. A broken power-law with the same slopes also results from the numerical integration of eq. (2.35) when the isotropic component is taken into account (see figure 6).

Over a range in luminosity, which is narrower for smaller values of f, the LF of beamed objects will be much flatter than the typical parent population LF: from eq. (2.36), with α=0, we have: $\Phi(L)\propto L^{-1.5}$, which must be compared, e.g., with the slope $\beta\simeq 2.6$ of the radio LF of steep-spectrum quasars.

The total fraction of objects which are jet-dominated ($f\delta^p>1$) sources is: $P_{jd}=(1-\cos\vartheta_c)$ which, for $\Gamma\gg 1$, is:

$$P_{jd}\simeq f^{1/p}/\Gamma=R_T^{1/p} \quad . \tag{2.38}$$

However, a sample of objects selected above a flux density I_o will favour Doppler-boosted bright sources, and so induce an excess of nearly face-on objects.

A modification of the Scheuer & Readhead unified scheme is due to Orr & Browne (1982), who suggested compact flat-spectrum quasars to be steep-spectrum quasars seen end-on. They used this idea to successfully predict the source counts for flat-spectrum sources, given those for steep spectrum ones. Radio data are broadly consistent with this scheme (Antonucci & Ulvestad 1985). The two radio (differential) LFs do have, in fact, the same slope (~2.6) for luminosities $>10^{32}$ erg $s^{-1}Hz^{-1}sr^{-1}$; however, the flat-spectrum LF does not flatten at lower luminosities as predicted (see, e.g. Phinney 1985). The spread in R is $\geq$2000:1, which suggests (for $\alpha\simeq 0$) $\Gamma\simeq 5$, hence $f\simeq 0.3$ (the observed minimum value of R being R_T=0.012).

A strong anti-correlation between the core-dominance parameter $R(\vartheta)$ and the line widths of broad Hβ has been found by Wills & Browne (1986): compact quasars have narrower lines, in the sense expected if the motion of the broad line gas is confined to a disk whose axis is perpendicular to the radio axis, and if compact sources are self-consistently seen almost face-on. The

higher R quasars are also of higher optical luminosity (~1 mag, Browne & Wright 1985), and on average a factor ~10 more X-ray luminous (Browne & Murphy 1987).

The case for bulk relativistic flow is strong, as we have seen, for blazar sources. The problem of the misaligned parent population of BL Lac objects has been addressed by Schwartz and Ku (1983). They have found that the local space density of BL Lacs with X-ray luminosity $\geq 10^{44}$ erg s^{-1} is similar to the space density of both Seyfert galaxies and optically selected quasars with the same luminosity, the BL Lac parent population being thus unlikely to be either Seyferts or QSOs (however, X-ray beaming may induce a bias against faint parent objects, see fig. 6).

Browne (1983) found that the space density of BL Lac objects with extended radio-luminosity (unaffected by relativistic beaming) $\geq 10^{29}$erg $s^{-1}Hz^{-1}sr^{-1}$ is: $\phi \geq 1.7 \cdot 10^{-7}$ $h^{-3}Mpc^{-3}$. The local space density of elliptical radio-galaxies with the same extended power is about a factor 60 higher than that of BL Lacs.

In the previous section we have suggested, on the basis of the Doppler factor distributions derived from SSC models, that the presence or absence of strong emission lines in blazar does not reflect a different degree of boosting at optical frequencies but rather an intrinsic difference between BL Lac objects and quasars.

It is also well known that radio galaxies have different emission-line properties: only FRII classical doubles (extended power $\geq 10^{32}$erg $s^{-1}Hz^{-1}sr^{-1}$, Fanaroff & Riley 1974) have strong nuclear emission lines. The more diffuse and weaker FRI might then represent the parent population of the line-less BL Lacs (Peacock 1987). This argument is supported by the extended radio luminosity-distribution of blazars (Antonucci & Ulvestad 1985) which show a clear separation between BL Lacs and HPQs at about

the FR borderline. The core-dominance parameter in FRI is $R_T \simeq 0.01$ and the most compact BL Lacs listed in Antonucci & Ulvestad (1985) are core dominated with $R_m \simeq 1000$. The range in $R(\vartheta)$ implies, for $\alpha=0$, Lorentz factors $\Gamma \geq 13$. However, the fraction of powerful elliptical radio galaxies which are BL Lacs, ~1/60, implies, from eq. (2.38), $R_T \simeq 4 \cdot 10^{-4}$ and $\Gamma \simeq 30$. Allowing for a likely substantial incompleteness in the BL Lac samples, i.e. the fraction of BL Lacs being closer to ~10%, it is possible to reconcile the observations with theory predictions.

An attractive alternative possibility is to introduce a distribution of Lorentz factors: $N(\Gamma)=A\Gamma^{-n}$, with $1 \leq \Gamma \leq \Gamma_{max}$. A power-law distribution of this form, with $n \geq 2$ and $\Gamma_{max} > 10$, would not produce many extreme core-dominated (R~1000) sources because only ~10% of objects would be highly beamed. The impact of a distribution of velocity on the shape of the ensuing luminosity function can be estimated as follows. If we adopt again, for simplicity, a one-component jet model, for $\Gamma \gg 1$ we can write the probability distribution in δ as:

$$P(\delta)=\delta^{-2} \cdot \int_{\Gamma_{min}}^{\Gamma_{max}} (\beta\Gamma)^{-1} N(\Gamma) d\Gamma \qquad (2.39)$$

where the lower integration limit $\Gamma_{min}(\delta)$ is equal to $1/\delta$ ($\vartheta=90^\circ$) if $\delta \leq 1$, and to $\sim\delta/2$ ($\vartheta=0^\circ$) if $\delta \gg 1$ (see figure 7). In the latter case, i.e. $L \gg 1$, we have: $P(\delta) \propto \delta^{-n-2}$, and, for $n \geq 2$, we derive:

$$P(L,1)=\left[A p^{-1} \Gamma_{max} 1^{(n+1)/p}\right] \cdot L^{-(n+p+1)/p} \qquad (2.40)$$

If we assume $n=2$, then $P(L,1) \propto L^{-(3+p)/p}$, which is steeper, as expected, than the distribution in eq. (2.34).

Consider the case of BL Lac objects. The only complete samples, obtained from X-ray surveys (Piccinotti et al. 1982,

Maccacaro et al. 1982), contains very few (4) BL Lacs, and most of unknown redshift. The X-ray luminosity function for a large number (29) of BL Lac objects that were not discovered in sistematic surveys has been estimated by Schwartz & Ku (1983). The slope of the differential X-ray LF is $\beta \simeq 2.1$, which is much flatter than the slope of the X-ray LF derived for, e.g. Seyfert galaxies $\beta=2.75$. The flatter BL Lac LF may be explained in the framework of a beamed population model. If we adopt an X-ray spectral index $\alpha=1$, a distribution in Γ with n=2 results in a beamed LF with $\beta=(3+p)/p=2$. On the contrary, the slope of the LF in eq. (2.36) (all sources with the same value of Γ) is $\beta=4/3$, probably too flat to be consistent with the observations (see figure 6).

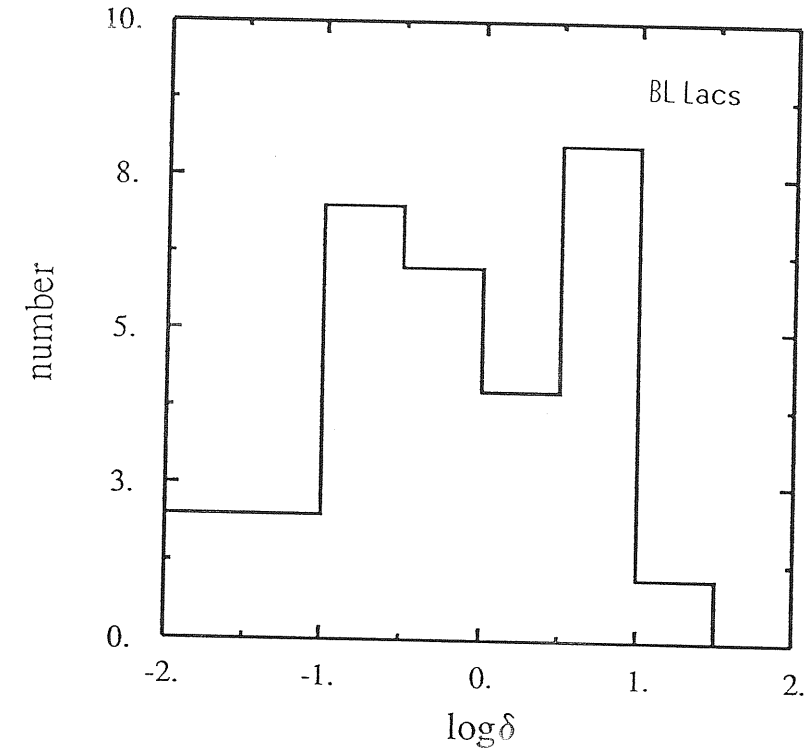

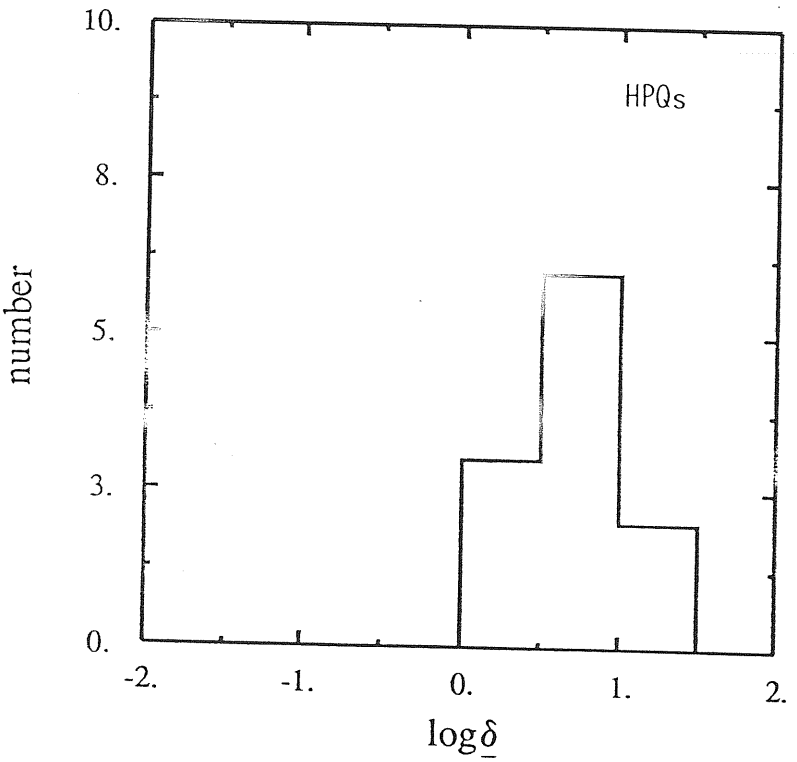

figure 5

Doppler factor distribution for the objects listed in Table 1.

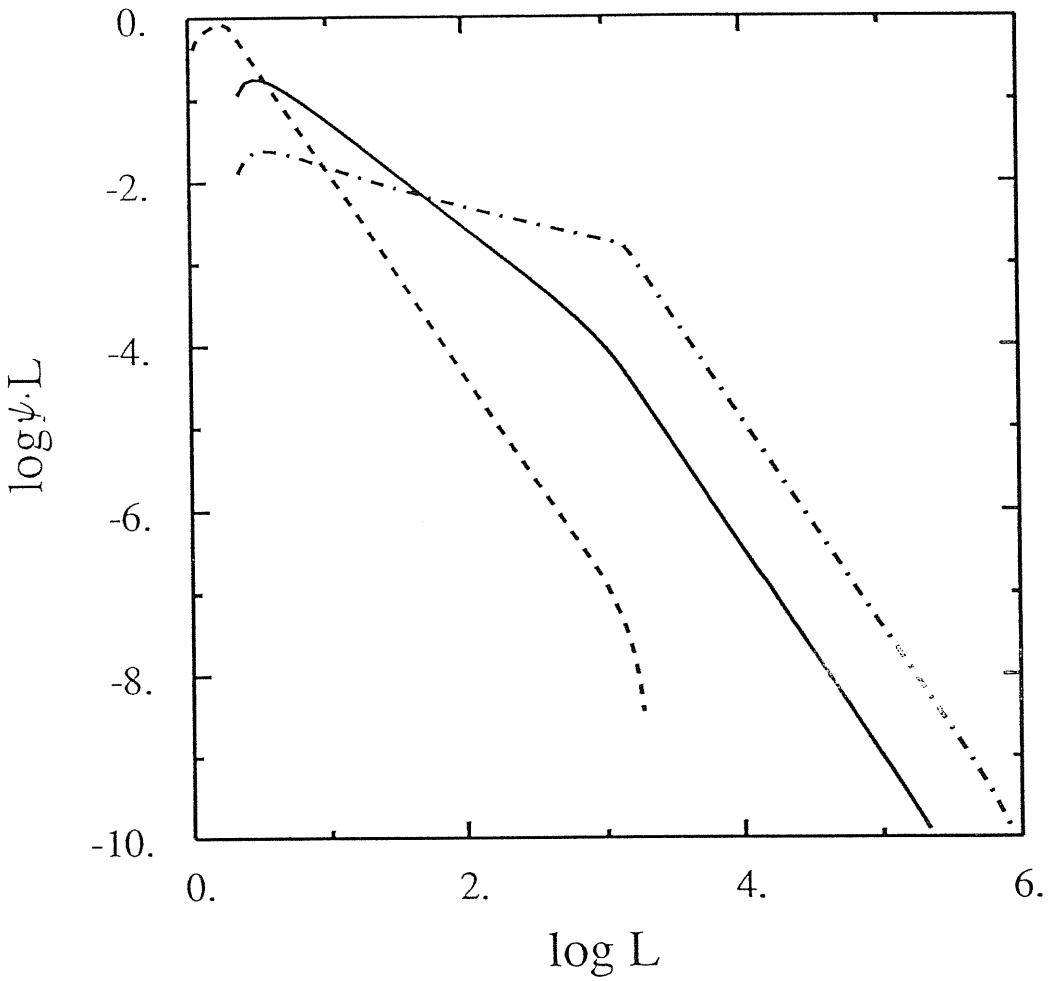

figure 6

The observed luminosity functions $\Psi(L)\cdot L$ (in arbitrary units) for a class of relativistically beamed sources. The intrinsic differential LF is $\phi(l)\propto l^{-3.5}$, $1\leq l \leq 1000$, with $L=(1+f\delta^{p})\cdot l$, $p=2.5$, $f=0.5$ (see text). A distribution of Lorentz factors is assumed: $N(\Gamma)\propto\Gamma^{-2}$, $1\leq \Gamma\leq 12$.

Dashed line: non-jet dominated sources defined by $0^{o}\leq \vartheta \leq \vartheta_{c}$.

Solid line: jet-dominated beamed sources with a distribution $N(\Gamma)$.

Dash-dotted line: jet-dominated beamed sources with Γ=const=12 .

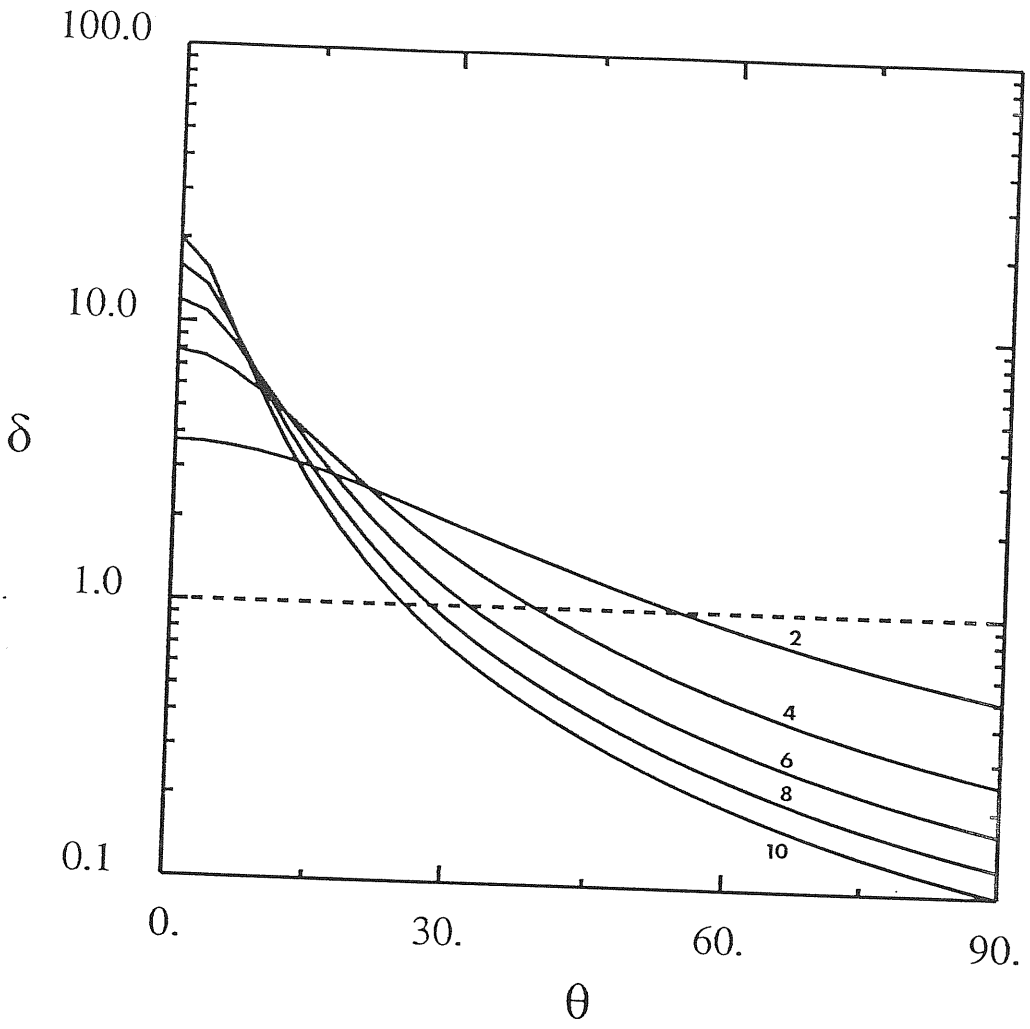

figure 7

Doppler factor δ vs the viewing angle ϑ, for different values of the Lorentz factor Γ=2,4,6,8,10. The maximum value of δ occurs at ϑ=0° and it is ≈2Γ. As Γ increases, the function δ(ϑ) becomes more sharply peaked. For increasing values of Γ, δ is equal unity at ϑ=55°, 39°, 32°, 28° and 25°.

Table 1: Input data for SSC and derived Doppler factors

	Name		z	θ_d (b) (mas)	ν_t (GHz)	S_t (Jy)	S_X(1keV) (Jy)	δ	Ref. (a)
	BL Lac objects								
	0048-097	OB 081	.....	0.4	5	0.71	6.6 (-8)	3.24	1, 2
	0212+73		.....	0.6	5	1.5	2.3 (-7)	2.82	3, 2
	0219+428	3C 66A	0.444	1.5	5	0.2	1.6 (-7)	0.09	1, 2
*	0235+164	AO	0.852	0.5	5	1.75	1.7 (-7)	6.19	1, 2
	0306+102	PKS	.....	0.5	5	0.73	1.1 (-7)	2.11	1, 2
	0316+41	NGC1275	0.018	0.3	22	1.2	1.8 (-5)	0.3	4, 2
	0454+84		.....	0.55	5	1.3	5. (-8)	3.71	3, 2
	0521-365	PKS	0.055	1.8	5	0.86	6.8 (-7)	0.16	5, 2
	0716+714		.....	0.35	5	0.5	2.2 (-7)	2.28	3, 2
*	0735+178	OI 158	0.424	<0.3	5	1.29	3.2 (-7)	7.2	6, 2
	0754+100	OI 090	.....	0.6	5	0.53	1.7 (-7)	1.06	1, 2
	0818-128	OJ 131	.....	0.8	5	0.47	7. (-8)	0.68	1, 2
	0829+046	OJ 049	.....	0.9	5	0.26	1.9 (-7)	0.26	1, 2
	0851+202	OJ 287	0.306	0.3	5	2.3	1.7 (-6)	8.7	7, 2
	1101+384	Mkn421	0.03	<0.3	5	0.24	1.4 (-5)	0.49	6, 2
	1147+245	B2	.....	0.9	5	0.39	8. (-8)	0.46	1, 2
	1215+303	ON 235	.....	0.7	5	0.33	8.5 (-7)	0.38	1, 2
	1219+285	ON 231	0.102	0.5	5	0.13	4.2 (-7)	0.23	8, 2
	1400+162	MC3	0.244	1.4	5	0.08	1. (-7)	0.04	1, 2
	1538+149	4C14.60	.....	0.6	5	0.56	1.5 (-7)	1.14	9, 2
	1652+398	Mkn501	0.034	<0.5	5	0.4	1.7 (-7)	0.35	9, 2
	1727+502	I Zw186	0.055	1.2	5	0.04	2.1 (-6)	0.01	1, 2
	1749+096	4C09.57	.....	0.2	5	1.43	3.5 (-7)	15.0	1, 2

Table 1: Input data for SSC and derived Doppler factors (continue)

	Name		z	$\theta_d^{(b)}$ (mas)	ν_t (GHz)	S_t (Jy)	S_x(1keV) (Jy)	δ	Ref.[a]
	BL Lac objects								
	1803+78		.....	0.4	5	1.8	1.6 (-7)	7.0	3, 2
	1807+698	3C 371	0.05	1.4	5	1.21	6. (-7)	0.36	10,2
*	2007+776		.....	0.4	5	1.17	1.1 (-7)	4.87	3, 2
*	2200+420	BL Lac	0.069	0.35	5	1.6	8.2 (-7)	4.39	7, 2
	2201+044	PKS	0.028	0.7	5	0.16	2.1 (-7)	0.17	1,11
	2254+074	OY 091	.....	1.0	5	0.14	1. (-7)	0.13	1, 2
	2335+031	PKS	.....	1.7	5	0.03	<2.3 (-8)	0.02	1, 2
	HPQs								
	0106+013	PKS	2.107	<0.4	5	2.3	2.2 (-7)	18.76	12,2
	0336-019	CTA 26	0.852	<1.0	5	2.1	4.7 (-8)	3.02	12,2
	0420-014	PKS	0.915	<0.7	5	1.5	5.2 (-7)	2.57	12,2
*	1253-055	3C 279	0.538	0.3	5	0.9	1.4 (-6)	4.15	7, 2
	1308+326	B2	0.996	0.5	5	1.97	3. (-7)	6.76	1, 2
*	1641+399	3C 345	0.595	0.3	22	6.9	6.6 (-7)	5.22	13,2
*	2223-052	3C 446	1.404	0.4	10.7	2.2	1.1 (-6)	3.74	14,2
	2230+114	CTA 102	1.037	<0.5	5	0.54	3.4 (-7)	1.85	9, 2
	2234+282	B2	0.795	<0.5	5	1.21	5. (-8)	5.17	9, 2
*	2251+158	3C454.3	0.859	<0.3	5	0.9	5.6 (-7)	5.93	7, 2
	2345-167	PKS	0.6	<0.4	5	2.5	1.8 (-7)	10.9	12,2

Notes to table 1

a) References:

1 Weiler and Johnston 1980

2 Ledden and O'Dell 1985

3 Eckart et al. 1982

4 Lawrence et al. 1985

5 Preuss and Fosbury 1983

6 Baath et al. 1981

7 Pauliny-Toth et al. 1981

8 Weistrop et al. 1985

9 Zensus et al. 1984

10 Pearson and Readhead 1981

11 Madejski and Schwartz 1983

12 Kellerman et al. 1971

13 Unwin et al. 1983

14 Brown et al. 1981

b) When the minor and major axes a and b of the source are given we adopt

$\theta_d = \sqrt{ab}$

*) Superluminal sources

CHAPTER III : ACCRETION FLOWS ONTO BLACK HOLES

III.1) Accretion with angular momentum

The details of accretion flows and energy generation are the subject of much current research and hot debate (for reviews on the subject see Rees 1984, Blandford 1984, Begelman 1985). The way in which gas flows into a black hole depends largely on the conditions where it is injected. If the gas has no angular momentum, it can flows in radially. In this case the efficiency ϵ of conversion of rest-mass energy into the emitted bremsstrahlung radiation which results from adiabatic compression is:

$$\epsilon=L/\dot{M}c^2\simeq 6\cdot 10^{-3}\cdot(n_\infty/1cm^{-3})\cdot(T_\infty/10^4K)^{-3/2}\quad M_8\ . \qquad (3.1)$$

Thus, in general, the spherical accretion of interstellar gas by a massive black hole tends to be an inefficient radiation mechanism (in contrast to spherical accretion onto a neutron star for which $\epsilon\sim 0.1$). For this reason, coupled with the large angular momentum expected in infalling gas and the observations of strongly aspherical radio structures such as jets, we will confine our attention to accretion with angular momentum.

Whenever the angular momentum per unit mass $l(r)$ exceeds $l_{ms}\equiv\sqrt{3}\ r_G c=1.6\cdot 10^{24}\ cm^2 s^{-1}\ M_8$, where l_{ms} is the specific angular momentum at the innermost stable circular orbit r_{ms}, centrifugal forces will become significant before the gas crosses the event-horizon. Particles with $l>l_{ms}$ will form a disk in the equatorial plane of the system. These particles will only be

accreted if viscosity (or other mechanisms, e.g. an hydromagnetic wind, Blandford & Payne 1982) acts to reduce their specific angular momenta below l_{ms}. The widely discussed central star-cluster in M87 (Dressler 1980) has a velocity dispersion $\sigma_v \simeq 350$ Km s^{-1}, and a size $R \geq 2$pc, which yield $l(R) \geq 2 \cdot 10^{26}$ $cm^2 s^{-1}$. In this example viscous torques (or others) must remove 99% of the gas angular momentum before the gas can plunge into the hole.

The gravitational binding energy of the unit mass at the inner edge of the disk is dissipated away as the gas drift through the disk, and is converted to internal energy. Friction between adjacent annuli causes, in fact, most of the mass to move into lower angular momentum, larger angular velocity, smaller radius orbits, while a tail of matter moves outward taking away the excess angular momentum (see, e.g. Pringle 1981). Viscosity damps out shearing orbital motion and the energy of the shearing motion is dissipated in the fluid as frictional heat.

If we denote with $t_k(r)$ the Keplerian orbital timescale and with $t_{in}(r)$ the inward drift timescale through the disk, the ratio t_k/t_{in} depends on the effective viscosity mechanisms. If this ratio is fixed, the global structure of the accreting flow is mainly governed by the ratio $\dot{m}$ of the accretion rate $\dot{M}$ to the critical accretion rate $\dot{M}_E \equiv L_E/c^2 = 0.2 \cdot M_8$ $M_\odot yr^{-1}$, ratio which determines the relative importance of gravity and radiation pressure.

The dynamical (i.e. rotational) timescale and the gravitational radius r_G, in fact, scale as mass M. The characteristic density scales then like $\rho \propto (\dot{M} \cdot t_{in})/r_G^3 \propto \dot{m}/M$. In the case of two-body cooling processes, the cooling timescale t_c is inversely proportional to the density, hence it is: $t_c/t_k \propto 1/\dot{m}$, independently on the mass.

The ratio t_c/t_k actually governs the flow pattern. If the flow is able to radiate away most of its binding energy on a dynamical timescale, a *thin accretion disk* will form. However, if $\dot{m}$ is small, the flow may be unable to cool effectively and may instead inflate to form a torus supported by gas pressure. The "virial" local temperature is given by:

$$T_v(r)=m_p c^2 \cdot r_G/(3k \cdot r) \quad . \qquad (3.2)$$

If $r \leq 600 r_G$, $kT_v(r) \geq m_e c^2$ and electrons will be subject to very efficient relativistic synchro-Compton cooling processes. So pressure gradients can balance against gravity in this region only if hot protons are decoupled from electrons: an *ion torus* would then form (Rees et al. 1982). This two-temperature thermal state (see also Shapiro, Lightman & Eardley 1976) relies on inefficient coupling between ions and electrons. Coulomb collisions alone provide inefficient coupling if: $\dot{m} < 50 \cdot \alpha^2$, where α is the viscosity parameter.

At sufficiently low accretion rates then, two thermal states are possible: a cool thin accretion disk which, if heated at the local virial temperature (e.g by an instability, see Shakura & Sunyaev 1976) may never cool back down to become a thick, hot torus. In particular, if the viscosity is large enough that the inflow time is shorter than the cooling time, ions are decoupled from electrons and provide the dominant kinetic pressure.

Moreover, in this region, any adiabatic heating mechanism will preferentially heat ions ($T_p \propto \rho^{2/3}$) than relativistic electrons ($T_e \propto \rho^{1/3}$). However, collective plasma processes may be much more efficient than Coulomb interactions in coupling electrons to ions. In this case electrons could drain energy from the ions and the torus would deflate. Whether or not a

two-temperature torus may exist in nature is still an open question.

Alternatively, consider a flow with $\dot{m} \gg 1$. The ratio of the photon diffusion timescale t_p to the dynamical timescale is: $t_p/t_k \simeq \tau_T \propto \dot{m}$, so the Thomson optical depth is large, photons are trapped and radiation pressure builds up to form a *radiation torus*. In geometrically thick disks radial pressure gradients are dynamically important and the rotation law will no longer be keplerian.

Thin accretion disks and radiation tori are mainly thermal emitters. A characteristic temperature may be associated with the Eddington luminosity and the Schwarzschild radius r_G:

$$T_E \equiv (L_E/4\pi r_G^2 \sigma)^{1/4} = (c^5/4K_T \sigma GM)^{1/4} \simeq 4 \cdot 10^5 \, M_8^{-1/4} \, ^\circ K \ .$$

We expect then thermal spectra which peak at ultraviolet frequencies, with harder spectra in the case of less massive objects. Ion tori, instead, are low density sources optically thin to electron scattering and mainly non-thermal emitters: thermal bremsstrahlung will be a source of gamma-ray photons and relativistic electrons will Compton upscatter synchrotron and f-f photons to the IR-gamma region of the spectrum.

A unified scheme for the different forms of AGNs has been proposed by Rees et al. (1982), Phinney (1983), Blandford (1984) and Begelman (1985), within the hypothesis that dissipative accretion flows onto supermassive black holes are the powerhouse in the nuclei of active galaxies. The basic classification parameter is naturally the dimensionless accretion rate $\dot{m}$.

At low rates $\dot{m} \ll 0.1$, the basic flow pattern would be an ion-supported torus, whose main attractive feature is in the low radiative efficiency. The starting point is in the inferred

small fuelling rates of double-jet radio sources with low nuclear luminosities; only few of them exceed $\sim 10^{42}$erg $s^{-1}=10^{-4}$ M_8 L_E. On the other hand, mechanisms of jet formation which require high or super-Eddington luminosities seem to be ruled out by the energetics of the extended (~Mpc) radio emission, with minimum energies $\sim 2\cdot 10^{62}$erg $=10^{7}\epsilon_{0.1} M_\odot c^2$. Indeed, in some cases, the extended radio luminosity is greater than the observed bolometric nuclear luminosity. The need, then, is for a mechanism which can very efficiently produce bulk ordered motion with a very low radiative efficiency.

Ion tori may provide this mechanism; moreover, they might offer the environment where the Blandford-Znajek (1977) process of extraction of spin energy from the black hole can operate. If the central black hole is nearly maximally rotating with $J=J_{max}=GM^2/c$ (spun up during the early phase of accretion, Thorne 1974), the rotational energy of the hole amounts to 29% of the rest-mass. An ordered magnetic field, supported by the torus, may pierce the ergosphere of the hole and tap its spin energy by an amount which is adeguate to supply the extended radio-sources energy requirements. Predominantly non-thermal sources, such as radio galaxies, would then be powered by ion tori accreting at $\dot{m}\ll 1$. In general terms, an increasing ratio of non-thermal to thermal emission would be associated with a decreasing $\dot{m}$. Bright radio-quiet QSOs may then be powered by radiation tori accreting at $\dot{m}\gg 1$, with black hole masses of order 10^8-10^9 $M_\odot$. Seyfert I galaxies might be either critical accreting tori onto 10^6-$10^7 M_\odot$ black holes and be short-lived objects, or the may represent the end point of quasar evolution (see chapter I). In the latter case they would be powered by thin disks accreting at $\dot{m}\approx 1$. Radio-loud quasars QSRs may represent as well an intermediate class

displaying both the non-thermal emission of radio galaxies and the thermal unpolarized optical continua of QSOs. Alternatively, their radio-jets may be formed in the funnels of radiation tori and be then powered by radiation pressure. The OVV quasars and the BL Lac objects may be respectively associated with beamed QSRs and FRI radio galaxies. A "unified" scheme becomes a real difficult task if one consider that duty cycles of activity, dust opacity, galaxy morphology and environment are probably extra degree of freedom.

III.2) Thin accretion disks

The structure of a steady, axisymmetric, non self-gravitating accretion disk is governed by five basic equations: conservation of mass, momentum (radial, azimuthal and vertical component) and of energy (see, e.g Pringle 1981, Frank, King, Raine 1985). We use a cylindrical coordinate system (r,φ,z) centered on the black hole, with $z=0$ the central plane of the disk. The momentum conservation equation reads: (r)

$$v_\varphi^2/r = \frac{\partial \phi}{\partial r} - 1/\rho \frac{\partial p}{\partial r} - v_r \frac{\partial}{\partial r} v_r - v_z \frac{\partial}{\partial z} v_z \qquad (3.3)$$

and (z):

$$0 = \frac{\partial \phi}{\partial z} - 1/\rho \frac{\partial p}{\partial z} - v_z \frac{\partial}{\partial z} v_z - v_r \frac{\partial}{\partial r} v_z \qquad (3.4)$$

where $\phi(r,z)$ is the gravitational potential of the hole. The rotation law is Keplerian if $v_\varphi = v_k = (r\frac{\partial \phi}{\partial r})^{1/2}$. This requires radial pressure gradient to be negligible compared to gravity force: $v_\varphi \gg v_s$, where v_s is the sound speed, i.e. the circular flow to be highly supersonic. Moreover it must be: $v_\varphi \gg v_r$, $v_\varphi \gg v_z$.

If h is the pressure scale-height of the flow in the

z-direction, the hydrostatic equilibrium (eq. (3.4) with $v_z=0$) gives: $v_s^2/v_\varphi^2 \simeq (h/r)^2$, which can be interpreted as the ratio between internal energy and gravitational potential energy. Hence the Keplerian condition $v_\varphi \gg v_s$ is satisfied if the flow is geometrically thin: $h/r \ll 1$; in this regime is not possible to accumulate an appreciable amount of heat within the disk.

Consider then Keplerian rotation in a Newtonian potential. Since in most cases the radial structure is of prime importance, vertically integrated equations -actually replaced by z-averaged quantities - are used. Mass and angular momentum conservation read:

$$2\pi r \Sigma v_r = -\dot{M} \tag{3.5}$$

and

$$\Sigma v_r \frac{d(rv_\varphi)}{dr} = (2\pi r)^{-1} \frac{dG}{dr} \tag{3.6}$$

where Σ is the surface density and G is the viscous torque:

$$G \equiv 2\pi r^3 \nu \Sigma \, d\Omega/dr \quad . \tag{3.7}$$

Here Ω is the Keplerian angular velocity and ν is the kinematic viscosity. Equation (3.6) can be integrated, the integration constant being determined by the zero torque condition at the inner edge r_{in}: $G_{in}=0$, to yield

$$G(r) = -\dot{M} \cdot (l(r) - l_{in}) \tag{3.8}$$

where $l_{in}=l(r_{in})$. The inner radius r_{in} of the disk coincides with the last marginally stable circular orbit $r_{ms}=3r_G$. A gas particle pushed slightly inward would find itself on an unstable orbit and fall without radiating into the black hole along a spiral trajectory.

The viscous heat production rate per unit area is given by: $Q(r)=(d\Omega/dr)\cdot G\cdot(2\pi r)^{-1}$ and, from eq. (3.8) and the definition of keplerian rotation, we derive:

$$Q(r)=3GM\dot{M}\cdot(4\pi r^3)^{-1}\cdot\left[1-(r_{in}/r)^{1/2}\right] \qquad (3.9)$$

Thus in steady state the dissipation rate does not depend on the major uncertainty in the theory, the viscosity ν, although local disk properties such as the surface density do depend, of course, on the size of ν. In the absence of a microphysical theory for viscosity, a phenomenological fruitful approach to the problem has been the condensation of our ignorance into a dimensionless parameter α (Shakura & Sunyaev 1973): $\nu=\alpha v_s h$, with α being a constant assumed ad hoc and h the vertical thickness of the accretion flow. The main mechanisms of angular momentum transport are magnetic, turbulence, molecular and radiative viscosity (but radiation and molecular viscosity are negligibly small and cannot lead to disk accretion). The accreting material will carry with it some seed magnetic field which will be amplified by the shearing motion; the magnetic pressure will probably be maintained at a significant fraction of the total gas pressure. General arguments give $\alpha\leq 1$. From eq. (3.8) and (3.9), we may write:

$$v_r=\alpha\cdot(h/r)^2\cdot v_k=\alpha\cdot(h/r)\cdot v_s \quad . \qquad (3.10)$$

In the thin disk limit $(h/r)\ll 1$: first, the radial disk velocity is self-consistently very small compared to v_k, and second, the cooling time is short compared to the viscous inflow timescale and local thermal equilibrium holds (hence heat generated at radius r is radiated at the same radius). Also, the timescale on which hydrostatic equilibrium is established in the

z-direction, given by $\sim h/v_s$, is comparable to the local Keplerian timescale and is self-consistently very short compared with the inflow timescale. It is therefore possible to decouple the vertical and radial behaviour of the disk.

Integrating eq. (3.9) over the disk area, we find that the total disk luminosity: $L=GM\dot{M}/(2r_{in})$, is half of the total available accretion energy, the other half of the potential energy being retained as kinetic energy and lost in the black hole perfect drain. In order to solve the disk variables, the hydrodynamic equations and the equation defining the viscosity coefficient have to be supplemented with two auxiliary equations: the equation of state and the radiative transfer equation.

If the thin disk approximation holds, the temperature gradient is again essentially vertical, and we can neglect heat flow in the radial direction. Vertical integration and thin disk approximation allows separation of the radial and vertical structure of the disk, reducing a 2-D problem to two 1-D problems.

One first solves the z-integrated disk variables as a function of radius. Going back to the non-integrated forms of the hydrostatic equilibrium and radiative transfer (in the diffusion approximation) equations, one subsequently solves for the vertical structure (Shakura & [illegible]nev 1973). The "standard" disk equations are algebraic ones, linear in their logarithmic version whenever gas or radiation pressure dominates (for a review, see Abramowicz 1986).

The main contribution to the opacity is expected to come from Thomson scattering and free-free opacity. In the inner disk regions radiation pressure is dominant and electron scattering on free electrons plays the main role. In this case the flux of radiation is proportional to the gravitational acceleration at the

disk surface:

$$F_r(r)=cg_z/k_T=cGMh/(k_T r^3) \quad . \tag{3.11}$$

From eq. (3.11) and (3.9), with $F_r(r)=Q(r)/2$, we obtain that at large radii the disk thickness is constant, depending only on the flux of accreting matter:

$$h_\infty=3k_T\dot{M}/(8\pi c) \quad . \tag{3.12}$$

This is expected because the radiation pressure force and the normal component of the gravitational force scale both as r^{-3}. The ratio h/r reaches its maximum at $r=(27/4)\cdot r_G$:

$$(h/r)_{max}=(4/81)\cdot h_\infty/r_G=(1/27)\cdot\dot{m} \quad . \tag{3.13}$$

We see that at high accretion rates $\dot{m}\gg 1$, the thin disk condition $(h/r)\ll 1$ breaks down; in particular, we may no longer neglect the radial pressure gradient nor the heat flow in the radial direction. The rotation law is no longer Keplerian and the equations for the radial and vertical structure of the disk must now be solved simultaneosly.

Let us focus on the inner disk regions, which are dominated by radiation pressure and Thomson opacity, at the fiducial radius $r=(27/4)r_G$, where the h/r ratio is a maximum (eq. 3.13). The inflow time there is given by:

$$t_{in}\simeq 0.6\ M_8\ (\alpha\cdot\dot{m}^2)^{-1}\ \mathrm{yr} \tag{3.14}$$

which, together with mass conservation equation, yields the electron scattering opacity integrated in the z-direction:

$$\tau_T\simeq 400\ (\alpha\cdot\dot{m})^{-1} \tag{3.15}$$

and electron density:

$$n \simeq 8 \cdot 10^{13} \cdot (\alpha \dot{m}^2 M_8)^{-1} \ cm^{-3} \ . \qquad (3.16)$$

The radiation energy density at the disk surface is given by:

$$U_d \simeq 3.3 \cdot 10^5 \ \epsilon_{0.1} \dot{m} \ M_8^{-1} \ erg \ cm^{-3} \qquad (3.17)$$

and radiation is thermalized with a temperature on the equatorial plane given by:

$$T_c = (\tau_T \cdot U_d / a)^{1/4} \simeq 4 \cdot 10^5 \ \epsilon_{0.1}^{1/4} \cdot (\alpha M_8)^{-1/4} . \qquad (3.18)$$

The dominant thermal emission mechanism is bremsstrahlung. The equipartition magnetic field in the disk interior can be roughly estimate as: $B = (8\pi \tau_T U_d)^{1/2}$. The ratio between the scale height of the flow and the Larmor radius is given by:

$$(h/r_L) \simeq 2 \cdot 10^{16} \ \epsilon_{0.1}^{3/8} \alpha^{-3/8} \cdot \dot{m} \ M_8^{5/8} .$$

Ordinary molecular viscosity will then be suppressed and magnetic viscosity will probably govern the shear flow ($\alpha_B \simeq 0.01$, Eardley & Lightman 1975).

The free-free opacity (for $x = h\nu/kT = 1$) is given by:

$$\tau_{ff} \simeq 0.04 \cdot (\alpha^{9/8} \dot{m}^3 M_8^{1/8} \epsilon_{0.1}^{7/8})^{-1} \ . \qquad (3.19)$$

From eq. (3.15) and (3.19) it is clear that, in these regimes, the emitted spectrum will be modified strongly by electron scattering.

The emitted radiation will be thermalized if the effective optical depth $\tau_* = (\tau_T \cdot \tau_{ff})^{1/2}$ is greater than unity. The condition for LTE can be written as:

$$\tau_* \simeq 4 \cdot (\alpha^{17/16} \dot{m}^2 M_8^{1/16} \epsilon_{0.1}^{7/16})^{-1} \ > 1 \ . \qquad (3.20)$$

Thus, at high accretion rates, LTE may be violated in the

inner regions of the disk. However, when the parameter:

$$y \equiv 4kT\tau_T^2/(m_e c^2) \simeq 40 \cdot \epsilon_{0.1}^{1/4} \dot{m}^{-2} \alpha^{-9/4} M_8^{1/4}$$

is greater than unity, the thermalization of photons may proceed due to multiple Compton scatterings. The radiation spectrum will have a Wien distribution $F_\nu \propto \nu^3 e^{-x}$ with a peak at $x=h\nu/kT=3$, and will never be that of an optically thin plasma.

At the fiducial radius, the ratio of the photon diffusion to the inflow timescale is given by:

$$t_p/t_{in} \simeq 10^{-3} \cdot \dot{m}^2 \qquad (3.21)$$

hence only in the limit $\dot{m} \gg 1$ would the accretion flow advect photons inward faster than they can diffuse in the z-direction.

III.3) Feeding the black hole, luminosity evolution and thin disk spectra

The search for a mechanism able to feed the central black hole and power the AGN active phase has led to studies of the dynamical evolution of dense stellar systems with massive black holes at the center of the cluster. The entire system evolves gravitationally, with stars suffering collisions with other stars (for a review see Lightman & Shapiro 1978) or tidal disruption by the black hole (Hills 1975), with the gaseous debris providing the necessary luminosity as they are subsequently accreted.

Consider a stellar distribution with core radius R_c, velocity dispersion σ_v and density n_c. Typical values expected in the core of quasars are : R_c=1pc, σ_v=350 Km s^{-1}, $n_c=10^8 pc^{-3}$. A central

black hole point mass M_8 will affect the stellar velocity field out to an accretion radius $R_a \simeq GM_8/\sigma_v^2 \simeq 3.6 \cdot 10^5 r_G$. The central two-body relaxation time is (Duncan & Shapiro 1983):

$$t_r = 0.45\ \sigma_c/(G^2 m^2 n_c \ln(0.5\ N_c)) \simeq 1.5\ 10^{10}\ \mathrm{yr}$$

where N_c is the number of stars with mass $m=1M_\odot$ interior to R_c.

The black hole at the center provides an effective sink for stars approaching too close to it, hence there is no possibility to establish an isothermal distribution, with $n_c(R) \propto R^{-2}$. Rather, a state is established in the core which involves a slow inward drift of stars; the equilibrium star density, approached within a relaxation time, approximates a power-law $R^{-7/4}$ in the inner cusp region $R<R_a$ (Bahcall & Wolfe 1976).

The tidal radius within which a star would be disrupted is:

$$R_T = 6 \cdot 10^{13}\ M_8^{1/3}\ \mathrm{cm} \simeq 2 r_G \quad .$$

Any star orbiting the black hole with such a low angular momentum to pass within R_T will be disrupted, the energy needed to unbind the star coming from its orbital kinetic energy, with the stellar material subsequently radiating as it spirals into the black hole. The collision radius at which the velocity dispersion $(GM_8/R_{coll})^{1/2}$ is comparable with the escape velocity from typical $1M_\odot$ stars:

$$R_{coll} = 7 \cdot 10^{15}\ M_8\ \mathrm{cm} \simeq 200 \cdot r_G$$

is much greater than R_T for any interesting value of the black hole mass. When the latter exceeds the critical value of $3 \cdot 10^8\ M_\odot$, ordinary stars can be swallowed whole (i.e. $R_T < r_G$), without generating much radiation. For $M_8 \simeq 1$, the star (physical) collisions-fed luminosity exceeds by a factor ~100 the luminosity

due to tidal disruption (Young, Shields & Wheeler 1977).

For parameters appropriate to the expected accretion rates in QSOs, Duncan & Shapiro (1983) have shown that direct physical collisions between stars are more important than gravitational two-body relaxation in driving the dynamical evolution of the core within a collision time $\sim 2 \cdot 10^8$ yr ($t_r \simeq 4.5 \cdot 10^9$ yr); in this case, the stellar density profile in the inner regions is well fitted by a power-law $n_c(R) \propto R^{-1/2}$. The brightest phase, in which the gas liberation rate $\dot{M}(t)$ is roughly constant, is found to last about a collision time, until the hole has essentially consumed the core; subsequently $\dot{M}(t)$ decreases and attains an asymptotic form $\dot{M} \propto t^{-1}$.

The fate of such gas once it has been made available is uncertain. If we assume that the debris of stellar disruption settle down into a viscous evolving accretion disk, then in steady state the gas may be provided to the central power source at the same rate as it is liberated, $\dot{M}(t)$. In this case, the time-dependent luminosity L(t) is directly proportional to the gas liberation rate and can be compared to the observed luminosity evolution of QSOs and AGNs. After a collision time, the bolometric emitted luminosity would then evolve with redshift z as:

$$L(z) = \epsilon \dot{M} c^2 \propto t^{-1} \propto (1+z)^{3/2} \qquad (3.22)$$

(for $\Omega_o = 1$). This evolution is too slow in comparison with the best fit luminosity-evolution law: $L(z) \propto (1+z)^{3.5}$, obtained from the observed QSOs optical counts (see I.3). However, eq.(3.22) gives no spectral information, dealing only with bolometric magnitudes. To match with the observed slope, the efficiency to produce blue optical radiation must be: $\epsilon \propto \dot{M}^{4/3}$.

In thin α-disk models (Shakura & Sunyaev 1973, hereafter SS),

different accretion regimes result in very different emitted spectra. Local energy balance gives the radiative flux and the surface effective temperature distribution $T_e(r)=(F(r)/\sigma)^{1/4}$. From eq. (3.9), with $r \gg r_{in}$, we derive $T_e(r) \propto r^{-3/4}$, which attains a maximum value :

$$T_{max}=1.2\cdot 10^5 \dot{m}^{1/4} M_8^{-1/4} \qquad (3.23)$$

at $r=(49/12)r_G$. Thermal radiation from optically thick material will thus be in the ultraviolet region. The sum-of-blackbodies flux (erg $s^{-1}cm^{-2}Hz^{-1}sr^{-1}$) observed at a distance D under an inclination angle i, is:

$$F_\nu=\cos i/D^2 \cdot \int_{r_{in}}^{r_{out}} B_\nu(T_e(r))\cdot 2\pi r dr \qquad (3.24)$$

where r_{out} is the outer edge of the disk and B_ν is the Planck function. For frequencies $\nu \ll kT_e(r_{out})/h$, the spectrum takes the Rayleigh-Jeans form $F_\nu \propto \nu^2$. For $\nu \gg kT_{max}/h$, the spectrum is dominated by the hottest part of the disk and drops off exponentially. For intermediate frequencies, from eq. (3.9) and (3.24) we can derive:

$$F_\nu \propto M^{4/3} \cdot \dot{m}^{2/3} \cdot \nu^{1/3} \qquad (3.25)$$

which is the characteristic (hence never observed) "flat" disk spectrum. For an arbitrary temperature distribution $T(r)\propto r^{-p}$, the planckian spectrum reads: $F_\nu \propto M^{(2-0.5/p)} \cdot \dot{m}^{0.5/p} \cdot \nu^{3-2/p}$.

Whenever opacity is dominated by Thomson scattering, the emitted spectrum will be a modified blackbody, with thermal equilibrium existing where the effective optical depth is large: $\tau_T \cdot \tau_{ff} > 1$ (see also chapter IV). In the case of a homogeneous atmosphere (Felten & Rees 1972) the emitted specific intensity is given by:

$$I_\nu = 8.2 \cdot 10^{-4} \cdot \rho^{1/2} \cdot T^{5/4} \cdot x^{3/2} e^{-x} / (1-e^{-x})^{1/2} \qquad (3.26)$$

with $x=h\nu/kT$, which integrated over frequency reads:

$$F = 8.2 \cdot 10^{7} \cdot \rho^{1/2} \cdot T^{9/4} \quad . \qquad (3.27)$$

In the inner disk regions, where radiation pressure dominates over gas pressure, the standard SS solution reads: $\rho \propto \alpha^{-1} \dot{m}^{-2} M^{-1} (r/r_G)^{3/2}$, which, together with eq. (3.6) and (3.27), gives: $T(r) \simeq 10^{7} \alpha^{2/9} \cdot \dot{m}^{8/9} \cdot M_8^{-2/9} (r/r_G)^{-5/3}$. Inserting these expressions in (3.26) and integrating over the disk surface, the emitted spectrum can be written as:

$$F_\nu \propto \alpha^{-2/15} \cdot \dot{m}^{7/15} \cdot M^{17/15} \cdot \nu^{-0.4} \quad . \qquad (3.28)$$

In the intermediate disk parts, gas pressure dominates over radiation pressure, with electron scattering still giving the main contribution to the opacity. In the case of an exponential varying atmosphere we have: $\rho = \rho_o e^{-z/H}$, with $H = r^3 kT(z_o)/(GMm_p z_o)$ and with z_o being the location of the photosphere. After thermalization, the plasma temperature is practically constant:

$$T \simeq \quad 10^{6} \alpha^{1/75} \cdot \dot{m}^{28/75} \cdot M_8^{-19/75} \cdot (r/r_G)^{-47/50} .$$

The emitted spectrum is given by:

$$F_\nu \propto \alpha^{-2/141} \cdot \dot{m}^{85/141} \cdot M^{179/141} \cdot \nu^{3/47} \quad . \qquad (3.29)$$

None of these spectral regimes seems to fit the luminosity evolution law derived from optical counts. This can be due to a different feeding mechanism at work(such as galaxy interactions, which however may act on relatively shorter timescales $\sim 10^{7}$yr, Stockton 1982. Short evolution timescales may also originate in the local mass supply from the accretion disk) or to our ignorance of the microphysics (e.g. α-viscosity law) of accretion processes.

The role of non-thermal emission processes in in accreting disks is poorly known. It is plausible that an accretion disk does pump energy into a outer,hot and tenous corona-like layer (Liang & Price 1977). A small population of highly relativistic electrons may take some fraction of the coronal energy density and radiate it as synchro-Compton emission. The radiation energy density at the disk surface U_d (eq. 3.17) provides a characteristic value to compare with the coronal energy densities (Begelman 1985). Following the discussion in II.2, an equipartition coronal magnetic field can be defined as:

$$B \simeq 3 \cdot 10^3 \; \epsilon_{0.1}^{1/2} \; \dot{m}^{1/2} \; M_8^{-1/2} \; G \; . \qquad (3.30)$$

The synchro-Compton emissivity of a relativistic (steep) distribution of electrons is:

$$j_{sc} \simeq 8/3 \cdot (\sigma_T / m_e c) \cdot \gamma_t \cdot U_d \cdot U_e \qquad (3.31)$$

where γ_t is the Lorentz factor of the electrons at the self-absorbed frequency (eq. 2.13, 2.14, 2.15) and U_e is the energy density in relativistic electrons. If H_c is the coronal scale-height, the ratio between the synchro-Compton radiation density and the thermal radiation density emitted from the disk is equal to:

$$U_{sc}/U_d \simeq 4 \cdot 10^4 \cdot \epsilon_{0.1}^{13/12} \; \dot{m}^{13/12} \; M_8^{1/12} \cdot (U_e/U_d)^{7/6} \cdot (H_c/r_G)^{7/6} \qquad (3.32)$$

where $U_{sc} = j_{sc} \cdot (H_c/c)$. So, to produce a non-thermal synchro-Compton flux which is comparable with the thermal flux, the necessary energy density in relativistic electrons is only a small fraction of the disk energy density: $U_e/U_d \simeq 10^{-3}$.

III.4) Radiation tori

The theory of low-viscosity, non self-gravitating thick accretion disks which are in hydrostatic equilibrium beyond their inner radius has been developed in the last few years by Jaroszynski, Abramowicz & Paczynski (1980), Paczynski & Wiita (1980), Abramowicz, Calvani & Nobili (1980), Wiita (1982). In the following we will make use of a pseudo-Newtonian potential of the form:

$$\phi(r,z)=-GM/(R-r_G) \tag{3.33}$$

where $R=(r^2+z^2)^{1/2}$. It has been pointed out by Paczynski & Wiita (1980) that an ad-hoc potential of this form does mimick the essential features of a Schwarzschild spacetime with regard to accretion flows. In fact, the specific angular momentum and binding energy of a test particle in a Keplerian orbit (in the equatorial z=0 plane) are given by:

$$l_k(r)=(GMr)^{1/2}\cdot r/(r-r_G) \tag{3.34}$$

and

$$e_k(r)=0.5GM(r-2r_G)/(r-r_G)^2 \quad . \tag{3.35}$$

Hence:

$$dl_k/dr=0.5(GMr)^{1/2}\cdot(r-3r_G)/(r-r_G)^2 \tag{3.36}$$

and

$$de_k/dr=-0.5GM(r-3r_G)/(r-r_G)^3 \quad . \tag{3.37}$$

Both l_k and e_k are non-monotonic functions of r, their derivatives changing sign at $r=3r_G$. Orbits are bound ($e_k>0$) if $r>2r_G=r_{mb}$ and stable ($dl_k/dr\geq 0$) if $r\geq 3r_G=r_{ms}$. At r_{ms} we have the

minimum angular momentum and the maximum binding energy (see figure 8). These effects are just like those in a Schwarzschild metric. The maximum efficiency of energy conversion is : $\epsilon=e/c^2=6.25\%$ at r_{ms}, compared with the correct value 5.72%.

The nucleus of the theory is in the study of the dynamical equilibria of non self-gravitating perfect fluids in pure rotation around black holes, discussed by Fishbone & Moncrief (1976), Abramowicz, Jaroszynski & Sikora (1978), Chakrabarti (1985).

The hydrostatic equilibrium equations read:

$$1/\rho \frac{\partial p}{\partial r} = -\frac{\partial \phi}{\partial r} + l^2/r^3$$
$$1/\rho \frac{\partial p}{\partial z} = -\frac{\partial \phi}{\partial z} \qquad (3.38)$$

Here, again, it is assumed $v_\varphi \gg v_r$ and $v_\varphi \gg v_z$ so the convective term is zero. The shape and equilibrium structure of the rotating ring can be computed by assuming a barotropic equation of state: $p=p(\rho)$. With this simplification, the specific angular momentum is constant on cylinders centred about the rotation axis: $l(R)=l(r)$ (von Zeipel's theorem) and the hydrostatic equilibrium equation can be integrated to yield:

$$\phi_{eff}(r,z)=GM/(R-r_G)+\int(l^2/r^3)dr \qquad (3.39)$$

where ϕ_{eff} is the total (gravitational plus centrifugal)effective potential $\phi_{eff}=\int dp/\rho$. Now, if one specifies *a priori* the distribution of specific angular momentum $l(r)$, the shape of the equipotential surfaces $\phi_{eff}=$const can be determined (it has been actually shown by Jaroszynski, Abramowicz & Paczynski (1980) that the shape of a torus does depend only on the *surface* distribution of angular momentum, and can be determined without explicit knowledge of the equation of state. However, self-consistency checks (such as the assumption of negligible

self-gravity) of the model do require an investigation of the interior structure).

We take the boundary condition on the surface of the torus, defined by h(r), to be the vanishing of the effective potential there. Then, by specifying the rotation law l(r), the inner edge r_{in} and the height at r_{in}, the shape of the disk can be computed.

Consider, from simplicity, a power-law distribution of angular momentum of the form: $l(r)=l_k(r_{in})\cdot(r/r_{in})^{2-q}$, such that rotation is keplerian at the inner edge r_{in} of the torus and at the pressure maximum r_c located in the equatorial plane within a few gravitational radii (see figure 8). Inside r_c rotation is faster than Keplerian, and the excess centrifugal force is balanced by an inward directed pressure gradient. Outside r_c the situation is reversed, with pressure force pointing outward and adding to the deficient centrifugal force. Material is allowed to remain in stable circular orbits inside r_{ms} but outside the marginally bound orbit r_{mb} (this is because surfaces whose inner edges lie inside this radius are open at infinity).

However, for $r_{mb} \leq r \leq r_{ms}$, the binding energy is reduced from its maximum value at r_{ms}, reaching zero at r_{mb}. In general, then, thick tori will be less efficient converter of rest mass to radiation than thin accretion disks.

At the inner radius r_{in}, a *cusp* forms in the equipotential surface (i.e. a critical equipotential surface which crosses itself). Material at the cusp will rotate in a keplerian unstable circular orbit. If material fills this equipotential surface, the cusp will act as a Lagrangian point in a mass-transferring binary, and a mechanism like the Roche-lobe overflow will cause dynamical mass-loss through the inner edge. Inside the cusp, in fact, the angular velocity is sub-Keplerian and matter will spill over into

the hole; the assumption of hydrostatic equilibrium clearly breaks down close to the cusp, where a transition occurs from a subsonic inward drift to a supersonic, nearly-radial free-fall (Abramowicz and Zurek 1981).

Close to the rotation axis hydrostatic equilibrium is not possible; a hollow axial region or "funnel" forms, with its walls supported by centrifugal acceleration. Matter in the vortex funnel (which becomes a paraboloid for a flow with l=const) will either fall into the hole on a dynamical timescale or will be expelled to infinity by radiation pressure. The very existence of this region of non-stationarity is a general relativistic effect: no stationary axisymmetric flow pattern can extend too close to the rotation axis of a black hole due to the finite extent of the relativistic potential barrier. Particles whose angular momentum is below threshold will plunge directly into the hole.

Radiation-pressure support and electron scattering opacity (as in the inner regions of α-disks) allow us to compute the flux radiated from the known surface of the torus. If the disk atmosphere is in radiative and hydrostatic equilibrium, the critical flux emitted per unit area is:

$$F_r(r)=-c/k_T \cdot g_{eff}(r)=-c/k_T \cdot (-\nabla\phi + \Omega^2 r) \qquad (3.40)$$

where g_{eff} is the effective gravity vector (including the centrifugal force) which is perpendicular to the surface of the disk.

Consider, for simplicity, a disk rotating in a Newtonian potential and having a conical shape $z=r\cdot tg\vartheta$, where ϑ is the angle the surface of the disk makes with the radial direction. The effective gravity is then: $g_{eff}=GMr^{-2}\cdot\cos^2\vartheta\cdot tg\vartheta$, and integrating the critical flux over the entire surface, we have:

$$L=2\cdot\int_{r_{in}}^{r_{out}} c(k_T r^2)^{-1}\cdot GM\cos^2\vartheta\cdot tg\vartheta\cdot(2\pi r dr/\cos\vartheta)=L_E\sin\vartheta\cdot\ln(r_{out}/r_{in})\ . \tag{3.41}$$

where the factor 2 arises from the simmetry. It is clear that the emitted luminosity can exceed the Eddington limit by a large amount if the conical funnel is extended and narrow enough.

The logarithmic dependence on the ratio r_{out}/r_{in} and the possibility of super-Eddington luminosities are general characteristics of radiation tori. The logarithmic enhancement of L over L_E occurs in fact in the funnel region which surrounds the rotation axis. The funnel is supported by the centrifugal force rather than by gravity; the large radiative pressure gradient necessary to balance against rotation enables $L/L_E \gg 1$.

The correct argument involving differential rotation has been given by Abramowicz, Calvani & Nobili (1980). It is found that it is the shear term $\propto (d\Omega/dr)^2$, which increases the luminosity over L_E, while the vorticity term $\propto (dl/dr)^2$ acts to reduce it. Vorticity-free (l=const), big shear configurations can then radiate the highest luminosity.

The intense radiation field emitted deep in the funnel might easily accelerate low-binding energy material from the walls. The steep funnel would then naturally endenger and collimate a pair of jets in opposite directions (Lynden-Bell 1978, Abramowicz & Piran 1980). Basically, narrower funnels are associated with fatter tori.

Realistic thick accretion disks will resemble toroidal figures in dynamical equilibrium if the radial inward drift is dynamically unimportant, or, more in general, if departure from hydrostatic equilibrium are small. In analogy with the approximate relationship given for thin disks in eq. (3.9), we can write :

$$v_\varphi \approx (h/r)v_s \approx v_s \quad ; \quad v_r \approx v_z \approx \alpha(h/r)^2 v_\varphi$$

so, because the disk is now geometrically thick, $(h/r)\approx 1$, the condition of subsonic poloidal motion implies a tighter constraint on the magnitude of the viscosity: $\alpha \ll 1$.

Within a thick torus there is no *local* energy balance because the generated heat can be transported both in the radial and in the vertical direction. However, there must be *global* mass, energy and angular momentum conservation. Integrating the critical flux over the entire surface we can find the emitted luminosity, as we have seen (eq. 3.40,3.41). To compute the luminosity generated in the torus we must integrate the total rate of dissipation in a cylindrical shell: $Q(r)dr = G(d\Omega/dr)dr$ between the inner and outer radii:

$$L_g = -\int_{r_{in}}^{r_{out}} \dot{M}(l(r)-l_{in})(d\Omega/dr)dr \qquad (3.42)$$

assuming dissipation and torques due to vertical shear to be negligible. The integration yields:

$$L_g = \dot{M}\left[e_{in} - e_{out} - \Omega_{out}(l_{out}-l_{in})\right] \quad . \qquad (3.43)$$

This formula is not symmetric with respect to the inner and outer edges because the torque at the inner edge vanishes, whereas it is non zero at the inner edge. For large tori, $\Omega_{out} l_{out} \to 0$ and $e_{out} \to 0$, and one has approximately that $L_g = \dot{M} e_{in}$. Of course, as $r_{in} \to r_{mb}$, $e_{in} \to 0$, and extremely large accretion rates ($\dot{M} \to \infty$) are necessary to support a torus with a given luminosity.

It is also obvious (eq. 3.42) that viscous torques do not generate any dissipation in a torus with a constant specific angular momentum distribution. At this point one generally assumes that there are no additional sources of energy (such as, e.g.

nuclear burning) a part from viscous dissipation and that negligible internal energy is advected in and out the torus. In this case the local thin disk energy balance $Q=2F_r$ can be replaced by a global condition $L_g=L$ and we can solve for the accretion rate $\dot{M}$. The knowledge of $\dot{M}$ allows us to give an a posteriori estimate of the viscosity α which is necessary to drive the accretion flow. From the definition of viscous torque (3.7) and eq. (3.8) we can solve for the average kinematic viscosity :

$$\nu=\dot{M}(1-l_{in})\cdot(2\pi r^3\Sigma)^{-1}\cdot(-d\Omega/dr)^{-1} \qquad (3.44)$$

and compute the dimensionless α-parameter at, e.g the pressure maximum r_c :

$$\alpha=\nu\Sigma/(v_s\bar{\rho}\,h^2)\approx 4\nu\Sigma/(p_c^{1/2}\rho_c^{1/2}\cdot h^2) \quad . \qquad (3.45)$$

Here p_c and ρ_c are the pressure and density at r_c, with $\bar{\rho}=(1/2)\rho_c$ as a reasonable estimate.

The very viability of some thick disk models has been recently put under question by the discovery (Papaloizou & Pringle 1984, 1985) that non-accreting tori are subject to global, non-axisymmetric dynamical instabilities. Work on understanding the physical causes of the instability has been focused on geometrically simple configurations, in particular slender tori and two-dimensional annuli (see Blaes 1986 and references therein). In the linear regime it is found that the quickest and most violent unstable modes are stabilized by steep angular momentum gradients (Goldreich, Goodman & Narayan 1986). Recent non linear calculations by Blaes & Hawley (1987) do show the stabilizing effect of specific angular momentum gradients; the angular momentum redistribution that is driven by the instability results in configurations which can be characterized by a

power-law angular momentum distribution. Disks with greater radial thickness saturate with flatter rotation laws. Moreover, disks with inner edges that overflow the potential cusp are quickly stabilized by the accretion flow (Blaes 1987).

The emission spectra of radiation tori and their relevance to active galactic nuclei will be the topics of the next chapter.

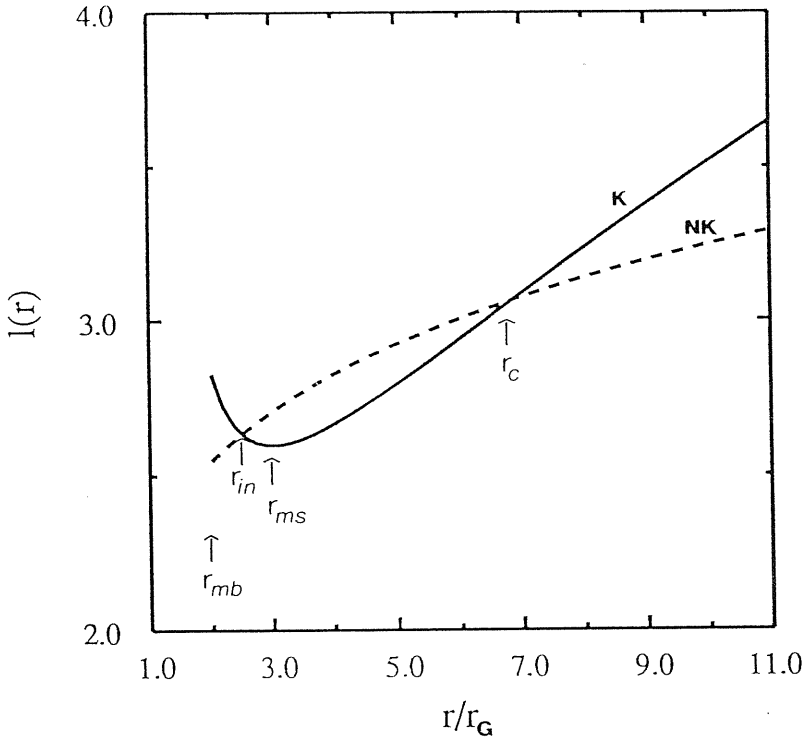
4.0
3.0
2.0
l(r)
K
NK
r_c
r_{in}
r_{ms}
r_{mb}
1.0
3.0
5.0
7.0
9.0
11.0
r/r_G

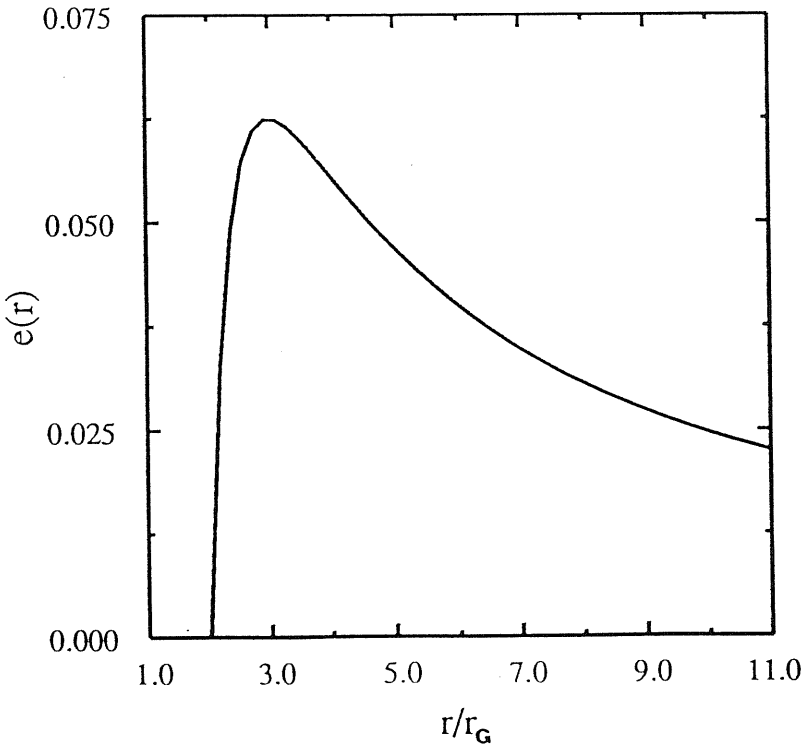
0.075
0.050
0.025
0.000
e(r)
1.0
3.0
5.0
7.0
9.0
11.0
r/r_G

figure 8

a) The specific angular momentum distribution (in units of $\sqrt{2}\,GM/c$*) for a pseudo-Newtonian potential.*

Solid line: the Keplerian distribution in the equatorial plane $z=0$.

Dashed line: a non-Keplerian distribution of the form $l(r)=l_k(r_{in})\cdot(r/r_{in})^{2-q}$, *with* $r_{in}=2.5\ r_G$ *and* $q=0.15$.

r_{in} = *location of the inner radius of the torus*

$r_{mb}=2\ r_G$ = *last marginally bound orbit*

$r_{ms}=3\ r_G$ = *last marginally stable orbit*

r_c = *location of the pressure maximum of the torus*

b) The distribution of Keplerian specific binding energy (in units of c^2*) for test particles orbiting in the equatorial plane. The binding energy is a maximum* $e_{max}=0.0625$ *at* r_{ms}. *At* r_{mb}, *it is* $e(r_{mb})=0$.

CHAPTER IV : RADIATION TORI AND THE UV/X EXCESS IN QUASARS

IV.1) The thermal bump

The 10-0.1 μm continuum of quasars and Seyfert galaxies can be decomposed into a single power-law $F_\nu \alpha \nu^{-\alpha}$,with α~1, plus a superimposed "bump" in the blue and near UV (Neugebauer et al 1979, Richstone & Schmidt 1980).

This optical/UV excess above the extrapolated non-thermal IR continuum has been attributed by Shields (1978) and later by Malkan & Sargent (1982) to a thermal component which peaks at ultraviolet frequencies and is approximately described by a single-temperature blackbody with $T \sim 2\text{-}3 \cdot 10^4$ K . It was argued by Shields (1978) that an accretion disk around a massive $\sim 10^9 M_\odot$ black hole could dominate at optical frequencies over the non-thermal power law and thus explain the flattening in the blue observed in quasar spectra. In a study of a sample of 8 Seyfert 1 and QSOs, Malkan & Sargent (1982) have shown that in at least the five more luminous objects an additional blackbody-like component is necessary to fit the spectra.

This component (lately named the *big bump* by Elvis & Lawrence 1985) does flatten the continuum starting at around 5500Å and must not be confused with the *little bump* which is a bend in the spectra at around 3500Å that is convincingly explained as a combination of Balmer continuum emission and a blending of hundreds of broad, permitted FeII lines (Wills, Netzer & Wills 1985). The optical/UV spectra would steepen at frequencies above

$\sim 2 \cdot 10^{15}$ Hz because of the exponential cut-off of this thermal component.

Much interpretative work has been devoted to geometrically thin disk accreting mass at a subcritical rate, i.e. $\dot{m} \ll 10$. In the blackbody approximation and in a pseudo-Newtonian potential, the maximum accretion disk temperature:

$$T_{max} = 6.3\ 10^{4} \cdot \dot{m}^{1/4} \cdot M_{8}^{-1/4} \quad K \qquad (4.1)$$

is achieved at $r \approx 5 r_G$ (cf eq. 3.15). The emitted spectrum peaks in the near-UV band, so it was natural to interpret the UV bump seen in quasars as the integrated thermal emission from an accretion disk around a $\sim 10^{8}\ M_{\odot}$ black hole.

Spectral fits with accretion disk models have been performed by Malkan (1983). The single blackbody fits of the IUE spectra of high-z QSOs appearently seem to have too little flux at the highest frequencies. A broader spectral distribution than a single Planck function, like a sum-of-blackbodies accretion disk spectrum, seems to improve the fit.

However, a well defined hump that looks very much like a single blackbody at $T \approx 27{,}500$ K is revealed in a plot νF_{ν} vs ν (Blandford 1984). Blandford (1984) has suggested that radiation tori may have star-like photosphere; this characteristic surface temperature would be determined by He recombination, which changes the material opacity.

It has been recently shown by Elvis et al (1986) that a single power-law of slope $\alpha \sim 1$ could cover five decades of frequencies from IR to X-ray in optically selected (PG) quasars, with the UV thermal component forming a bump on top of it. However, in at least one object, the quasar PG 1211+143, a soft

X-ray excess has been detected at energies ≤1 KeV (Elvis,Wilkes & Tananbaum 1985).

If thermal in origin, this excess would naturally be connected with the UV bump and interpreted as the hot tail of a single, very luminous thermal component with a much higher peak temperature $T_{max} \sim 0.5\text{-}1 \cdot 10^6$ K. More recently, other examples of quasars with soft X-ray excesses have been reported (Singh, Garmire & Nousek 1985, Arnaud et al 1985, Pounds et al 1986).

Observations of the maximum temperature T_{max} are then of great importance for disk models, because it constrains the mass and the accretion rate of the central engine. Thin disk model fits to the UV/soft X-ray excesses require $L \gg L_E$ or,equivalently, $\dot{m} \gg 10$ (Bechtold et al 1987).

The sum-of-blackbodies approximation on which these fits are based is somewhat doubtful. Opacity effects in real disks are very important (see III.2); in the inner regions the electron scattering opacity will strongly modify the blackbody spectrum. At high accretion rates ($\dot{m} \geq 1$), the diffusion approximation is no longer valid (see eq. 3.20) and Comptonization may play a relevant role in the formation of the spectrum.

Modification of the disk spectrum due to opacity effects require higher temperatures to radiate the same luminosity; hence soft X-ray excesses may be produced at much lower accretion rates. However, fuelling rates which exceed the Eddington one, $\dot{m} \geq 10$, are still needed (Czerny & Elvis 1987). In this regime, where radiation pressure is dynamically important, the standard theory of thin disk is no longer appropriate. Under this conditions it is expected that the disk will rather puff up to form a thick radiation supported torus.

Very little work has been done to express the theory of thick

accretion disks in a form suitable for observational scrutiny (for a review, see Abramowicz, Calvani & Madau 1987). Instead, general theoretical arguments have been used to place self-consistency constraints on the models, but these still leave a wide range of possible configurations. In the next section we will compute the thermal emission spectrum of a geometrically and optically thick radiation torus under a number of simplifying assumptions.

We may try to guess a priori what will be the characteristic spectral emission feature of a thick accretion disk; from eq. (3.40), in fact, we know that the critical radiation flux emitted per unit disk surface area does follow the surface distribution of effective gravity. However, the latter is much larger in the funnel, where the dominant contribution in the balance of forces comes from centrifugal acceleration, than in the outer regions which are dominated by the gravitational pull of the hole. Hence the inner regions will be much hotter than the outer ones.

The observed spectrum will be strongly dependent on the inclination angle of the system. Due to the donut shape, occultation of the innermost hottest parts of the torus will occur at large angles between the rotation axis and the line of sight.

It is actually found (Madau 1987) that the inner, very hot and luminous, funnel-shaped region dominates the emission from tori which are viewed more *pole-on*, i.e. at small viewing angles from the symmetry axis of the torus. This gives rise to a UV/soft X-ray thermal component such as that seen, e.g., in the quasar PG 1211+143. On the other hand, tori viewed nearly *edge-on*, i.e. at large viewing angles from the symmetry axis, do appear less luminous and cooler, possibly accounting for the optical/UV bump.

IV.2) The model

In the following we will study the physical properties of a radiation torus (consider as a toroidal, isolated star that is supported by radiation pressure) which is in hydrostatic equilibrium in the gravitational (pseudo-Newtonian) potential of the hole. Cylindrical coordinates (r,φ,z) will be used; the self-gravity of the torus is taken to be negligible (this assumption will be checked a posteriori).

We have to specify a distribution of specific angular momentum per unit mass $l(r)$. The acceptable forms of $l(r)$ are restricted by the requirements of local dynamical stability ($dl/dr\geq 0$) and inward accretion ($d\Omega/dr<0$). Moreover, configurations with a flat distribution of angular momentum may be prone to global, non-axisymmetric instabilities (Papaloizou & Pringle 1984). We will therefore consider a two-parameter angular momentum distribution :

$$l(r)=l_{in}\,(r/r_{in})^{2-q} \qquad (4.2)$$

where l_{in} is the value of the Keplerian angular momentum per unit mass at the cusp radius r_{in}. From eq. (3.39) and (4.2) we can write:

$$\phi_{eff}(r,z)=GM/(R-r_G)+l_{in}^2 r^B/(r_{in}^{B+2}\cdot B) + C \qquad (4.3)$$

where $R=(r^2+z^2)^{1/2}$, C is the integration constant and $B=2-2q$.

The boundary condition at the surface is $\phi_{eff}=0$. The surface of the torus passes through the cusp at $r=r_{in}$ and $z=0$ (the height of the cusp is neglected). We can then derive the integration

constant and write:

$$\phi_{eff}=GM/(R-r_G)-GM/(r_{in}-r_G)+l_{in}\cdot(r^B-r^B_{in})/(r^{B+2}_{in}\cdot B) \quad . \qquad (4.4)$$

On the surface h(r) it is $\phi_{eff}=0$, and the shape of the torus is found to be:

$$h(r)=\left[\left(\frac{(r_{in}-r_G)B\ r^B_{in}-r_G(r^B-r^B_{in})}{(r_{in}-r_G)B\ r^{B-1}_{in}-(r^B-r^B_{in})}\right)^2-r^2\right]^{1/2} \quad . \qquad (4.5)$$

The outer radius r_{out} of the disk can be computed by solving $h(r_{out})=0$:

$$r_{out}=\frac{Br^B_{in}(r_{in}-r_G)-r_G(r^B_{out}-r^B_{in})}{Br^{B-1}_{in}(r_{in}-r_G)-(r^B_{out}-r^B_{in})} \quad . \qquad (4.6)$$

Rather than assuming a value for the exponent q, one can equivalently specify the outer edge of the torus. The shape h(r) will then be fully determined by specifying the inner and outer radii of our disk.

We assume a barotropic equation of state $p=K\rho^\gamma$, with K=const and $p=p_{gas}+p_{rad}$. If β denotes the ratio of gas pressure to total pressure, we have (all the symbols have their usual meaning):

$$p=\left[3k^4\mu^{-4}a^{-1}m_p^{-4}\cdot(1-\beta)/\beta^4\right]^{1/3}\rho^{4/3}$$

$$T=\left[3k\mu^{-1}a^{-1}\cdot(1-\beta)/\beta\right]^{1/3}\rho^{1/3} \qquad (4.7)$$

The gas is taken to be fully ionized, with $\mu=1/2$. A sequence of barotropic models can now be constructed by varying the ratio, β, of the gas pressure to the total pressure. We assume β to be constant throughout the torus (see also Wiita 1982, Abramowicz,Henderson & Ghosh 1983). Radiation-pressure support implies $\beta\ll 1$, subject to the constraints of self-consistency imposed by the conditions of hydrostatic equilibrium and

negligible self-gravity.

The distributions of density and temperature inside the torus are given by:

$$\rho(r,z)=4.82\cdot 10^{12}\beta^4/(1-\beta)\cdot\phi_{eff}^3(r,z) \quad \text{gr cm}^{-3}$$

$$T(r,z)=6.81\cdot 10^{11}\beta\cdot\phi_{eff}(r,z) \quad \text{K} \quad . \tag{4.8}$$

Free boundary conditions, i.e. $\rho=0$, T=0 on the surface, are assumed. It is found that the opacity is dominated by electron scattering. For central temperatures which exceed $T\simeq 10^8$ K, the energy due to nuclear fusion may exceed that due to viscous dissipation.

The assumption that the gravitational potential is determined by the central massive object is valid only if the total mass of the disk M_{disk} is less than the mass of the black hole M. The constraint $M_{disk} < M$ is found to be rather important in building self-consistent models (Abramowicz, Calvani & Nobili 1980, Wiita 1982), actually providing more restrictions that the ones imposed by the onset of gravitational instabilities (which require the density in the disk at radius r to be much less than M/r^3, Paczynski 1978). The total mass of the disk, in units of 10^8 $M_\odot$, is given by:

$$M_{disk,8}=7.85\cdot 10^{12} M_8^3\cdot\beta^4/(1-\beta)\cdot\int_{r_{in}}^{r_{out}} dr \int_0^{h(r)} \phi^3(r,z)\,r\,dz \quad . \tag{4.9}$$

Fully general-relativistic models in which self-gravity is important are currently under study (Lanza 1986).

If the disk atmosphere is in radiative and hydrostatic equilibrium, then the radial dependence of the effective temperature is given by:

$$\sigma T_{eff}^4(r) = \frac{c}{k_T}(1-\beta)\left[\frac{G^2M^2}{(R-r_G)^4} + l^4 r^{-6} - \frac{2GMl^2}{R(R-r_G)^2 r^2}\right]^{1/2} \qquad (4.10)$$

where k_T is the Thomson opacity and the term in the square brackets is the effective gravity.

The total luminosity is calculated by integrating equation (4.10) over the entire disk surface. The ratio L/L_E is proportional to the logarithm of the ratio $Q=(r_{out}/r_{in})$ (see eq. 3.41). For Q>50, I derived:

$$L/L_E \approx 3.8 \log Q - 2.43 \quad . \qquad (4.11)$$

As the inner radius cannot change by much ($2r_G \leq r_{in} \leq 3r_G$), it is the outer radius that really matters. Also, the structure of the disk at small radii is not sensitive to the disk structure at very large radii.

Quantities related to the actual accretion flow through the disk can be estimated by applying the global energy balance condition. It turns out that, for a $\sim 10^8$ $M_\odot$ black-hole, the thickness of the flow at r_{in} -and, consequently, the amount of internal energy swallowed by the hole- is small provided $\beta > 10^{-6}$ (Abramowicz 1985). In this case, the condition of global energy balance enables one to determine, *a posteriori*, the accretion rate, $\dot{M}$, and the viscosity parameter α which are necessary to drive the accretion flow (see III.4).

IV.3) The Spectrum

A thick disk model with parameters : $r_{in}=2.7r_G$, $r_{out}=500r_G$,

$M=10^8 M_\odot$, $\beta=3\ 10^{-4}$, is investigated in the rest of the chapter. The actual size of the disk is then $\sim 10^{16}$cm, much smaller than the estimated radius $\sim 10^{17}$cm of the broad emission line region in quasars (Gondhalekar,O'Brien & Wilson 1986). Table 2 summarizes the relevant quantities of the model. The subscript "c" denotes values computed at the pressure maximum $r_c \simeq 8.4 r_G$. In a thick disk, most of the energy is released around r_c. The adopted value of the parameter β corresponds to a massive torus with a large optical depth. In this case the pressure scale-height is much smaller than the disk thickness and the atmosphere is very thin (see Blandford 1985). The dimensionless accretion rate is $\dot{m} \simeq 100$.

As electron scattering provides most of the opacity inside the torus, the emergent photons are thermalized on the surface where the effective absorption optical depth $\tau_* = \{\tau_{ff}(\tau_{ff}+\tau_T)\}^{1/2}$ is unity, τ_T and τ_{ff} being the electron scattering and free-free optical depth ,respectively. For sufficiently high frequencies, scattering dominates free-free absorption and the photosphere lies well below the last scattering surface, as shown in figure 9.

In figure 10 the effective temperature distribution given by eq. (4.10) is depicted. Similarly to what is found in thin disk models, the effective temperature has a sharp peak at a radius $r \simeq 4 r_G$, which is well inside the funnel. It then decreases roughly as $T_{eff} \propto r^{-2/3}$ in the region where the balance of forces is dominated by the centrifugal acceleration term l^2/r^3, and finally becomes constant in the outer region, where pressure gradients balances against gravity and the isobars are almost spherical. For comparison, the effective temperature distribution for a thin disk model with same values of M and $\dot{M}$ is also shown.

To include the effect of Thomson opacity on the spectrum, a homogeneous, isothermal atmosphere is assumed here (Shakura &

Sunyaev 1973). Then, since $k_T \gg k_{ff}(\nu)$, the emergent specific intensity is given by:

$$I_\nu = 3.2\cdot10^{-15} T_s^{11/4} \{\beta/(1-\beta)\}^{1/2} x^{3/2} e^{-x} (1-e^{-x})^{-1/2} \qquad (4.12)$$

where $x=h\nu/KT_s$. The total modified blackbody flux is:

$$F=3.2\cdot10^{-4} T_s^{15/4} \{\beta/(1-\beta)\}^{1/2} . \qquad (4.13)$$

The surface temperature T_s derived by combining eq. (4.10) and (4.13) is appreciably higher than the effective temperature T_{eff}; the emitted spectrum is therefore harder than that of a simple sum-of-blackbodies.

It is important to note the weak dependence of the temperature T_s on the parameters :

$$T_s \propto M^{-4/15} \beta^{-2/15} .$$

Any change of β will affect the temperature and density profiles, and the location of the photosphere will vary as well, keeping the temperature T_s almost constant, independently of β (cf Begelman 1985). The scaling of the viscosity parameter α with β ($\alpha\propto\beta^{-4}$) is such that the temperature of the photosphere will be very weakly dependent on α.

A detailed analysis of the spectral regime can be performed a posteriori. Consider first the frequency ν_o at which the scattering and absorption coefficients are equal: for $x>x_o=h\nu_o/kT_s$ electron scattering will modify the emission spectrum. For the model considered here it is $x_o\simeq10^{-2}$, so scattering is indeed important over most of the spectrum. The frequency ν_c for which Compton upscattering of photons becomes important is defined by $y(\nu_c)=1$, where $y(\nu)$ is the frequency dependent Compton parameter (Rybicki & Lightman 1979):

$$y(\nu)=4kT_s\cdot\tau_T^2(\nu)/(mc^2) \quad . \tag{4.14}$$

Here $\tau_T(\nu)$ is the electron scattering optical depth between emission and escape from the medium, so it is measured from an effective absorption optical depth, $\tau_*(\nu)$, of order unity. Comptonization will affect the emerging radiation significantly for $x \geq x_c=h\nu_c/kT_s$; if $x_c \ll 1$, inverse Compton will go to saturation and a Wien peak will be produced around $3kT_s$. For the model considered here it is $x_c \geq 1$, thus inverse Compton scattering may be neglected since the majority of photons undergo coherent scattering.

For an observer at a distance D, the flux at frequency ν from the disk is given by:

$$F_\nu = \frac{1}{D^2}\int_\Sigma I_\nu(n)\ n\cdot N\ d\Sigma \tag{4.15}$$

where N is the outward normal to the surface area element $d\Sigma=r\cdot[1+(dh/dr)^2]^{1/2}\ dr\ d\varphi$, and n is the direction of the line of sight. We assume that the surface of the disk radiates isotropically, I(n) independent of n for $n\cdot N>0$.

Let us specify a line of sight in the plane $\varphi=\pi/2$ and denote with ϑ_o the angle between the line of sight and the rotation axis. Represented in the Cartesian coordinates (X,Y,Z), with the Z axis being the symmetry axis of the system, the unit vectors can be written as:

$$n=y\sin\vartheta_o+z\cos\vartheta_o \quad ; \quad N=x\sin\vartheta\cos\varphi+y\sin\vartheta\sin\varphi+z\cos\vartheta$$

and we have $I_\nu(n)=0$ for $n\cdot N\leq 0$.

The self-shadowing of the disk must be taken into account. Geometrical thickness causes, in fact, occultation of the innermost (and the hottest) regions for high-inclination systems.

Consider the element of area at the point $P_o \equiv (r_o, \pi/2, z_o)$ on the surface of the funnel, whose outward normal N_o is perpendicular to the line of sigh, and denote with R the vector connecting P_o to a generic point $P \equiv (r, \varphi, z)$ on the funnel walls:

$$N_o = -y\cos\vartheta_o + z\sin\vartheta_o \quad ; \qquad R = x r\cos\varphi + y(r\sin\varphi - r_o) + z(z - z_o) \quad .$$

The condition $R \cdot N_o = 0$ yields the range of integration over φ in eq. (4.15), which is obviously limited by the eclipsing effect .The observed disk spectrum will then strongly depend on the viewing angle ϑ_o.

The resulting disk spectrum is shown in figure 11, where the specific luminosity $4\pi D^2 F_\nu$ is plotted versus the frequency ν for different inclination angles. As expected from figures 9 and 10, disks seen more edge-on ($\vartheta_o \simeq 90^\circ$) look cooler and underluminous, the observed bolometric luminosity being only a fraction ~1/10 of the total energy output. Since the temperature in the outer parts of the disk is roughly constant, the spectrum is approximately that of a single-temperature modified blackbody. In the model considered here it peaks at log ν~15.3 (1500 Å) and then falls off exponentially. The temperature of the outer regions, however, does depend on the particular choice of the outer edge of the torus. The logarithmic enhancement of the emitted luminosity with increasing r_{out} (eq. 4.11) actually occurs mainly in the inner regions. The luminosity of the outer, spherical body of the torus is always close to ~L_E. The outer temperature then scales as $T_{out} \propto r_{out}^{-1/2}$.

At smaller inclination angles, the funnel region becomes more and more visible. The hottest parts of the disk start contributing to the integrated spectrum, which therefore hardens and flattens at high frequencies, the spectral turnover always occurring

between ~1500-1200 Å. The dependence on the inclination angle of the observed luminosity at a given frequency $\bar{\nu}$ is depicted in figure 12 for $\log\bar{\nu}$=15.5, 16, 16.5,and 17. The self-shadowing of the disk has a dramatic effect at the highest frequencies. The curves rise steeply up to the point where the angle ϑ_o is roughly equal to the funnel opening angle $\psi\approx 20^\circ$and most of the innermost regions become visible, then flatten at smaller angles. Soft X-ray emission is observed only at inclination angles smaller than ψ, the associated probability P=1-cosψ being equal to ~8% for the model considered.

In these calculations we have neglected the relativistic effects on the propagation of radiation from the disk, namely the Doppler shift, the gravitational redshift and the gravitational focusing effect. For a thin disk around a Schwarzschild hole these are minor effects except for an observer near the equator, who sees radiation from the innermost regions to be blueshifted and strongly focused (Cunningham 1975). This enhancement cannot be directly observed in thick accretion disks because of the strong eclipsing effects at and near the equatorial plane. However, it will affect somewhat the flux of radiation falling on the funnel surface. The problem of scattered radiation will be discussed in detail in the next section.

IV.4) The reflection effect

So far mechanical equilibrium between gravity, centrifugal force and pressure of the outgoing radiation has been assumed. However, when we consider the funnel surface, the incoming

radiation from the other parts of the funnel must be included in the balance of forces, the local effective gravity determining in this case the net radiative flux perpendicular to the surface (Sikora 1981).

Within the funnel, in fact, each photon will in general scatter many times before escaping either to infinity or falling down into the black hole. As a result of multiple scatterings, the surface brightness will be much larger than the net flux. If the opening solid angle of the funnel is Ω, then the surface brightness will be enhanced by a factor $\leq 2\pi/\Omega$ (it would be equal to $2\pi/\Omega$ in the limiting case where all the photons emitted in the funnel were collimated within an angle Ω).

It is then important to include this *reflection effect* in our calculations, to get the correct angle-averaged radiation luminosity. In the following we will assume an empty funnel in which the radiation is scattered isotropically off the surface elements of the disk. This does imply that the local thermal state of the emitting material at $\tau_*=1$ is not modified by the incoming flux. This is a reasonable approximation because we have seen that, in the conditions envisaged, the Thomson opacity dominates at frequencies $x \geq 10^{-2}$; hence most of the photons are thermalize well below the last scattering surface . Low energy incoming photons, however, will be absorbed in the upper atmospheric layers and the local temperature of the emitting gas will increase.

Newtonian approximation will be used in the following.

The balance of forces normal to the surface is now given by the integral equation:

$$F_e(r) - F_{in}^N(r) = c/k_T \cdot g_{eff}(r) \qquad (4.16)$$

where F_e is the sum of the flux which is locally generated and

the flux which is scattered isotropically and F^N_{in} is the normal component of the incoming flux:

$$F^N_{in}=1/\pi \int F_e R\cdot N \, d\Omega \qquad (4.17)$$

where $d\Omega$ is the element of solid angle associated with the direction R within which the incoming radiation is seen at the given point. It is the integral term which takes into account the radiative interaction between different zones of the funnel.

The distribution of emitted flux F_e has been obtained (see also Sikora 1981) by subdividing the surface of the funnel into a large, finite number of emitting rings and by approximating eq. (4.16) as

$$F_{e,i} - 1/\pi \sum_j B_i^j F_{e,j}=c/k_T \cdot g_{eff,i} \qquad (4.18)$$

We have then to solve the set of linear algebraic equations which results from equation (4.18). The elements of the diagonally dominant matrix B_{ij} represent the fraction of the radiation emitted from the jth ring which reaches the ith ring.

Consider a pair of points (P_i, P_j) respectively on the ith and jth ring and denote with N_i and N_j the outwar normal vectors to the surface area elements at those points. We can then write:

$$B_{ij}=\int_{\Omega_{ij}} \frac{(N_i\cdot R)}{|R|} \, d\Omega \qquad (4.19)$$

where R is the vector connecting P_i to P_j and Ω_{ij} is the solid angle within which an observer located at the ith ring sees the jth ring. The solid angle element is:

$$d\Omega=\frac{(N_j\cdot R)}{|R|^3} d\Sigma_j=\frac{(N_j\cdot R)}{|R|^3} r_j\cdot[1+(dh/dr)_j^2]^{1/2} d\varphi \, \Delta r \qquad (4.20)$$

where Δr is the mesh-size. A grid of 350 points has been used to

approximate eq. (4.16). The integration over φ in eq. (4.19) can be performed analitically using elementary functions. However, self-shadowing of the funnel surface, which again limits the range of integration over φ in eq. (4.19), must be taken into account.

A substantial increase of the surface brightness results, as may be seen in figure 13 for the model of radiation torus considered above. It is important to stress that the tangential components of the external radiative force are left unbalanced. This will have little effect on the equilibrium structure at large optical depths, but strict hydrostatic equilibrium will not be maintained in a surface layer of thickness $\leq 1/\rho k_{es}$ (Nityananda & Narayan 1982). Upward acceleration of the funnel walls will occur; the outflowing matter will probably carry away, in the optically thin case, a particle luminosity $\leq L_E$ (Narayan,Nityananda & Wiita 1983).

We have assumed, in fact, that the mass outflow does not make the funnel optically thick and ignored any modification of the radiation field by the moving walls. To compute how the multiple scatterings of photons do modify the spectrum of the disk, equation (4.18) has to be solved at each frequency, the local specific intensity being given by equation (4.12).

The resulting spectrum is shown in figure 14 for different inclination angles; comparison with figure 11 clearly shows the luminosity enhancement due to the multiple reflections. The dependence of the observed specific luminosity on the viewing angle is depicted in figure 15. The hard photons emitted in the innermost regions of the disk, regions which are shadowed for high inclination angles, will be scattered by the funnel walls into the line of sight. That is why the self-occultation effect at the highest frequencies is less pronounced than in figure 12. In

particular, soft X-ray emission will be observed now at viewing angles which are much larger than Ψ, up to $\vartheta_o \approx 50^o$. In this case we should expect to see a fraction of soft X-ray emitting sources of about ~35%.

The luminosity emitted per logarithmic frequency interval is plotted in figure 16 in the case of face-on view ($\vartheta_o = 0^o$). In the same figure the emission spectra of a thin disk and of a radiation torus without the inclusion of the reflection effect are shown for comparison.

IV.5) Conclusions

The nature and the shape of the ultraviolet continuum in quasars are debatable. There are strong evidences that a large fraction of the luminosity emitted by active nuclei is produced in the ultraviolet band, maybe well beyond the Lyman edge. Thermal emission from an accretion disk is an attractive, although not unique, explanation.

Thin accretion disk models are very popular; spectral fits in the simple sum-of-blackbodies approximation have been performed by Malkan (1983), who has interpreted the steepening of the UV continuum shortward of λ~1500 Å as the exponential cut-off of the thermal spectrum. However, the basic problem with this interpretation is that this portion of the spectrum concides with the natural scale energy of atomic physics and strong absorption by the gas along the line of sight is likely to occur.

In fact, IUE observations of moderate redshift ($1 \leq z \leq 2$) quasars (Bechtold et al. 1984) show a redshift-correlated

steepening in the continuum at about ~1200 Å, from a power-law in the optical $\alpha_o \approx 0.5$ to $\alpha_L \approx 3\text{-}5$ shortward Lyα. This probably arises from Lyman continuum absorption by intervening neutral H along the line of sight.

Recent high-resolution observations of very high-z QSOs ($z \geq 2.7$, Steidel & Sargent 1987) do indicate that the steepening in the continuum slope shortward Lyα is not intrinsic to the quasar but is due to the effect of blanketing of Lyα, Lyβ, Ly continuum absorption by a cosmological distribution of intervening ,neutral Lyα clouds (see also I.4). This is consistent with the absence of a turnover in $z<0.5$ objects (Kinney et al. 1985). The apparent steepening observed in IUE low-resolution spectra would then be completely unrelated to the intrinsic continuum of the hypothetical accretion disk; the inferred blackbody peak temperature $T \approx 30{,}000$ K would be then too low and just reflect the absorption cut-off at Lyα.

In principle, it might be possible to use the observed relative strengths of optical and UV emission lines to infer informations about the extreme-UV continuum shape (for a critical discussion, see Krolik 1986). The problem with emission line diagnostics is basically that the ionization parameter (i.e. the ratio of the ionizing photon density to the gas density) is much more important than the exact shape of the ionizing spectrum (provide it extends above the relevant ionization thresholds) in determining the line ratios. A grid of photoionizing models computed by Kallman & Krolik (1987) using three different UV spectra (a *bare power-law*, a 10 *eV bump* and a 80 *eV bump*) gave undetermined results, the relative fluxes of many emission lines being rather insensitive to the input spectrum.

The observed UV spectrum might also be too steep and too

faint to produce the total emission-line flux, as recently pointed out by Netzer(1985). An energy budget problem actually arises from standard photoionization models; apparently, the total line emission and Balmer continuum flux is about 8 times the Lyα flux (in case B recombination, the number of Lyα photons escaping the cloud equals the number of ionizing photons absorbed by it). Again, a much flatter intrinsic Lyman continuum ($\alpha<0.4$) might be required.

Observational determinations of the frequency where the thermal component peaks are thus very uncertain. In this respect, the extreme cases of disk spectra extending up to the highest frequencies may be represented by those quasars (such as PG 1211+143, Mkn 335,Mkn 841) with a large excess of soft X-ray emission above the extrapolation of the >2 Kev power-law spectrum. This soft X-radiation would be emitted from the innermost parts of the disk, while the optical/UV continuum would originate in the outer, cooler disk regions. The interpretation of this excess as the hot ($T\leq 10^6$K) tail of the accretion disk spectrum, besides making this UV/X feature dominate the luminosity of the source, requires highly super-Eddington accretion rates.

Opacity effects in more realistic thin disk models have been recently explored by Czerny & Elvis (1986). These effects strongly modify the simple sum-of-blackbodies spectrum, making it harder and so alleviating the super-Eddington problem. These authors explain the observed spectral flattening at ~1500 Å as being due to the onset of electron scattering, and they also discuss the importance of occultation effects. However, these models still require $L \geq L_E$, i.e. they imply an accretion regime in which radiation-supported tori, rather than thin accretion disks, are expected to form.

We were then led to investigate a thick disk model which depends on the following parameters: the black-hole mass M, the angular momentum distribution l(r) (which in turn determines $\dot{M}$) and the ratio of the gas pressure to the total pressure β. We have computed the resulting thermal emission spectrum; opacity effects due to coherent electron scattering have been taken into account. More importantly, the self-shadowing and the multiple reflection effects have been self-consistently included.

A striking dependence of the spectrum on the viewing angle of the observer is found. Different inclinations result in a range of apparent luminosities and color temperatures, the UV continuum being flatter for increasing luminosities. If the IR power-law is a distinct component (as variability data suggest, see Cutri et al. 1985) and it is emitted isotropically, the thermal to power-law flux ratio increases for decreasing viewing angle, and an anti-correlation between the optical/UV luminosity and the IR/optical continuum slope is expected. The existence of such a correlation has been recently suggested by Wandel (1987).

Within this model, it is then natural to interpret optical/UV bumps peaking at $\lambda \leq 1500$ Å as due to thermal emission from thick accretion disks seen almost equator-on ($\vartheta_o = 90^\circ$). Soft X-ray emission would be observed at small inclination angles.

As a result of multiple scatterings of photons off the funnel walls, the surface brightness in the funnel is greatly enhanced. The distribution of luminosity at infinity is such that, along the rotation axis, the effective luminosity exceeds the Eddington limit by more than a factor of twenty, which is four times the luminosity averaged over all angles (see figure 17). At inclination angles which are smaller than the funnel opening angle Ψ, luminosities of order 10^{47} erg/sec will be observed from thick

accretion disks orbiting black hole of mass only $\sim 5 \cdot 10^7 M_\odot$!

Some of the implications of an anisotropic ionizing continuum for photoionization models of the BLR have been recently discussed by Netzer (1986). Generally speaking, line emitting clouds at small inclination angles would be subject to a stronger ionization flux and so emit mostly high-excitation lines compared with clouds near the equatorial plane, which would emit mainly low-excitation lines. The angular dependence of the ionization parameter and of the covering factor would be a critical feature of the model. Physical parameters of the BLR could crucially differ from previous standard estimates.

The strong soft X-ray emission observed nearly pole-on could actually inhibit the very formation of clouds near the disk rotation axis. In the standard two-phase instability model (Krolik, McKee & Tarter 1981) a steep soft X-ray spectrum would not lead to the formation of a two-phase medium, with cold ($\sim 10^4$K) line emitting clouds being pressure-confined by a hot ($\sim 10^8$ K) intercloud medium, the hot-phase temperature being determined by the balance of Compton heating and cooling (Guilbert,Fabian & McCray 1983). Now, if one assumes power-law emission in the X-ray band to be spherically symmetric, cooling dominates heating at small angles and no two-phase medium is formed. A BLR would thus form only at high inclination angles (Fabian et al 1986, Bechtold et al 1987).

Soft X-ray excesses have been observed in radio-quiet, optical bright QSOs. It has already been suggested by Blandford (1984) that in a simplified unified scheme for different types of active galaxies, controlled by the parameters $\dot{m}$-M, radio-quiet QSOs may be identified with supercritical accreting tori. The geometrical effect of the absorption of primary ionizing photons

by a toroidal thick configuration has been invoked for radio-quiet QSOs as a possible explanation for the presence of strong nuclear Fe II optical lines (Boroson, Oke & Persson 1985, see also I.1). Basically, radio-quiet QSOs (and compact flat spectrum objects) have stronger Fe II emission lines than steep-spectrum extended radio quasars.

A possible explanation is that the optically thick torus which we suggest may power the radio-quiet QSOs (and which may produce and collimate a radio-emitting outflow at, say $\dot{m}>100$, in the case of flat-radio sources) does shadow the outer, line emitting material from the inner source of hard, ionizing radiation. The softer ionizing flux observed closer to the equatorial plane would allow a lower ionization stage of the iron, thus increasing the strength of the optical Fe II emission. Subcritical accretion disks would instead be characterized by a higher flux of ionizing radiation which can get out into the surrounding material and this would ionize Fe^{+} and reduce the Fe II emission lines. If this picture is correct, an obvious test is to check for the presence of strong Fe II emission lines in the spectra of the objects which show a soft X-ray excess.

The idea of a strong and anisotropic far-UV continuum may then have many important and exciting consequences. A discussion of such possibilities needs more careful modelling and will be subject of future work.

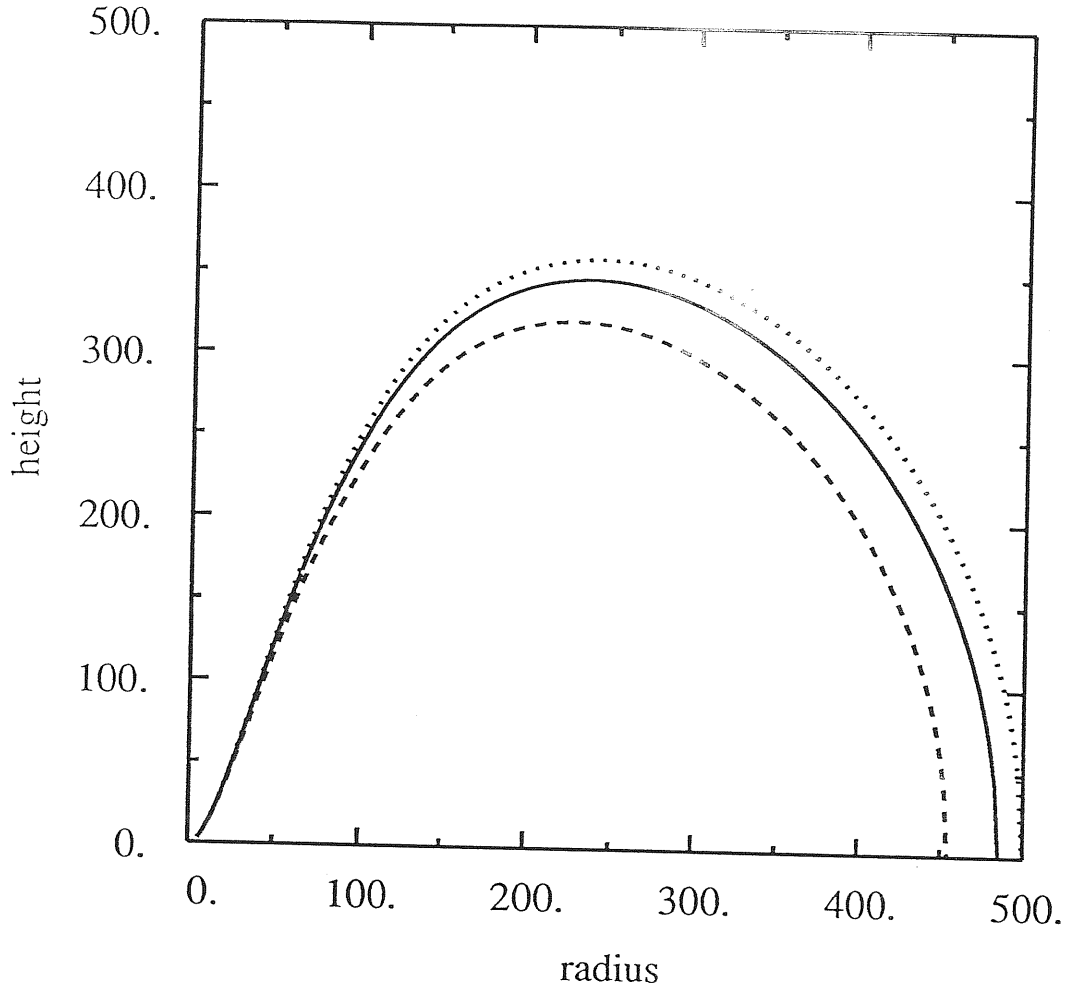

figure 9

Meridional cross-section of a radiation torus with model parameters: $r_{in}=2.7r_G$, $r_{out}=500r_G$, $M=10^8 M_\odot$, $\beta=3\cdot10^{-4}$. *The zero-pressure (dotted curve), last-scattering* $\tau_T=1$ *(solid curve), and thermalization* $\tau_*(\nu)=1$ *for* $\nu=kT/h$ *(dashed curve) surfaces are plotted. Height and radius are in units of* r_G. *The optical depth is evaluated as* $\tau=K\rho H$, *where K is the specific opacity and H is the pressure scale-height:* $H=p/\nabla p$.

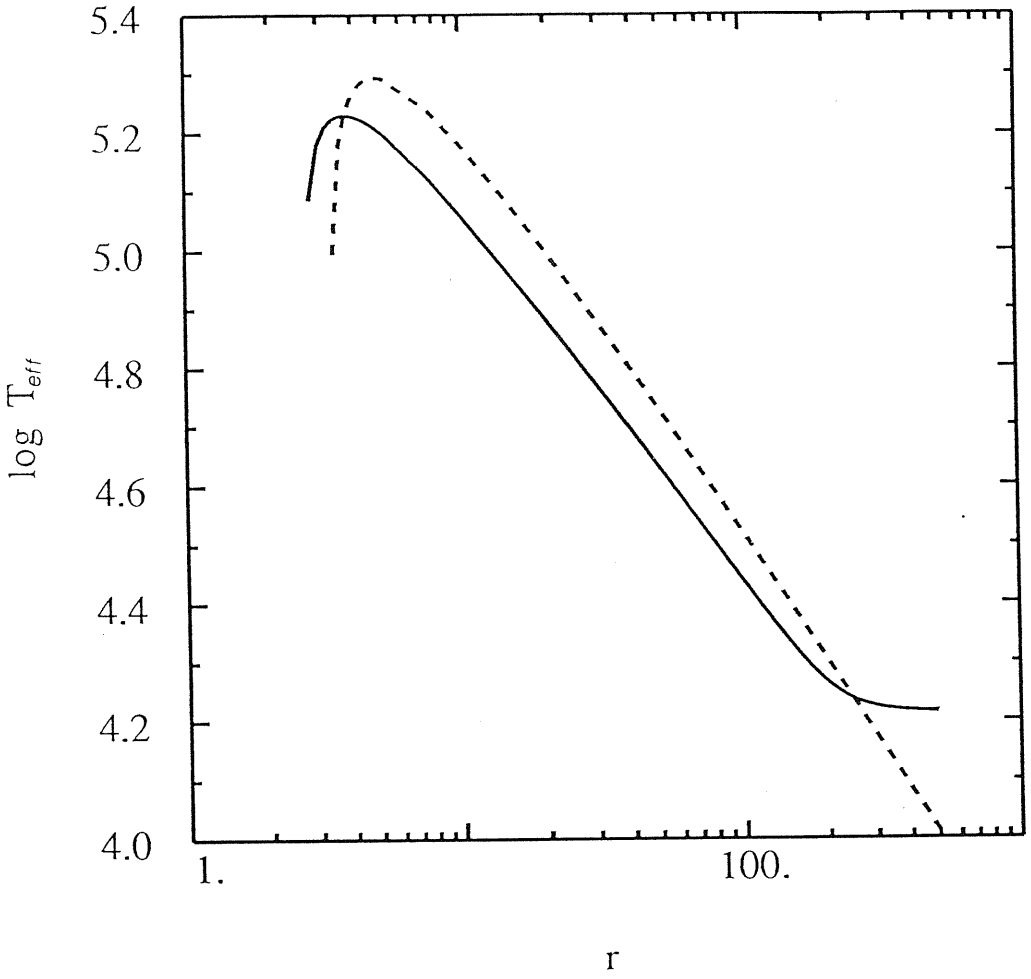

figure 10

The effective temperature distributions for a radiation torus (solid curve) and for a thin accretion disk with the same values of M and $\dot{m}$ (dashed curve). the radius is in units of r_G .

Thin disk: $T_{eff} \propto r^{-3/4}$.

Radiation torus: $T_{eff} \propto l^{1/2} r^{-3/4}$ *where the centrifugal force dominates in the balance of force, and* $T_{eff} \sim const$ *where gravity dominates and the isobars are almost spherical.*

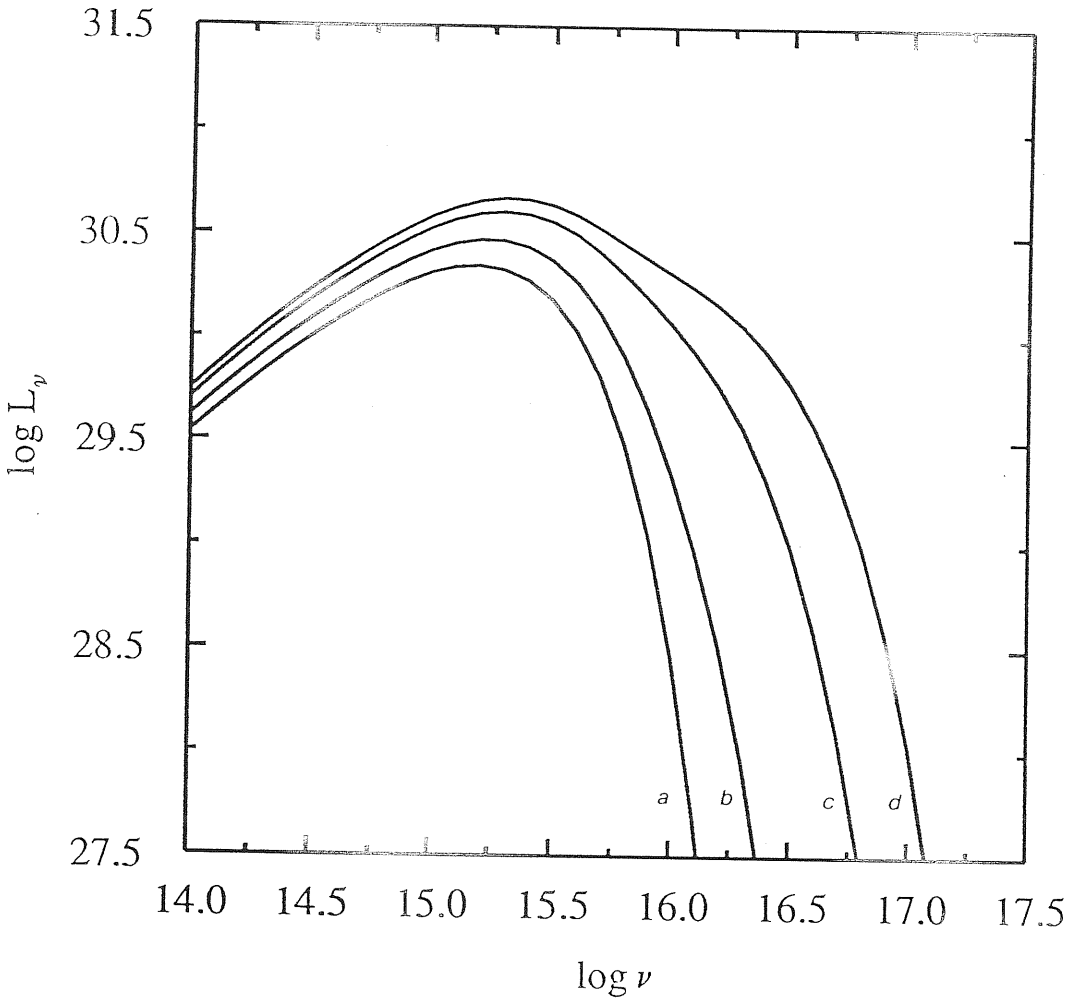

figure 11

Thick disk spectra for different angles, ϑ, of inclination between the rotation axis and the line of sight. Curves labeled a,b,c,d are computed for ϑ=90° (edge-on view), 50°, 25°, and 0° (pole-on view),respectively.

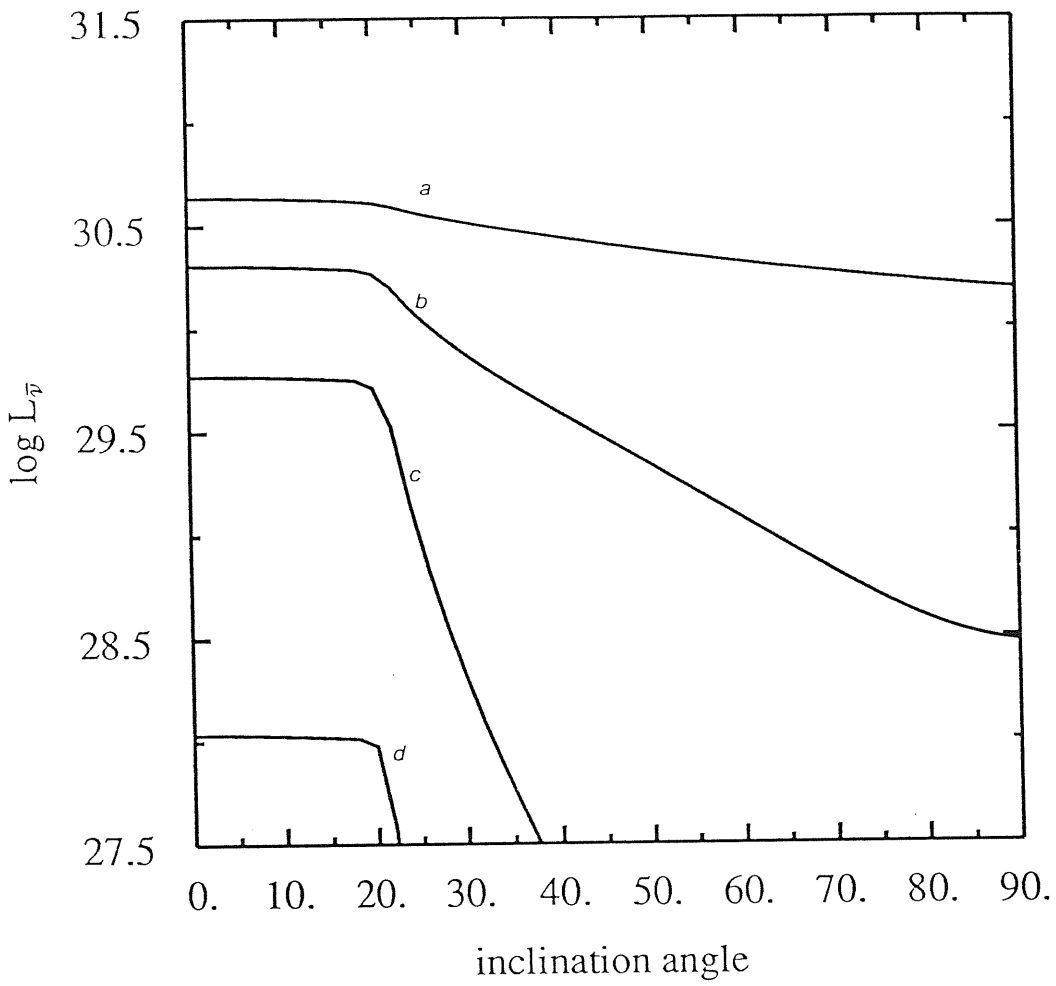

figure 12

Dependence on the inclination angle of the specific luminosity observed . Curves labeled a,b,c,d are computed for $\log\bar{\nu}$ *= 15.5, 16, 16.5, and 17, respectively.*

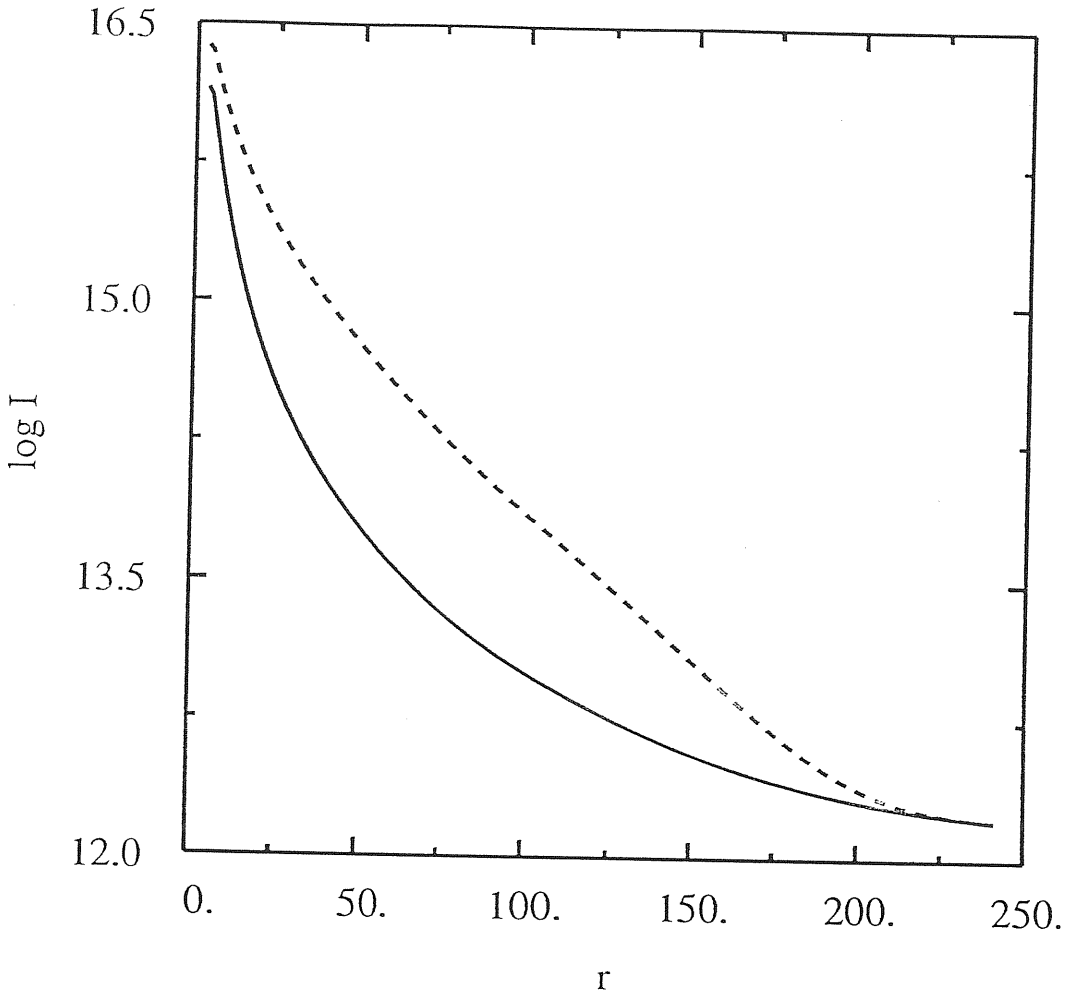

figure 13

The surface brightness (dashed curve) and effective gravity or net flux (solid curve) vs radius in the funnel (in units of r_G*). Note the enhancement due to the reflection effect.*

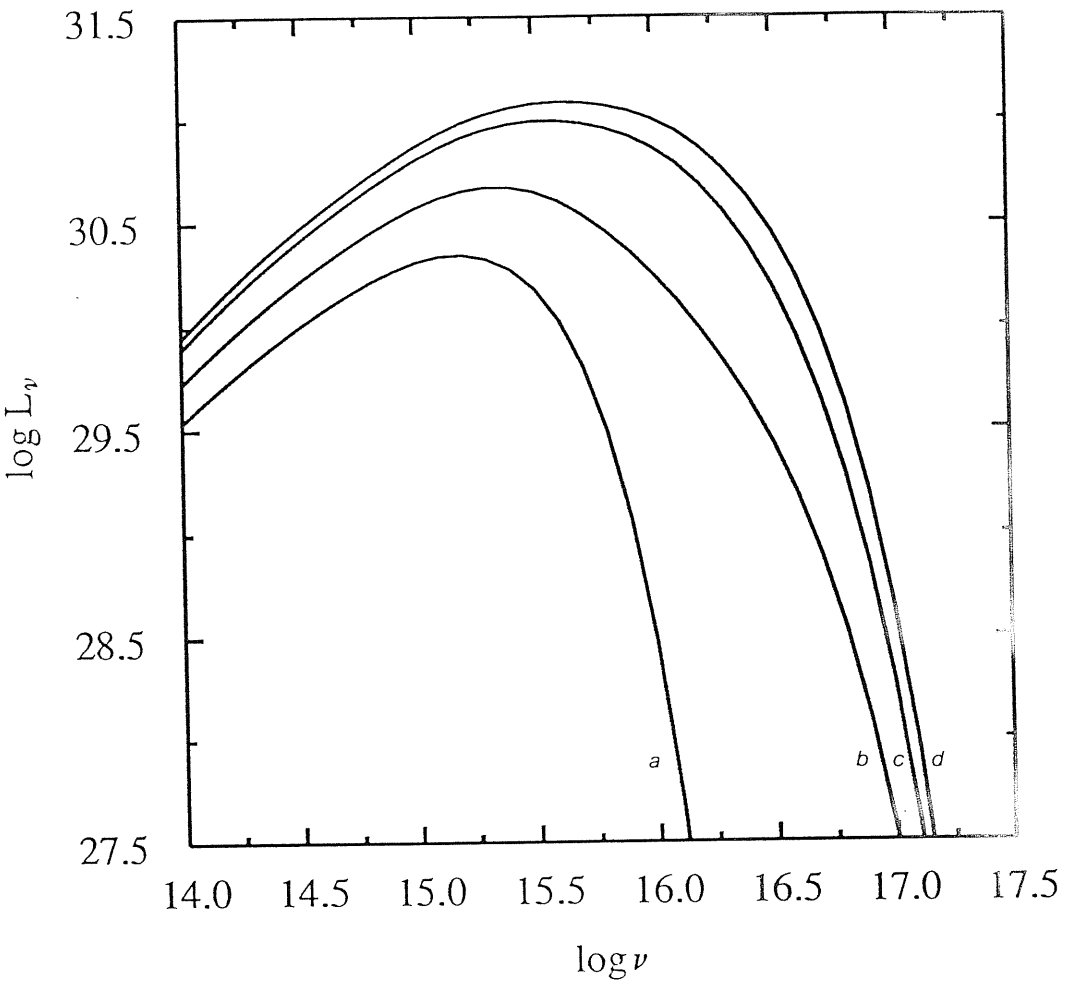

figure 14

Thick disk spectra for different inclination angles. The effect of multiple scatterings of photons off the funnel walls has been included. Curves labeled a,b,c,d are computed for $\vartheta = 90^\circ, 50^\circ, 25^\circ, o^\circ$.

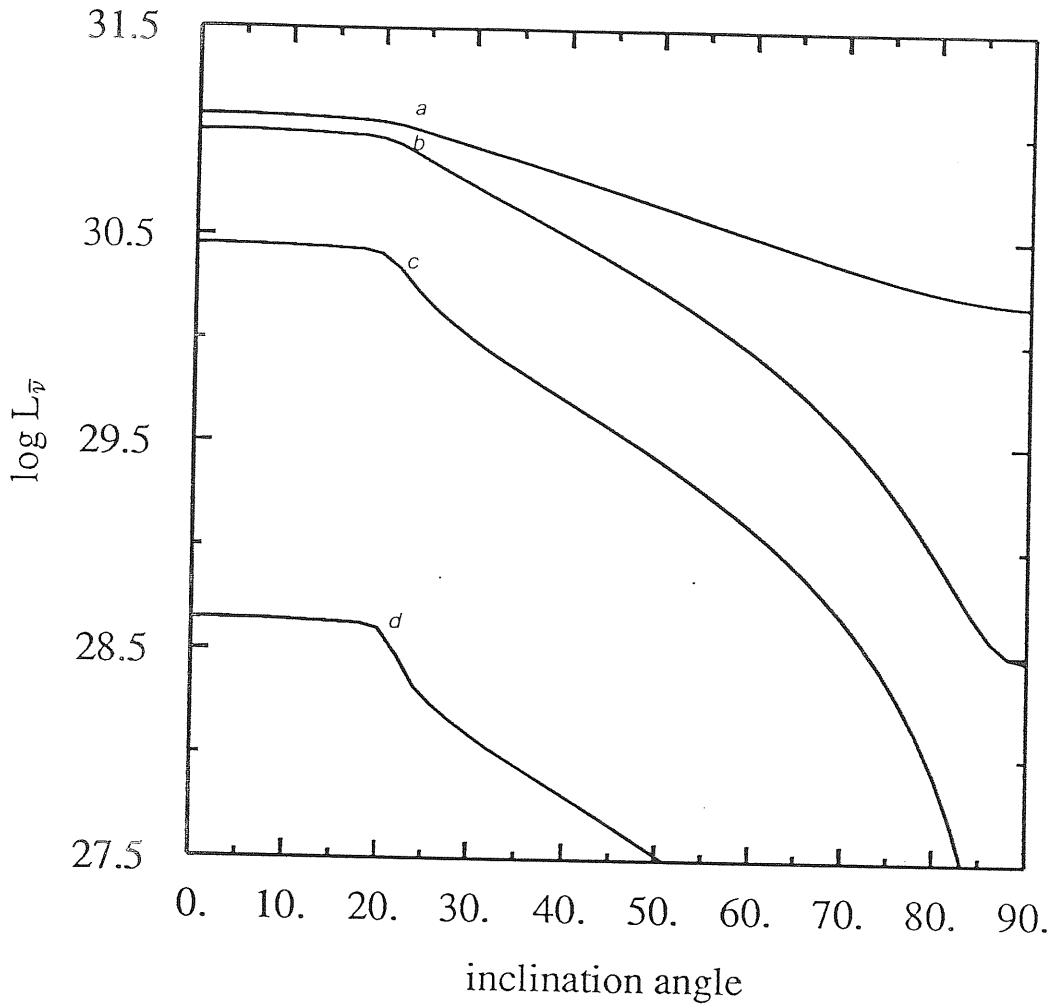

figure 15

Dependence of the specific luminosity on the inclination angle. The effect of multiple scatterings is included. Curves labeled a, b, c, d are computed for $\log\bar{\nu}$ *= 15.5, 16, 16.5, and 17.*

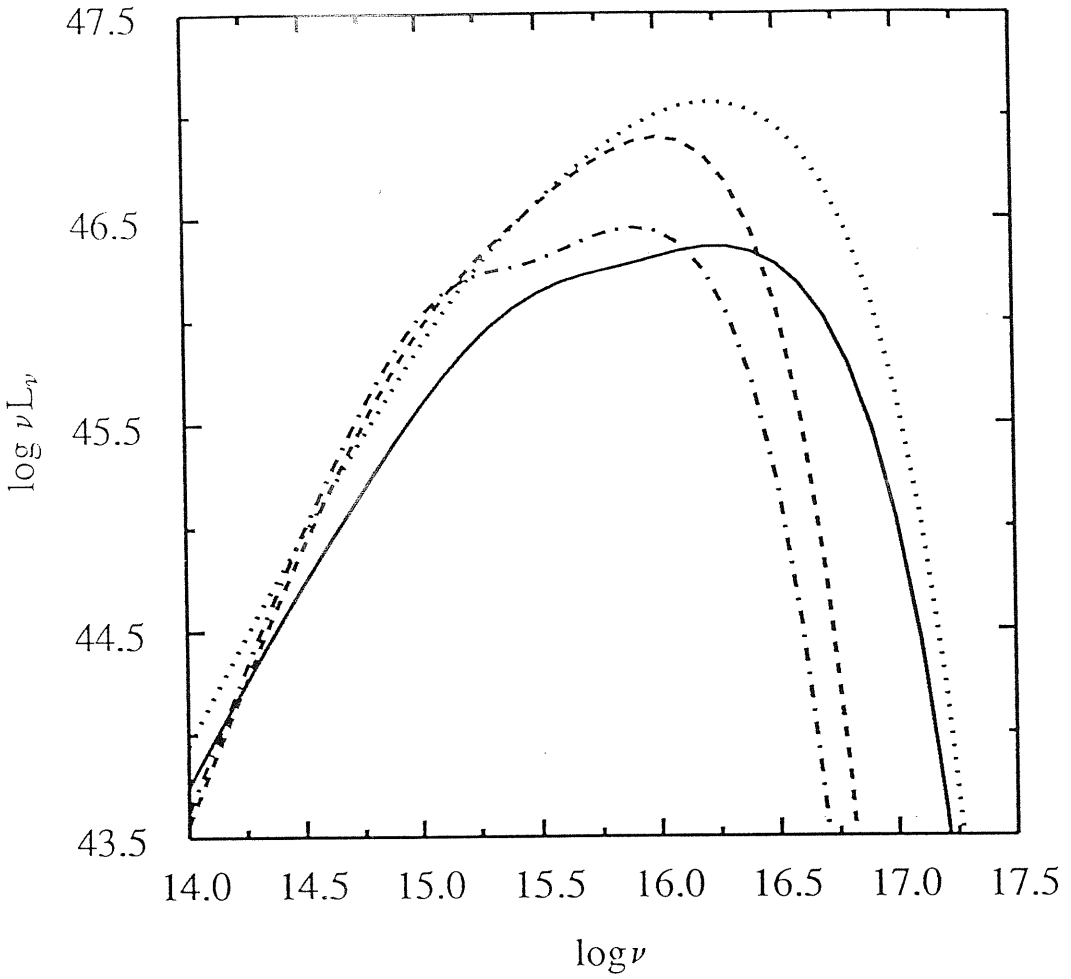

figure 16

Spectra at ϑ=o° (pole-on view) replotted in terms of luminosity per logarithmic frequency interval.

Solid line: thick disk spectrum without reflection effect.

Dash-dotted line: same, in the sum-of-blackbodies approximation.

Dotted-line: thick disk spectrum with reflection effect.

Dashed line: thin accretion disk spectrum with same M, $\dot{m}$, and size.

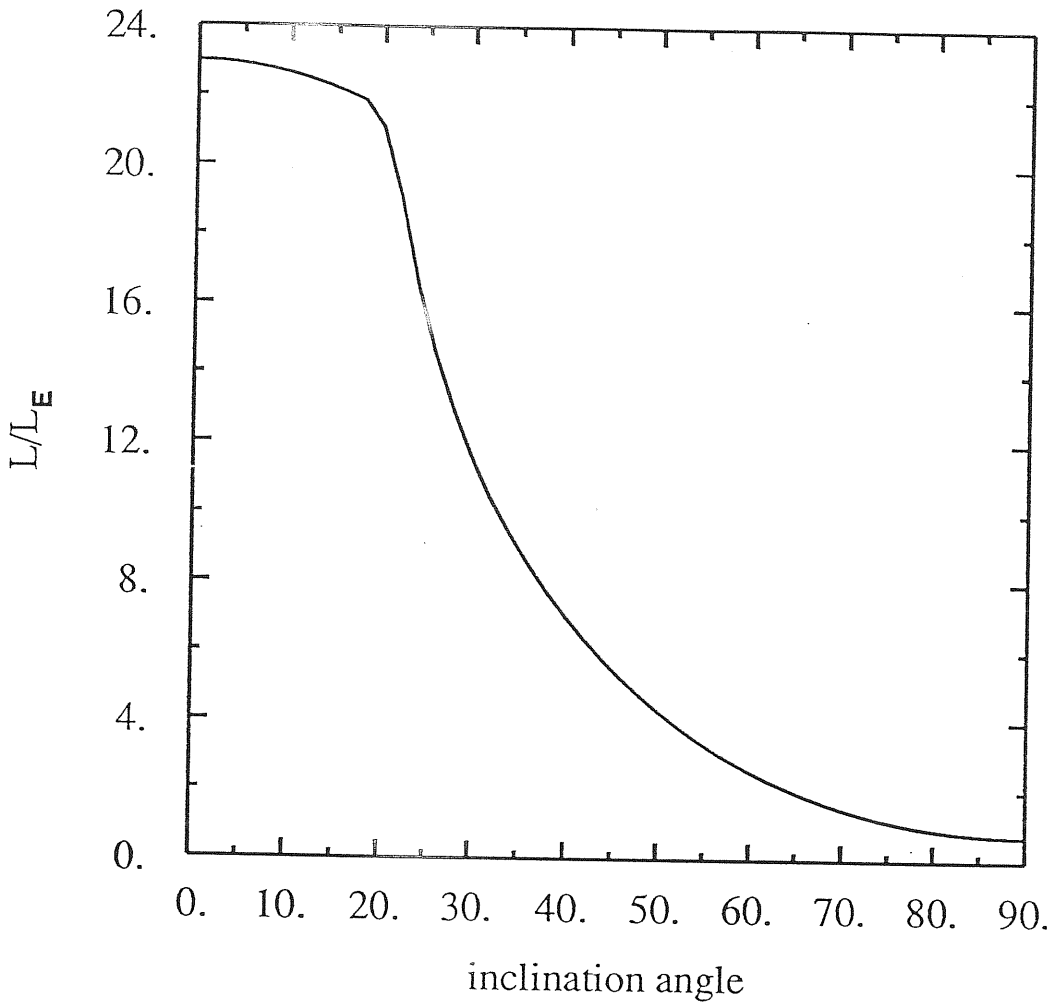

figure 17

The distribution of luminosity at infinity, as a function of the inclination angle from the rotation axis.

Table 2

The Thick Accretion Disk Model : Characteristic Values

$r_{in} = 2.7\ r_G$	$L \simeq 6\ L_E$	$M_{disk} \simeq 2.4 \cdot 10^6\ M_\odot$
$r_{out} = 500\ r_G$	$\dot{M} \simeq 20\ M_\odot/yr$	$\alpha_c \simeq 4. \cdot 10^{-7}$
$M = 10^8\ M_\odot$	$\epsilon \simeq 6\%$	$\rho_c \simeq 2. \cdot 10^{-6}\ gr/cm^3$
$\beta = 3 \cdot 10^{-4}$	$\Psi \simeq 23^\circ$	$T_c \simeq 7.6 \cdot 10^6\ K$

dynamical timescale at r_c :	$t_d = 2\pi/\omega$	$\sim 10^5$ sec
thermal timescale at r_c :	$t_{th} \simeq t_d/\alpha$	$\sim 10^4$ yr
viscous timescale at r_c :	$t_{vi} \simeq t_{th}/(h/r)^2$	$\sim t_{th}$

$\Psi \equiv$ half-opening angle of the funnel

References

Abramowicz,M. A. 1985,Publ.Astron.Soc.Japan,37,727 .

Abramowicz,M. A.,Calvani,M.,and Madau,P. 1987,Comments Astrophys., in press .

Abramowicz,M. A.,Calvani,M.,and Nobili,L. 1980,Ap.J.,242,772 .

Abramowicz,M. A.,Henderson,P. F.,and Ghosh,P. 1983, M.N.R.A.S.,203,323 .

Abramowicz,M. A.,and Piran,T. 1980,Ap.J.(Letters),241,L7 .

Abramowicz,M. A., and Zurek,W. H. 1981,Ap.J.,246,314 .

Angel,J. R. P.,and Stockman,H. S. 1980,Ann.Rev.Astr.Ap.,18,321 .

Antonucci,R. J., and Miller,J. S. 1985,Ap.J.,297,621 .

Antonucci,R. J., and Ulvestad,J. S. 1985,Ap.J.,294,158 .

Arnaud,K. A. et al. 1985, M.N.R.A.S.,217,105 .

Baath,L. B. et al. 1981,Astr.Ap.,96,316 .

Bahcall,J. N., and Wolfe,R. A. 1976,Ap.J.,209,214 .

Bajtlik,S.,Duncan,R. C., and Ostriker,J. P. 1987,preprint.

Bassani,L.,Dean,A. J., and Sembay,S. 1983,Astr.Ap.,125,52 .

Beall,J. A. et al. 1978,Ap.J.,219,836 .

Bechtold,J.,Czerny,B.,Elvis,M.,Fabbiano,G.,and Green,R. F. 1987, Ap.J.,314,699 .

Bechtold,J. et al 1984,Ap.J.,281,76 .

Bechtold,J.,Weymann,R.J.,Lin,Z., and Malkan,M.A. 1987,Ap.J.,315,180 .

Begelman,M. 1985,in "Astrophysics of Active Galaxies and Quasi-Stellar Objects",ed. J.S. Miller (Oxford:Oxford University Press),p. 411 .

Begelman,M. C.,Blandford,R. D., and Rees,M. J. 1984,Rev. Mod. Phys., 56,225 .

Blaes,O. M. 1986,Ph.D. thesis,SISSA,Trieste .

Blaes,O. M. 1987, M.N.R.A.S.,in press .

Blaes,O. M., and Hawley,J. F. 1987,preprint.

Blandford,R. D. 1984,in Proceedings of the Manchester Conference on Active Galactic Nuclei,ed. J. Dyson (Manchester:University Press),p. 281 .

Blandford,R. D. 1985,in "Numerical Astrophysics",eds. J. Centrella, J. LeBlanc,and R. L. Bowers (Boston:Jones and Bartlett Publishers, Inc.),p. 6 .

Blandford,R. D., and Konigl,A. 1979,Ap.J.,232,34 .

Blandford,R. D., and Payne,D. G. 1982,M.N.R.A.S.,199,833 .

Blandford,R. D., and Rees,M. J. 1974,M.N.R.A.S.,169,395 .

Blandford,R. D., and Rees,M. J. 1978,in Pittsburgh Conference on BL Lac objects, ed. A. M. Wolfe (Univ. Pittsburgh Press),p. 328 .

Blandford,R. D., and Znajek,R. L. 1977,M.N.R.A.S.,179,433 .

Blumenthal,G. R., and Gould,R. J. 1970,Rev. Mod. Phys.,42,237 .

Boyle,B. J.,Fong,R.,Shanks,T., and Peterson,B. A. 1987,M.N.R.A.S., 227,717.

Boroson,T. A., and Oke,J B. 1984,Ap.J.,278,11 .

Boroson,T. A.,Persson,S. E., and Oke,J. B. 1985,Ap.J.,293,120.

Brown,R. L. et al. 1981,Astrophys. Letters,21,105 .

Browne,I. W. A. 1983,M.N.R.A.S.,204,23P .

Browne,I. W. A., and Wright,A. E. 1985,M.N.R.A.S.,213,97 .

Browne,I. W. A., and Murphy,D. W. 1987,M.N.R.A.S.,226,601 .

Carrasco,L.,Dultain-Hacyan,D., and Cruz-Gonzales,I. 1985,Nature, 314,146 .

Carswell,R. F. et al. 1984,Ap.J.,278,486 .

Cavaliere,A. and Morrison,P. 1980,Ap.J.,238,L63 .

Chakrabarti,S. K. 1985,Ap.J.,288,1 .

Cheng,F.,Danese,L.,de Zotti,G., and Franceschini,A. 1985,M.N.R.A.S., 212,857 .

Cohen,M. H., and Unwin,S. C. 1984,IAU Symposium 110,VLBI and

Compact Radio Sources,eds Fanti,R.,Kellerman,K.I. and Setti,G.Reidel, Dordrecht,p. 95 .

Cruz-Gonzales,I., and Huchra,J. P. 1984,Astr.J.,89,441 .

Cunningham,C. T. 1975,Ap.J.,202,788 .

Cutri,R. M.,Wisniewski,W. Z.,Rieke,G. H., and Lebofski,M. J., Ap.J.,296,423 .

Czerny,B.,and Elvis,M. 1987,Ap.J.,in press .

Davis,M., and Huchra,J. 1982,Ap.J.,254,437 .

Dressler,A. 1980,Ap.J.,240,L11 .

Duncan,M. J., and Shapiro,S. L. 1983,Ap.J.,268,565 .

Eardley,D. M., and Lightman,A. P. 1975,Ap.J.,200,187 .

Eckart,A. et al. 1982,Astr.Ap.,108,157 .

Edelson,P. A., and Malkan M. A. 1986,Ap.J.,308,59 .

Elvis,M.,Green,R. F.,Bechtold,J.,Schmidt,M.,Neugebauer,G.,Soifer, B. T.,Mathews,K.,and Fabbiano,G. 1986,Ap.J.,310,291 .

Elvis,M., and Lawrence,A. 1985,in "Astrophysics of Active Galaxies and Quasi- Stellar Objects",ed. J.S. Miller (Oxford:Oxford University Press),p. 289 .

Elvis,M.,Wilkes,B. J.,and Tananbaum,H. 1985,Ap.J.,292,357 .

Fabian,A. C.,Guilbert,P. W.,Arnaud,K. A.,Shafer,R. A.,Tennant, A. F., and Ward,M.J. 1986,M.N.R.A.S.,218,457 .

Fabian,A. C., and Rees,M. J. 1979,in "X-ray Astronomy", eds. Baity & Peterson, Oxford Pergamon .

Fanaroff,B. L., and Riley,J. M. 1974,M.N.R.A.S.,167,31P .

Feigelson,E. D. et al. 1986,Ap.J.,302,337 .

Ferland,G. J., and Netzer,H. 1983,Ap.J.,264,105 .

Felten,J. E., and Rees,M. J. 1972,Astr.Ap.,17,226 .

Fishbone,L. G., and Moncrief,V. 1976,Ap.J.,207,962 .

Frank,J.,King,A. R., and Raine,D. J. 1985,"Accretion Power in Astrophysics",Cambridge Univ. Press .

Gear,W. K. 1985,Ap.J.,291,511 .

Gehren,T.,Fried,J.,Wehiner,P. A., and Wyckoff,S. 1984,Ap.J.,278,1 .

Ghisellini,G. 1987,M.N.R.A.S.,224,1 .

Ghisellini,G.,Maraschi,L.,Tanzi,E. G., and Treves,A. 1986,Ap.J.,310,317 .

Ghisellini,G.,Maraschi,L., and Treves A. 1985,Astr.Ap.,146,204 .

Goldreich,P.,Goodman,J., and Narayan,R. 1986,M.N.R.A.S.,221,339 .

Gondhalekar,P. M.,O'Brien,P.,and Wilson,R. 1986,M.N.R.A.S.,222,71 .

Gould,R. J. 1979,Astr.Ap.,76,306 .

Guilbert,P. W.,Fabian,A. C.,and McCray,R. 1983,Ap.J.,266,466 .

Guilbert,P. W.,Fabian,A. C.,and Rees,M. J. 1983,M.N.R.A.S.,205,593 .

Hills,J. G. 1975,Nature,254,295 .

Hoyle,F.,Burbidge,G. R., and Sargent,W. L. W. 1966,Nature,209,75 .

Jaroszynski,M.,Abramowicz,M. A.,and Paczynski,B. 1980,
Acta Astr.,30,1 .

Jones,T. W.,O'Dell,S.L., and Stein,W. A. 1974,Ap.J.,188,353 .

Kallman,T., and Krolik,J. H. 1987, in preparation .

Keel,W. C. 1985,in "Astrophysics of Active Galaxies and Quasi-Stellar Objects",ed. J.S. Miller (Oxford:Oxford University Press),p. 1 .

Kellerman,K. I. et al. 1971,Ap.J.,169,1 .

Kellerman,K. I., and Pauliny-Toth,I. J. K. 1981,Ann.Rev.Astr.Ap.,19,373 .

Kinney,A. L.,Huggins,P. J.,Bregman,J. N., and Glassgold,A. E. 1985,
Ap.J.,291,128 .

Konigl,A. 1981,Ap.J.,243,700 .

Koo,D. C., and Kron,R. G. 1982,Astr.Ap.,105,107 .

Koo,D. C., and Kron,R. G. 1987,preprint .

Krolik,J. H. 1986,to be published in the proceedings of the George Mason University Workshop on Supermassive Black Holes .

Krolik,J. H.,McKee,C. F., and Tarter,C. B. 1981,Ap.J.,249,422 .

Lanza,A. 1986,Ph.D. thesis,SISSA,Trieste .

Lawrence,A. 1987,P.A.S.P.,99,309 .

Lawrence,A., and Elvis,M. 1982,Ap.J.,256,410 .

Lawrence,C. R. et al. 1985,Ap.J.,296,458 .

Ledden,J. E., and O'Dell,S. L. 1986,Ap.J,298,630 .

Liang,E. T. P., and Price,R. H. 1977,Ap.J.,218,247 .

Lightman,A. P., and Shapiro,S. L. 1978,Rev. Mod. Phys.,50,437 .

Lind,K. R., and Blandford,R. D. 1985,Ap.J.,295,358 .

Lynden-Bell,D. 1978,Physica Scripta,17,185 .

Maccacaro,T. et al. 1982,Ap.J.,253,504 .

Madau,P. 1987,to appear in the Ap.J. .

Madau,P.,Ghisellini,G., and Persic,M. 1987,M.N.R.A.S.,224,257 .

Madjeski,G. M., and Schwartz,D. A. 1983,Ap.J.,275,467 .

Malkan,M. A. 1983,Ap.J.,268,582 .

Malkan,M. A., and Moore,R. L. 1986,Ap.J.,300,216 .

Malkan,M. A.,and Sargent,W. L. W. 1982,Ap.J.,254,22 .

Marano,B.,Zamorani,G., and Zitelli,V. 1987,preprint .

Maraschi,L.,Ghisellini,G.,Tanzi,E. G., and Treves,A. 1986,Ap.J.,310,325 .

Marscher,A. P. 1980,Ap.J.,235,386 .

Marshall,H. L. 1985,Ap.J.,299,109 .

Marshall,H. L. 1987,preprint .

Mathez,G. 1976,Astr.Ap.,53,15 .

Miley,G. 1980,Ann.Rev.Astr.Ap.,18,165 .

Miller,J. S. 1981,P.A.S.P,13,681 .

Moore,R. L., and Stockman,H.S. 1984,Ap.J.,279,465 .

Morini,M. et al. 1986,Ap.J.,306,L71 .

Murdoch,H. S.,Hustead,R. W.,Pettini,M., and Blades,J. C. 1986,
Ap.J.,309,19 .

Narayan,R.,Nityananda,R.,and Wiita,P. J. 1983,M.N.R.A.S.,205,1103 .

Netzer,H. 1985,Ap.J.,289,451 .

Netzer,H. 1987,M.N.R.A.S.,225,55 .

Neugebauer,G.,Oke,J. B.,Becklin,E. E.,and Matthews,K. 1979, Ap.J.,230,79 .

Nityananda,R.,and Narayan,R. 1982,M.N.R.A.S.,201,697 .

Orr,M. J. L., and Browne,I. W. A. 1982,M.N.R.A.S.,200,1067 .

Osmer,P. S. 1982,Ap.J.,253,28 .

Paczynski,B. 1978,Acta Astr.,28,91 .

Paczynski,B.,and Wiita,P. J. 1980,Astr.Ap.,88,23 .

Papaloizou,J. C. B.,and Pringle,J. E. 1984,M.N.R.A.S.,208,721 .

Papaloizou,J. C. B.,and Pringle,J. E. 1985,M.N.R.A.S.,213,799 .

Pauliny-toth,I. I. K. et al. 1981,Ap.J.,248,61 .

Peacock,J. A. 1987,in the proceedings of the Erice School on "AGNs, Neutron Stars and Jets",in press .

Peacock,J. A., and Gull,S. F. 1981,M.N.R.A.S.,196,611 .

Pearson,T. J., and Readhead,A. C. S. 1981,Ap.J.,248,61 .

Phinney,E. S. 1983,Ph.D. thesis, Cambridge University .

Phinney,E. S. 1985,in "Astrophysics of Active Galaxies and Quasi-Stellar Objects",ed. J.S. Miller (Oxford:Oxford University Press),p. 453 .

Phinney,E. S. 1987, in preparation .

Piccinotti,G. et al. 1982,Ap.J.,253,485 .

Pounds,K. A.,Stanger,V. J.,Turner,T. J.,King,A. R.,and Czerny,B. 1987, M.N.R.A.S.,224,443 .

Preuss,E., and Fosbury,R. A. E. 1983,M.N.R.A.S.,204,783 .

Pringle,J. E. 1981,Ann.Rev.Astr.Ap.,19,137 .

Rees,M. J. 1966,M.N.R.A.S.,135,345 .

Rees,M. J. 1967,M.N.R.A.S.,137,429 .

Rees,M. J. 1984,Ann.Rev.Astr.Ap.,22,471 .

Rees,M. J.,Begelman,M. C.,Blandford,R. D., and Phinney,E. S. 1982, Nature,295,17 .

Richstone,D. O.,and Schmidt,M. 1980,Ap.J.,235,377 .

Rybicki,G. B.,and Lightman,A. P. 1979,"Radiative Processes in Astrophysics", (New York:Wiley) .

Sargent,W. L. W.,Young,P. J.,Boksenberg,A., and Tytler,D. 1980, Ap.J. Suppl.,42,1 .

Sargent,W. L. W., and Boksenberg,A. 1983,in "Quasars and Gravitational Lenses",24th Liege Astrophysical Coll.,p. 518 .

Schechter,P. 1976,Ap.J.,203,297 .

Scheuer,P. A. G., and Readhead,A. C. S. 1979,Nature,277,182 .

Schmidt,M. 1972,Ap.J.,176,273 .

Schmidt,M. 1978,Physica Scripta,17,329 .

Schmidt,M.,Schneider,D. P., and Gunn,J. E. 1986,Ap.J.,306,411 .

Schmidt,M.,Schneider,D. P., and Gunn,J. E. 1987,Ap.J.,316,L1 .

Schwartz,D. A., and Ku,W. H. M. 1983,Ap.J.,266,459 .

Shakura,N. I.,and Sunyaev,R. A. 1973,Astr.Ap.,24,337 .

Shakura,N. I.,and Sunyaev,R. A. 1976,M.N.R.A.S.,175,613 .

Shapiro,S. L.,Lightman,A. P., and Eardley,D. M. 1976,Ap.J.,204,187 .

Shields,G. A. 1978,Nature,272,706 .

Sikora,M. 1981,M.N.R.A.S.,196,257 .

Singh,K. P.,Garmire,G. P.,and Nousek,J. 1985,Ap.J.,297,633 .

Smith,E. P.,Heckman,T. M.,Bothun,G. D.,Romanishin,W., and Balick, B. 1986,Ap.J.,306,64 .

Soltan,A. 1982,M.N.R.A.S.,200,115 .

Steidel,C. C., and Sargent,W. L. W. 1987,Ap.J.,313,171 .

Stockton,A. 1982,Ap.J.,257,33 .

Stockton,A., and McKenty,J. W. 1987,Ap.J.,316,584 .

Svensson,R. 1986,in "Hydrodynamics in Stars and Compact Objects", IAU Coll 89, in the press

Terrel,J. 1959,Phys. Rev.,116,1041 .

Thorne,K. S. 1974,Ap.J.,191,507 .

Unwin,S. C. et al. 1983,Ap.J.,271,536 .

Unwin,S. C. et al. 1985,Ap.J.,289,109 .

Urry,M. C. 1984,Ph.D. thesis,University of Maryland.

Urry,M. C., and Shafer,R. A. 1984,Ap.J.,280,569 .

Veron,P. 1983,in "Quasars and Gravitational Lenses",24th Liege Astrophysical Coll.,p. 210 .

Wandel,A. 1987,Ap.J.,316,L55 .

Wardle,J. F. C.,Moore,R. L., and Angel,J. R. P. 1984,Ap.J.,279,93 .

Weedman,D. W. 1985,in "Astrophysics of Active Galaxies and Quasi-Stellar Objects",ed. J.S. Miller (Oxford:Oxford University Press),p. 497 .

Weedman,D. W. 1986,in "Structure and Evolution of AGNs",eds. Giuricin,G. et al.,Reidel,Dordrecht,Holland .

Weiler,K. W., and Johnston,K. J. 1980,M.N.R.A.S.,190,269 .

Weistrop,D.,Shaffer,D. B.,Hintzen,P., and Romanishin,W. 1985,Ap.J.,292,614 .

Wiita,P. J. 1982,Ap.J.,256,666 .

Wills,B. J., and Browne,I. W. A. 1986,Ap.J.,302,56 .

Wills,B. J.,Netzer,H., and Wills,D. 1985,Ap.J.,288,94 .

Wolstencroft,R. D.,Gilmore, G., and Williams,P. M. 1982,M.N.R.A.S., 201,479 .

Yee,H. K. C., and Green,R. F. 1984,Ap.J.,280,79 .

Young,P. J.,Shields,G. A., and Wheeler,J. C. 1977,Ap.J.,212,367 .

Zamorani,G. et al. 1981,Ap.J.,245,357 .

Zdziarski,A. A. 1986,Ap.J.,305,45 .

Zensus,J. A.,Porcas,R. W., and Pauliny-toth,I. I. K. 1984,Astr.Ap.,133,27 .